MOUNTAIN-PLAINS CONSORTIUM

MPC 18-366 | H. Mahmoud, R. Atadero, K. Rager,
A. Harper-Smith, and M. Memari

Effect of Service Temperature on Joint Removal in Steel Bridges

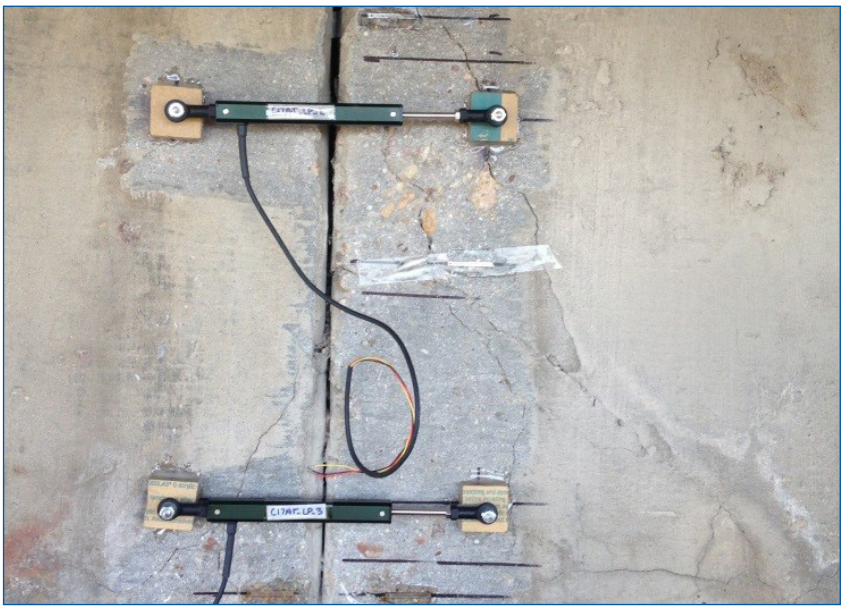

MOUNTAIN-PLAINS CONSORTIUM REGION 8

A University Transportation Center sponsored by the U.S. Department of Transportation serving the Mountain-Plains Region. Consortium members:

Colorado State University
North Dakota State University
South Dakota State University
University of Colorado Denver
University of Denver
University of Utah
Utah State University
University of Wyoming

Effect of Service Temperature on Joint Removal in Steel Bridges

Hussam Mahmoud (PI)
Rebecca Atadero
Karly Rager
Aura Lee Harper-Smith
Mehrdad Memari

Department of Civil and Environmental Engineering
Colorado State University
Fort Collins, CO 80523

August 2018

Acknowledgements

The funds for this study were provided, in part, by the United States Department of Transportation to the Mountain-Plains Consortium (MPC). Matching funds were provided by Colorado State University. The data for this study was provided by Colorado State Patrol and Colorado Department of Transportation, which is greatly appreciated.

Disclaimer

ABSTRACT

Bridge expansion joints are a particularly troublesome component of bridges and many departments of transportation (DOTs) are looking for a solution to deteriorating expansion joints on highway bridges. Bridge expansion joints create a break in the structural continuity of a bridge, allowing clogging gravels and corroding chlorides to enter. They are designed to absorb thermal movements of the bridge between two bridge elements. There are three main issues regarding expansion joints: maintenance, knowledge about thermal movements, and costs.

In order to prevent deterioration due to expansion joints, the joints must be cleaned regularly and replaced promptly after failure. However, most DOTs do not have the personnel, time, or resources to maintain their districts' expansion joints, which leads to bridge deterioration. Other similar maintenance and component issues have been addressed using a life-cycle cost analysis (LCCA). For this to be used on expansion joints the main issues of thermal knowledge, maintenance, and costs must first be addressed.

The main goals of this project are to 1) expand understanding of thermal loading effects on bridge expansion joints and 2) conduct an LCCA for joint elimination and retrofits for bridges in Colorado. These objectives were accomplished utilizing data from in-field instrumentation and finite element models. The study has been developed jointly between the Colorado Department of Transportation (CDOT) and researchers at Colorado State University.

Three main tasks were conducted to achieve the objectives: 1) collect and analyze long-term thermal loading data from existing bridges to assess thermal loading impacts on joints; 2) perform a parametric study using a calibrated finite element model to further understand joint behavior and retrofit options under thermal loads; 3) perform an LCCA for bridge expansion joint retrofitting, including impacts on bridge superstructure.

The significance of this work includes the results of data collection and analysis, the parametric studies, and the LCCA findings. The results of the numerical analysis show that clogged joints induce some localized stress, more so for the steel bridge, but do not significantly affect the global performance of the superstructure. The results also show that a reduction in moment demand on the superstructure is not apparent until a full-moment connection is utilized as a joint replacement. The parametric study and data analysis of thermal gradients indicate a stark need for further research into thermal gradients experienced by bridges. Finally, the LCCA concluded that a retrofit continuous bridge design would provide the most cost-effective design by decreasing joint replacement costs and pier cap corrosion. The modeling approach outlined in this study and the LCCA framework can be applied to any bridge and be used by CDOT to determine the viability of joint elimination for any bridge in Colorado.

TABLE OF CONTENTS

LIST OF FIGURES

List of Tables

1. INTRODUCTION

1.1 Statement of the Problem

Degradation of United States' public infrastructure has attracted attention from the public and governing agencies alike. A challenge facing transportation departments is management of leaking and clogged expansion joints in bridge structures, which result in significant deterioration to bridge substructures and superstructures. The need for a different maintenance strategy or a new solution to bridge expansion joints is ever pressing.

Bridge expansion joints create a break in the structural continuity of a bridge. They are designed to absorb thermal movements of the bridge between two bridge elements. Notably, expansion joints and bearings require regular maintenance throughout their life span in order to function properly and thus inhibit damage to the bridge superstructure (Hawk, 2003). A clogged joint can induce undesired stresses into the girders and abutments. A leaking joint can introduce corrosion into the superstructure below, primarily the pier caps (Lam et al., 2008). Deicing salts and chemicals used in colder regions increase the likelihood of corrosion beginning in the superstructure if a leaking joint is present. Additionally, bridges located in the mountains, where chains are used on vehicles, can experience more extensive deterioration. These issues are what caused expansion joints to be named by the American Association of State Highway and Transportation Officials (AASHTO) as the second most common bridge maintenance issue behind concrete bridge decks (AASHTO, 2012).

There are three main issues regarding expansion joints: maintenance, knowledge about thermal movements, and costs. Expansion joints are very susceptible to a lack of maintenance because DOTs lack the people and resources to regularly maintain their numerous bridge expansion joints. A bridge expansion joint needs to be cleaned every few months and repaired to protect it from clogging and leakage due to a damaged or worn out seal. However, this type of maintenance is beyond the scope of DOTs; consequently, removing the expansion joints from existing bridges altogether might solve this maintenance issue. The second issue is a lack of current research regarding thermal effects on bridge joints, including how much movement and stress are induced by thermal loads. Without knowing how important expansion joints are to bridge behavior, bridge movement, and stress, it is hard to know how removing the expansion joints would affect the overall structure. Finally, costs are an issue that needs addressing. Costs are important in any long-term decision such as this. DOTs need to know what makes the most economic sense regarding expansion joints. The economic issue could be addressed utilizing a life-cycle cost analysis (LCCA) in conjunction with data analyzing the effects of temperature on joint behavior. Consequently, a more cost-effective solution could be obtained for deteriorating expansion joints in existing bridges that does not require frequent extensive maintenance and uses knowledge of thermal effects.

The use of LCCA in infrastructure design, maintenance, and repair is becoming more prevalent around this country and globally. The public is becoming more interested in how officials use tax dollars, and thus encouraging agencies to look into and utilize better methods of infrastructure analysis for higher cost efficiency (Al-Wazeer et al., 2005; Ozbay et al., 2004). Stanford University defines LCCA concisely as the "process of evaluating the economic performance of a building (or other piece of infrastructure) over its entire life" (Stanford University, 2005). An LCCA of expansion joints on existing bridges in this manner could build on results of data regarding thermal behavior of bridge joints.

1.2 Objectives and Scope of Research

The overall goal of this study is to increase understanding of thermal loading and movement exhibited by bridges in Colorado and to provide recommendations for the elimination of deck joints in existing bridges. Specific objectives of this goal were developed through discussion and coordination among researchers at Colorado State University (CSU) and the Colorado Department of Transportation (CDOT). Four main tasks were identified: 1) collection of long-term thermal loading data to assess joint movement of two bridges, 2) development and validation of finite element models of one steel bridge and one concrete bridge, 3) assessment of joint elimination options, and 4) assessment of the life-cycle cost and the implications associated with joint removal.

The long-term data collected in Task 1 can provide information to DOTs about the actual movement of the selected bridges and joints. This can then be compared with the deck joint movement and thermal loading requirements outlined in the AASHTO LRFD Bridge Design Specifications. Development of the finite element models in Task 2 can help assess the stresses induced in the bridge from different connection types and thermal loading scenarios. Development of retrofit connection types in Task 3 can provide CDOT with options to confidently eliminate deck joints in bridges. Assessment of the life cycle cost (LCC) implications in Task 4 can help CDOT make decisions about which bridges to retrofit to eliminate deck joints and when a joint eliminating retrofit is the most appropriate option. The content of this report includes:

- A literature and background review
- Bridge selection and field instrumentation
- Load-controlled tests for validating the finite element models
- Parametric studies analyzing the joints response to different clogging stiffness, thermal gradients, and retrofit options
- LCCA of bridge expansion joints and retrofitting

2. BACKGROUND AND LITERATURE REVIEW

2.1 Introduction

To achieve a thorough understanding of the problem and the state of the current research relating to the elimination of deck joints, an extensive literature review was performed. Topics such as origins of code provisions, local behavior at joints, global bridge performance, leading agencies in the field, thermal loads, and LCCA are included in this section.

2.2 Girder to Abutment Consideration

Various structural systems have been developed to allow for thermal movements while reducing or eliminating deck joints. Placing the joints at the ends of approach slabs or only at the abutments is one method used. Allowing rotation of the abutments is another method that has been utilized. This section aims to discuss these differences and the nomenclature put into place by transportation agencies.

Integral bridges are bridges without deck joints (*AASHTO LRFD Bridge Design Specifications,* 2012) and have been increasingly used in recent years by government agencies (Burke Jr., 1990; Tsiatas and Boardman, 2002; Wasserman, 1987). Although the current AASHTO code provides an umbrella definition for integral bridges, some state or local transportation agencies have developed definitions for fully integral bridges and semi-integral bridges. In an integral bridge, the total longitudinal movement is accommodated through thermal stresses in the superstructure, rotation of abutments, piers, or foundations, or a combination of those. Therefore, understanding integral bridge behavior is a vital part of designing the other elements of the structure that must accommodate the longitudinal thermal movement.

Fully integral bridges are characterized by the absence of deck joints, and have a girder system that is monolithic with the abutment. Often, the foundation piles supporting the abutment are constructed to accommodate longitudinal movement from the bridge superstructure through rotation. Constructing the abutment foundation from steel H-piles that are weak-axis oriented (to be rotationally flexible) is one method used. Alternatively, a structural hinge can be used at the base of the abutment to prevent moment buildup (Albhaisi and Nassif, 2014; Wasserman, 1987). For fully integral bridges, a joint is often placed at the end of the approach slab, where a leak would not as adversely affect the structural integrity of the bridge (Husain and Bagnariol, 2000).

Semi-integral bridges, however, are characterized by the absence of deck joints throughout the spans and by girders that are not monolithic with the abutment. Instead of a monolithic girder-abutment connection, a bearing is used at the seat of the abutment to allow global bridge movements. The foundation system for a semi-integral bridge is rigid and the approach slab is continuous with the bridge deck. Semi-integral bridges require less maintenance than bridges with multiple deck joints. However, the bearings must be inspected and maintained – a concern not relevant to fully integral bridges. An advantage to using semi-integral bridges is that they can be longer than fully integral bridges, because they have expansion joints at the abutments. The expansion joints at the abutments allow for some thermal movement, whereas fully integral bridges allow for no thermal movements without inducing stresses in the structure (Husain and Bagnariol, 2000). Although a fully integral bridge and a semi-integral bridge are both considered integral bridges by the current AASHTO definition, the physical difference between the structural systems is noteworthy when further understanding of bridge movements and stresses are of interest.

2.3 Leading Agencies

Samples of past experiences published by transportation agencies are presented. The agencies discussed are not necessarily an exhaustive list, but are those with a significant history of published work relating to elimination of deck joints or the analysis of thermal loading.

2.3.1 Tennessee Department of Transportation

The Tennessee Department of Transportation (TDOT) has published many articles and reports describing its experience with integral bridges (Wasserman 1987, 1999, and 2014). During the past several decades, almost all bridges in Tennessee have been constructed without deck joints up to several hundred feet. In extreme cases, bridges that could not be built entirely continuous were constructed with a bearing at the abutment to allow for global bridge movements, making them semi-integral bridges. Steel bridges in Tennessee have been constructed with entirely continuous superstructures up to a length of 127 m (416 ft.). When bridges without deck joints or joints at the abutments were studied, the stresses in the bridges were lower than expected. However, TDOT admits to not fully understanding why these integral bridges perform so well (Wasserman, 1987). Through experience, they have become more confident in increasing the length of their integral bridges. However, to develop a generalized procedure that can be followed with confidence by all bridge designers, it is necessary to better understand how these structures behave spatially, thermally, and throughout seasonal cycles rather than relying on past experience, which lacks analytical explanations.

2.3.2 Transportation Ministry of Ontario

The Transportation Ministry of Ontario (MTO) has also found success with integral bridges since implementing the deck elimination retrofit program in 1995. MTO focuses on connecting the slabs over the joint and leaving the girders discontinuous (Ontario Ministry of Transportation, 2014). Due to the variability of superstructure types, material, and loading scenarios, three retrofit designs were developed and used: 1) casting a deck and concrete diaphragm monolithically with the girders, 2) casting a thin flexible deck, and 3) casting a flexible deck de-bonded from girders. Generally, limits on skew, girder end rotations, and girder heights help guide designers to a retrofit choice. All three options were found feasible for steel girder systems. To avoid cracking caused in the negative moment regions, fiber reinforced concrete was suggested (Lam et al., 2008). MTO limited eligibility for the retrofit program to bridges with less than a 20° skew, a total bridge length of less than 492 ft. (150 m), and an angle subtended by a ~ 98 ft. (30 m) arc along the length of the structure that is less than 5° (Husain and Bagnariol, 2000). Details of MTO's program provide a suitable starting point for retrofitting bridges in Colorado to eliminate deck joints.

2.3.3 Colorado Department of Transportation

Many state DOTs, including the Colorado Department of Transportation (CDOT), also limit the length or skew of integral bridges (CDOT, 2012). Provisions in the CDOT Bridge Design Manual for integral bridges provide limits on bridge length. Bridge lengths are limited to 640 ft. (195 m) for steel bridges (CDOT, 2012). Further analysis of the thermal effects and connection types could help validate, tighten, or loosen these restrictions in some scenarios.

2.4 Types of Retrofit Connections

In addition to reducing maintenance and repair costs, integral bridge construction and retrofit programs can potentially increase the bridge's load rating and design life. However, there needs to be a greater understanding of the thermal effects induced in a jointless bridge so bridge designers can confidently

implement integral bridges. It has been shown that substantial differentials of stresses and movement occur in bridge girder systems due to thermal effects (Chen, 2008; Koo et al., 2013). Additionally, state departments have used numerous methods of connecting two simple spans. These different connections and bridge conditions may have varying benefits, load-rating implications, and LCC implications.

A study completed with the Rhode Island Department of Transportation at the University of Rhode Island investigated the effect that converting a simple span bridge to a continuous span bridge would have on load ratings (Tsiatas and Boardman, 2002). Linear, two-dimensional models were developed to examine the potentially increased moment capacity of bridges that were converted from simple spans with deck joints to continuous structures without deck joints. Multiple retrofit connection types that had been used by state transportation agencies were included in the study, including deck only, deck and top flange, deck and bottom flange, deck, top and bottom flange, and full moment splice. The results of the study indicated that moment capacity increased only when the deck and bottom flange, deck, top and bottom flange, and full moment splice retrofits were implemented. However, the deck only connection type was found to be the least expensive and most popular with government agencies. Based on the two-dimensional model, these connection types had the highest potential for cracking and did not increase the load carrying capacity of the bridge (Tsiatas and Boardman, 2002).

2.5 Thermal Effects on Bridges

One of the main considerations of deck joint elimination is longitudinal movement. Longitudinal thermal movement is currently accounted for in Section 3 of the AASHTO Bridge Design Specifications. The global thermal longitudinal movement has been shown to be accurately predicted by the average temperature of the bridge (Moorty and Roeder, 1992). Some methods used to accommodate longitudinal movements in integral bridges include flexible pile foundations (Albhaisi and Nassif, 2014) or an appropriately selected bearing or a hinge at the bottom of an abutment (Wasserman, 1987). However, the total bridge performance and local behavior cannot be entirely described by the average temperature of the structure. The uneven heating and resulting thermal stresses may also require consideration in order to eliminate deck joints without adversely affecting structural performance.

Thermal gradients are the most uneven at times of heating or cooling of the bridge. Heat transfer due to direct radiation from the sun, conduction, or convection occurs every time the ambient air temperature changes – usually every morning and evening. Bridge orientation, length of concrete overhang, depth of girders, height of concrete slab, and girder spacing are all parameters that affect how evenly the bridge gains and loses heat (Chen, 2008). Commonly, uneven bridge movements are accommodated through pier, bearing, joint, and girder movement or rotation. Notably, however, an integral bridge would not possess a joint to allow for uneven movements of a superstructure. A more detailed study on thermal stress distribution for bridges in Colorado could allow integral bridges to be designed confidently with longer lengths, greater skew angles, and greater curvature.

The coefficient of thermal expansion, commonly expressed as μ or α, describes the increase in length of a material for a given increase in temperature. Change in length of a homogeneous material due to uniform change in temperature can be expressed in Equation 1:

$$\Delta L = \Delta T * \alpha * L_0 \qquad \text{(Eq. 1)}$$

where ΔL is the change in length, ΔT is the change in temperature or the final temperature minus the initial temperature, α is the thermal expansion coefficient, L_0 is the original length of the material considered. A negative result for the change in length corresponds to a shortening of the material, and a positive value for the change in length corresponds to an increase in length of the material. Concrete has a coefficient of thermal expansion that is about 8% less than that of steel (Chen, 2008), and this results in a

change in length of a steel girder that is about 8% greater than what a concrete girder would experience. When these two materials are rigidly connected, such as in a steel composite bridge, the change of length is restricted and corresponding stresses develop.

A concept worthy of recognition is the difference in timing between critical thermal movements and critical thermal stresses. The maximum expansion and contraction from setting length for global bridge movement occurs during the warmest days in summer and the coolest nights in winter, respectively. However, the maximum thermal stresses due to uneven heat transfer in the superstructure occur during the warming of the bridge in the early afternoon or the cooling of the bridge in the evening (Moorty and Roeder, 1992). Verification of this concept and further understanding of the heating and cooling cycles on Colorado bridges can be further understood with temperature data from instrumentation of in-service bridges.

Thermal stresses are localized stresses due to overall temperature change and temperature gradients along any axis (transverse, longitudinal, or vertical) of a bridge. Currently, thermal gradient in the transverse direction is not accounted for in AASHTO LRFD Bridge Design Specifications. The thermal gradient in the vertical direction is mentioned in the current AASHTO provisions, but does not need to be considered if "experience has shown that neglecting temperature gradient in the design of a given type of structure has not led to structural distress" (*AASHTO LRFD Bridge Design Specifications,* 2012). The ambiguity of this statement leads many practitioners to neglect the thermal stresses that result from thermal gradients in the vertical direction. However, these stresses have been shown to exist on the order of +/- 5 ksi in a daily heat cycle of a steel box girder superstructure in Texas (Chen, 2008). This could be significant depending on how economically the bridge was designed initially.

2.6 Increasing Popularity

Overall, the use of integral bridge retrofits and construction has recently increased in popularity in the United States and Canada. As of 2002, over 500 existing bridges in the two countries have been made continuous (Tsiatas and Boardman, 2002). The bridge types that have been retrofitted are up to six-span structures with spans up to 300 ft. (~91.5 m) (Wasserman, 1987). Although the popularity of bridges without deck joints is increasing, one of the current barriers to more universal use of integral bridges is the lack of understanding of thermal gradients in bridges. To improve the success of joint elimination retrofit programs and new construction for bridges without deck joints, increased understanding of the thermal effects in bridges is requisite. Knowledge of thermal effects, especially with regard to local behavior at connections, will allow researchers and designers to develop a more diverse palate of retrofit options and improve estimates of LCC, load rating, and expected stresses.

2.7 Global Bridge Performance

The global performance of an integral bridge under thermal loading is a function of multiple parameters. Total longitudinal movement of the superstructure, the rotation of piers, abutments, and foundations that accommodate the longitudinal movement, the effect of curvature, length, and skew, and a potentially improved moment capacity and seismic performance are all of interest to a practitioner designing an integral abutment bridge. Multiple studies have been completed on these parameters of interest for integral bridges; however, most have focused on concrete girder systems (Tsiatas and Boardman, 2002). Less work has been completed on steel girder performance and connection retrofit types in steel bridges than for concrete superstructures.

2.7.1 Longitudinal Movement

A case study has shown that the total longitudinal movement of a bridge can be predicted by the bridge's average temperature (Roeder, 2003), and this is the method currently described by the AASHTO Bridge

Design Specifications, specifically in sections 3, 5, and 15 (*AASHTO LRFD Bridge Design Specifications,* 2012). This global expansion and contraction of the superstructure is the primary focus of design codes (Zhu et al., 2010). The coolest and warmest temperatures expected for steel bridges with concrete decks are described by a temperature contour map of the United States and are experienced in the coldest nights of winter and warmest days of summer, respectively. The contour map showing the maximum design temperature, developed by Roeder in 2002, is shown as an example in Figure 2.1. The minimum design temperatures are also provided by AASHTO LRFD Bridge Design Specifications in Chapter 3.12, but only the maximum temperature is shown in this paper to illustrate the method. The expected extreme temperatures for steel bridges have a greater range than for concrete bridges.

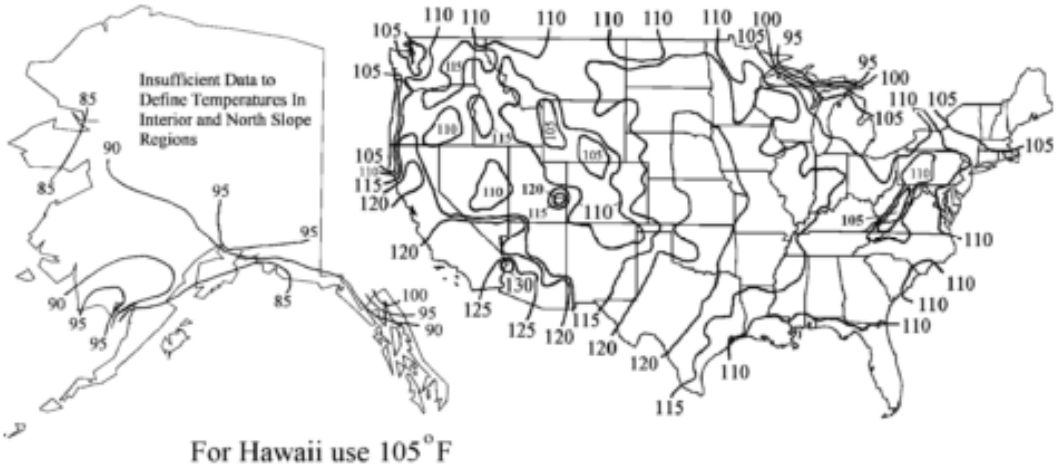

Figure 3.12.2.2-3—Contour Maps for $T_{MaxDesign}$ for Steel Girder Bridges with Concrete Decks

Figure 2.1 Maximum expected temperature for steel bridges with concrete decks

In addition to the difference in longitudinal bridge movement due to differences of the coefficient of thermal expansion, concrete girders generally contain a larger volume and mass than steel girders. Therefore, concrete superstructures act more as a heat sink and do not reach the air temperature as quickly as steel superstructures (Wasserman, 1987). For these reasons, concrete girder bridges are often designed for less extreme longitudinal movement than bridges with steel girders. In integral bridge construction or deck joint elimination candidates, this difference in longitudinal thermal movement is manifested in codes through more restrictive maximum length limits on steel integral bridges than for concrete integral bridges; ~400 ft. (120 m) to ~500 ft. (150 m is considered the longer end of the spectrum for integral bridge construction in steel bridges (Burke Jr., 1990).

One method used to allow the longitudinal thermal movement of integral bridges is placing a hinge at the bottom of the abutment or pier to prevent moment buildup (Loveall, 1985; Wasserman, 1987). The top of the abutment will rotate away from the bridge during warmer days due to thermal expansion and will rotate toward the bridge superstructure during cooler days due to thermal contraction. This method has been used with success by the Tennessee Department of Transportation (TDOT).

Another method used to accommodate longitudinal thermal movement of integral bridges is flexible foundations beneath the abutments. Typically, a single row of weak-axis-oriented H piles that can rotate when the bridge expands and contracts is used (Pugasap et al., 2009; Zhu et al., 2010). Zhu et al. completed a calibrated finite element model of pier footings to examine the robustness of the AASHTO provisions for the movements and soil stresses encountered under the footings due to thermal loads. The pressures encountered were well within the allowable bearing pressure. However, the focus of the study was on the pier footings, rather than the single row piles. Lastly, the girders were constructed of concrete

rather than steel, and the soil considered was not clay, which is commonly considered a problematic soil in Colorado.

Kim and Laman completed another parametric study in 2010 to examine the thermal effects on flexible rotations. A finite element model was developed, and the influence of the thermal expansion coefficient, span length, backfill height, backfill stiffness, and pile soil stiffness was considered. It was concluded that the backfill height and the backfill soil stiffness have relatively insignificant effects on the global bridge responses. However, as the pile soil stiffness increases, the maximum pile lateral force and pile moment also increases. Of the parameters of interest, the thermal expansion coefficient and span length influence the girder axial force, pile lateral force, pile moment, and pile head displacement significantly (Kim and Laman, 2010). Finally, the authors conclude by recommending that the effects of thermal stresses are included in all integral abutment bridges.

2.72 Effects of Bridge Geometry (Skew and Curvature)

Effects of curvature and skew have been examined to determine if global longitudinal bridge movements can or cannot be totally described by the one-dimensional AASHTO provisions in cases where the curvature and skew of the bridge are significant. Several transportation agencies have set limits on the skew and curvature of bridges eligible for integral construction and retrofits (Burke Jr., 1990; CDOT, 2012; Husain and Bagnariol, 2000). Further understanding of connection retrofits could help loosen the restraints on skew and curvature limitations. That being said, special attention should be given to skewed and curved bridges since field observations have confirmed the high potential for crack development within long and continuous skewed bridges (based on a discussion with Matt Greer from FHWA).

A three-dimensional finite element model was developed and verified by Moorty and Roeder (1992) to examine effects of skew, length, width, girder depth, cloud cover, wind speed, air temperature, bridge temperature differentials, and horizontal curvature in bridges under thermal loading. Their studies were performed on bridges with bearings between the girder system and the piers and abutments. Bridges with horizontal curvature were found to exhibit significant radial displacements near the center of curvature and significant tangential displacements at a point farthest away from rigid supports. Also, radial displacements were found to increase as the curvature of the bridge increased. Lastly, the radial displacements were shown to increase when the stiffness of bearings were greater (Moorty and Roeder, 1992). This is of importance to integral bridges where the superstructure connects monolithically with the piers and abutments. The stiffness in these connections is many orders of magnitude greater than the stiffness of a bearing. Therefore, it is not unreasonable to expect significant stress buildup in connections or significant radial movements in curved bridges without bearing pads that are subjected to thermal expansion and contraction along their longitudinal axis.

The finite element model developed by Moorty and Roeder also considered the effects of skew. The longitudinal and transverse deflections due to thermal loads were found to vary in the transverse direction in skewed bridges. Displacements were greatest at points farthest away from rigid supports. Lastly, it was recommended that bearings used on skewed bridges be unguided (not restricted to a single line of movement) to allow for transverse movements (Moorty and Roeder, 1992). In an integral bridge without bearings, however, these movements would be restrained, and the bridge would need to be able to accommodate these stresses through movement in a different location or with the strength of structural elements.

Questions remain about the effects of curvature and skew in integral bridges. However, understanding the movement of non-integral bridges provides a link to how the stresses would accumulate in curved and skewed integral bridges. Current AASHTO commentary (Section C3.12.2.1) states that bridges with large skew or curvature should not be built upon bearings that only allow movement in the longitudinal

direction due to expected radial or tangential movement. Understanding of the restraints and connections used, combined with structural solid mechanics, could yield an estimate for the accumulated stresses. Or the vertical supports could be decreased in stiffness to allow for the thermal movements to occur without the accumulation of stress.

2.7.3 Potential Increase in Moment Capacity

Eliminating deck joints and making the girders and deck continuous has the potential to increase moment capacity. However, due to the multiple ways a bridge can be connected and made continuous, the extent of the increased load rating is largely dependent on which detail is used and what elements of the superstructure become connected (Tsiatas and Boardman, 2002). A study conducted in 2002 by Tsiatas and Boardman examined deck only, deck and top flange, deck and bottom flange, deck, top and bottom flange, and full moment splice connections. The study concluded that no increase in moment capacity was exhibited when deck only and deck and top flange connections were used. The deck only and deck and top flange connections were also found to possess the highest potential for cracking due to the negative moment experienced in the bridge over the piers or supports.

Connections that did improve the moment capacity of the bridge included the deck, top and bottom flange connection and the full moment splice connection (Tsiatas and Boardman, 2002). Unsurprisingly, these connections are more expensive and laborious to construct. However, for bridges expected to carry more traffic in the near future, this option may be worth considering. Worth noting is that the model used to draw these conclusions was two-dimensional. It is uncertain whether this model included some of the benefits or disadvantages of the local behavior of the connection types considered. A three-dimensional model and more field verification of this model would strengthen the claims asserted.

2.8 Local Superstructure Behavior

The parameters and areas of interest of local behavior for bridges with deck joints differ from those without. Local superstructure behavior of interest for bridges with deck joints includes corrosion of girders under leaking joints, joints unable to perform due to debris buildup, and performance of joints and bearing pads under extreme temperatures. Local superstructure behavior of interest for integral bridge construction and retrofits (bridges without deck joints) includes lateral-torsional buckling (LTB) risk, thermal stress differentials in the superstructure cross-section, stresses in connections, rotation at girder ends, shear lag at girder ends, and understanding the advantages and disadvantages of numerous connection types. Local behavior of these forms could be non-linear and not fully described by two-dimensional models. Instead, verified, detailed three-dimensional finite element analysis would increase the understanding of the complex behaviors exhibited. An examination of previous research completed in these areas of interest follows.

2.8.1 Corrosion

Corrosion, one of the central issues with deck joints, is caused in the superstructure when deck joints leak (Hawk, 2003; Lam et al., 2008). This corrosion at the deck joints, which are commonly located at the piers, abutments, or other vertical supports, causes the structural integrity of the superstructure and bearings to deteriorate. Often, local behavior of the bearings, connections, girders, pier caps, and piers under these decks will be adversely affected. The use of deicing chemicals, and their subsequent runoff from roadways, increases the rate of corrosion to girder systems under deck joints (Tsiatas and Boardman, 2002). When deck joints leak, maintenance and, eventually, replacement are necessary to maintain a safe structure. Various bridges in Colorado have suffered from similar deterioration. The Colorado Bridge Enterprise (CBE) was formed in 2009 to provide funding to repair, reconstruct, and replace bridges designated as structurally deficient or functionally obsolete, and rated as poor. A list of bridges that fall

under these conditions can be found in the CBE list at https://www.codot.gov/programs/BridgeEnterprise/documents/faster-statewide-bridges.

2.8.2 Blocked Expansion

In order to function properly, expansion joints must be able to freely expand and contract without significantly affecting the road's driving surface. As illustrated in Figure 2.2, debris buildup in an expansion joint less than six months old can prevent it from closing in warmer weather to accommodate thermal loads (Chen, 2008). Routine maintenance is required to keep expansion joints in working order.

Figure 2.2 Debris in expansion joint in service for less than six months (Chen, 2008)

If excessive debris is allowed to build up in an expansion joint, pavement growth (PG) can occur. PG, as defined by the Michigan Department of Transportation (MDOT), is the widening of joints from debris buildup. Another major cause of PG is from concrete pavement that expands over time, causing joints to close. This phenomenon has been observed in bridges on I-225 and I-25 in Colorado, and has been successfully addressed with pavement relief joints.

If traffic removes a compression seal or debris builds up from other causes, the effect on the structure can be severe. When a joint with debris buildup opens farther because of reduced average bridge temperature, the debris settles farther into the joint and takes up the entire new width of the joint opening. This is very damaging because, at this point, the joint will not be able to close any farther than the current cool weather, wider debris opening. As a result of this increased opening, more debris is allowed to build up, and the distance from one end of the pavement to the other "grows." If the average bridge temperature were to increase, the joint would not be able to close to alleviate thermal stresses. However, if the temperature only decreases to a greater extent, the joint will open farther, and the newly added debris will settle into the joint and prevent even more movement, as shown in Figure 2.3. This cycle continues if the bridge deck joint is not maintained and significant stresses can be induced into the bridge local connections, bearing pads, and superstructure elements (Rogers et al., 2012). Eliminating deck joints would allow for reduction of damage or reduction of maintenance cost to prevent damage.

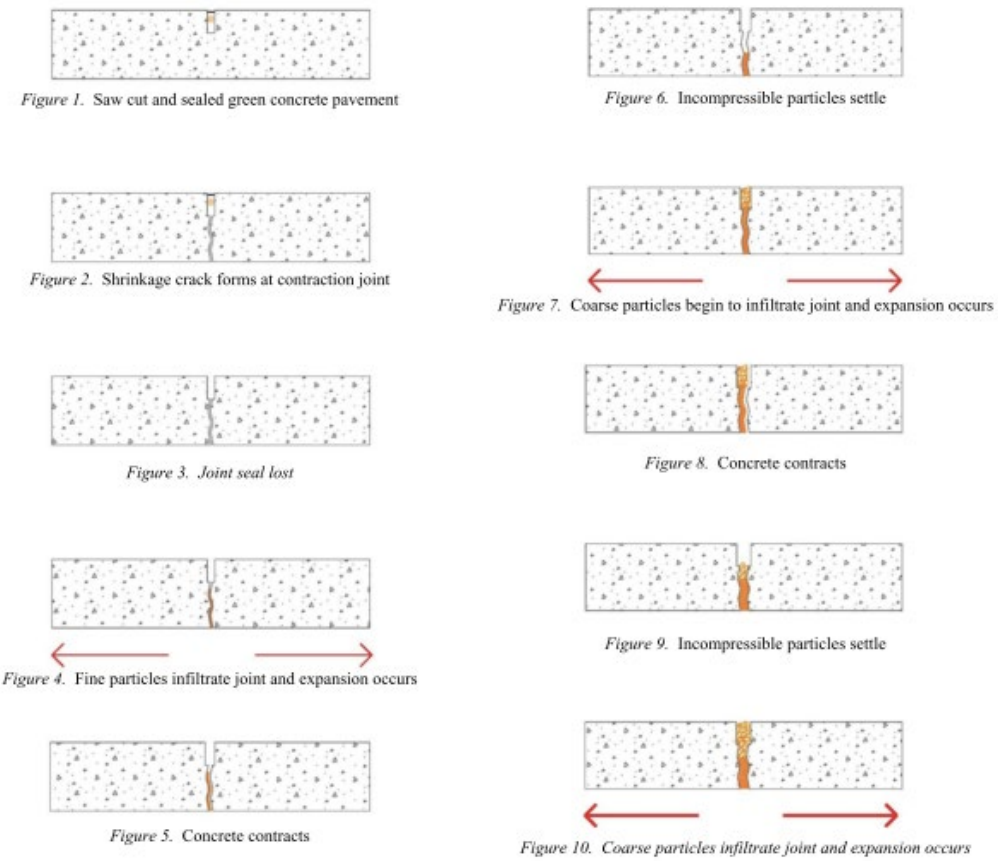

Figure 2.3 Cycles of pavement growth (Rogers and Schiefer, 2012)

2.8.3 Lateral Torsional Buckling Risk for Steel Girders

In bridges constructed without deck joints originally or retrofitted such that deck joints are eliminated, a potential lateral-torsional buckling risk occurs in composite steel girder systems. Positive moment regions of the bridge (near mid-span) exhibit compressive stresses on top of the superstructure cross-section. Since most steel girder systems are composite with a concrete deck, the neutral axis of the cross-section is raised, and the majority of the compressive stresses are carried in the concrete deck in the positive moment regions of the bridge. The compression that occurs in the top flange is relatively small, and the flange is held in place by a composite concrete deck. However, in the negative moment regions of the bridge, which are commonly where a deck joint is eliminated and the bridge can be made continuous, the new cross-section under negative moment will exhibit compressive stresses on the bottom flange of steel girders not supported or carried by a composite concrete deck (Vasseghi, 2013). These high compressive stresses in the bottom of the section below the neutral axis and the tensile forces experienced above the neutral axis cause a potential for lateral-torsional buckling or kicking-out-of-plane. Analysis of this type of behavior is requisite to making a superstructure continuous and stable.

Compact steel sections are cross-sections not at risk of lateral-torsional buckling. Whether or not standard compact sections, as specified by American Institute of Steel Construction (AISC Code), are clear of this risk in all integral bridges could be verified by numerical modeling or laboratory tests. Sections not classified by the AISC as compact should definitely be analyzed for this behavior before a retrofit or new construction of an integral steel bridge is completed. The stresses occurring in the connections and girder system are a function of what kind of connection and girders are in place. Therefore, an analysis of buckling behavior for current and possible retrofit connections and girder systems would be a helpful step

in quelling the potential for lateral-torsional buckling. Lateral bracing in the form of stiffeners or torsional bracing in the form of diaphragms or cross frames can be implemented near the part of the girder in compression to prevent lateral torsional buckling (Vasseghi, 2013; Segui, 2012).

2.8.4 Temperature Gradient

Another significant factor to consider when eliminating deck joints is uneven temperature in the transverse and vertical direction across a bridge and girder cross-section. During times of the day in which the ambient air temperature is changing, the entire bridge is also changing in temperature through radiation, convection, and conduction. This could cause deck cracking, which has been observed in Colorado bridges as a result of continuity. Undoubtedly, the mix designs and placement are other contributors to deck cracking. Radiation is the energy emitted by the sun in the form of electromagnetic waves through the medium of the atmosphere. Usually, only the deck receives direct solar radiation, while the girder system does not. Convection is the mode of heat transfer between the bridge's solid surface and the adjacent air in motion (e.g., wind) and involves the combined effects of fluid motion and conduction. The outer girders and deck may experience the effects of convection to a greater extent than the interior girders. Conduction is the transfer of energy of more energetic particles in one solid to less energetic particles in another solid through direct contact (Cengel, 2012). The constant and inconsistent temperature changes across the cross-section manifest themselves in uneven expansion or, if restrained, uneven thermal stresses in the bridge structure.

In 2008, Li et al. completed a study on the thermal loading and expansion joint movement of Confederation Bridge, an existing, long-span concrete girder bridge. Though not a steel bridge, the methodology to analyze and monitor a concrete bridge would be similar for a steel bridge. Temperature differentials in the vertical and transverse direction in the girder cross-section were examined with three years of data gathered from thermocouples installed on the bridge. The rate of temperature change and temperature gradient was discovered to develop in different rates and patterns in the transverse direction, rather than in the vertical directions (Li et al., 2008). It was also found that shallow sections did not need to consider temperature variation in the transverse direction (the direction perpendicular to traffic flow). Though this seems like a promising way to simplify a design method, what constitutes a shallow section was not explicitly stated by the authors. Rather, the shallowest section of the bridge, a concrete box girder with a height of 177 in. (4.5 m), was the shallowest section considered and it did not appear to have significant temperature variation in the transverse direction (Li et al., 2008). A boundary between shallow sections and deep sections is never explained, but a qualitative conclusion that shallow sections have negligible temperature variation in the transverse directions helps further understanding about thermal effects in a cross-section. However, a quantitative definition of shallow in relation to other parameters would be more useful to a practitioner designing an integral bridge.

Another notable study was performed by French et al. in 2013 to assess the thermal gradient effects in the Interstate 35 St. Anthony Falls Bridge in Minneapolis, MN. This post-tensioned concrete box girder bridge was monitored over three years. Finite element modeling in ABAQUS was developed and gradients from two code provisions were considered. Vertical thermal gradients from AASHTO LRFD Bridge Design Specifications developed by Imbsen et al. (1985) and the New Zealand Bridge design code developed by Priestley (1978) were considered. A fifth-order design thermal gradient, as specified by the New Zealand Bridge Design Code, was determined to be the most appropriate for this bridge with the top surface temperature matching the temperature assigned in the AASHTO provisions for Minneapolis (French et al., 2013). Additionally, the global structural demand modeled with the AASHTO provisions of vertical thermal gradient were found to be much lower than the measured stresses (French et al., 2013). This study further encourages the examination of the vertical gradient developed by Imbsen et al. (1985) in AASHTO for other bridge girder types and in other geographical locations.

Further studies performed by Chen (2008) were conducted to analyze temperature differentials and the corresponding thermal stresses in steel bridges in Texas. This study is particularly relevant because the bulk of research involving elimination of deck joints and thermal gradients has been conducted on concrete girder bridges. Analysis in this study involved finite element models verified by field monitoring and experimental testing performed in the Ferguson Structural Engineering Laboratory in Austin, Texas. The dissertation addresses the robustness of thermal stresses that occur in bridges accounted for in the current AASHTO Bridge Design Specifications. Also, stresses that are not currently accounted for in the AASHTO Bridge Design Specifications are examined (Chen, 2008). According the temperature contour map provided by AASHTO, the temperatures range is cooler in Colorado than in Texas. The maximum expected temperature for Colorado and Texas is 100°F - 110°F and 105°F - 115°F, respectively. The minimum expected temperature in Colorado and Texas is approximately minus 30°F - 0°F and 10°F - 40°F, respectively (AASHTO, 2012, Figure 3.12.2.2-1 and Figure 3.12.2.2-2). The range of expected temperatures for Colorado is larger than in Texas; therefore, the stresses found in steel bridges in Texas may actually be less than what a similar steel bridge in Colorado would experience.

Although current AASHTO provisions only require consideration of the total longitudinal thermal movement based on the average bridge temperature, stresses due to temperature differentials in the cross-section were shown to commonly be above +/- 5 ksi (34.5 MPa) in steel box girder bridges in Texas. Though different girder widths, depth, and bridge location would change the value of these stresses, it is clear that the significance of these stresses is worth analyzing in Colorado's steel bridges if an order of magnitude of 5 ksi (34.5 MPa) is reached on a regular basis in Texas steel bridges.

The heating and cooling of steel girder systems with composite bridge decks was analyzed in Chen's research. Due to the differences in thermal expansion coefficient and different exposure to radiation, convection, and conduction, the heating and cooling of a composite girder cross-section is non-uniform, as shown in Figures 2.4 and 2.5. If these two components of the superstructure, the deck and the girder, are restrained in the same place, thermal stresses will develop due to the uneven heating or cooling of the structure. Accounting for these additional stresses through increases in material strength, flexible piles, hinged abutments, and/or bearings could help alleviate stresses in this local behavior.

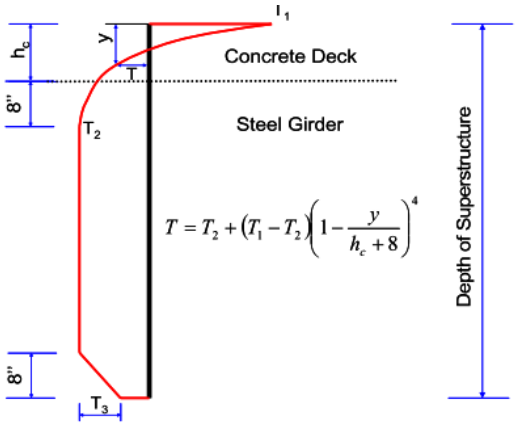

Figure 2.4 Vertical temperature distributions of heating of steel composite girders (Chen, 2008)

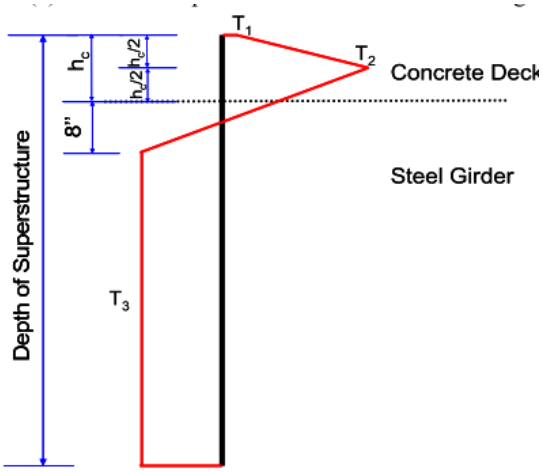

Figure 2.5 Vertical temperature distributions of cooling of steel composite girders (Chen, 2008)

Regarding integral bridges, material strength must be increased, or movement must be allowed to accommodate these uneven movements to occur. Non-integral bridges with expansion joints can expand or contract at slightly different rates without inducing stresses because of the gap that is present. For example, if the concrete deck heats and expands sooner than the steel girder below it due to solar radiation on the deck, the gap in the expansion joint would close more near its top and less near its bottom. However, this uneven expansion joint opening would induce no stresses. For integral bridges, on the other hand, any uneven thermal expansion or contraction would induce a stress in the element because it is not allowed to move independently from the adjacent span at the vertical supports. Movements would need to be absorbed through pier deflection, foundation deflection, strength of material, bearing movements, girder deformation, or a combination of all these (Chen, 2008). It should be noted that for both integral and non-integral bridges, stresses at the interface of the steel girders and concrete deck would be expected due to the uneven heating shown in Figure 2.4 and 2-5. The magnitude of these stresses is relatively unexamined, but it is worth analyzing for design of shear studs and connections between the deck and the girder system.

Effort also was made in this study to identify the conditions with the greatest thermal effects. It was found that bridges with north-south orientation, shorter lengths of the concrete deck overhang, deeper steel girder webs, thinner concrete decks, and wider girder spacing resulted in the most extreme cases of thermal stresses (Chen, 2008). Though this is a qualitative result, it may be beneficial to know these most extreme conditions to strategize a way to reduce thermal effects in the design of a new bridge.

2.8.5 Temperature Data

Lastly, a statistical analysis was performed to compare the temperature data found with the expected values provided in the AASHTO Bridge Design Specifications. The temperatures provided in AASHTO are meant to show the minimum and maximum temperatures expected in a region with a 100-year return period. This study found that, for the Houston area, the AASHTO code provided a lower bound temperature with a return period of only 16 years. The authors recommended that the expected minimum temperatures be adjusted to a true 100-year return period (Chen, 2008). This discrepancy in temperature data is concerning for the bridge designs in Colorado as well. Statistical analysis for minimum and maximum bridge temperatures in Colorado may help designers construct bridges in a more accurate temperature range than provided in the current AASHTO provisions or help AASHTO modify their provisions.

2.8.6 Influence of Temperature Compared with Other Variables

Another case study performed on the Tamar Bridge, a 335-m span suspension bridge in Plymouth, United Kingdom, intended to examine the effects of environmental loading on the bridge from temperature, wind, and traffic. Out of levelness, tension response in cables, bridge temperature, and wind loading were all monitored during the study. It was determined that out of levelness, tension response of cables, and stresses across the girder system were most driven by the effects of temperature (Koo et al., 2013). Wind and traffic loading were found to have an insignificant effect in comparison. It was also found in this study, like in others, that the temperature of the bridge deck is routinely warmer than the supporting superstructure below (Koo et al., 2013), which reaffirms that shear stresses will exist at the connections between the two elements if rigidly connected. Overall, this study showed that the effects of temperature differentials in the cross section are significant in local behavior, such as stresses, out of levelness, and deformation.

2.9 LCCA Process

LCCA involves determining all costs associated with a piece of infrastructure over its design life. These costs range from design and construction to maintenance and user costs to environmental and vulnerability costs (Frangopol and Liu, 2007; Marques Lima and de Brito, 2010; Hawk, 2003; Safi et al., 2015; Kim et al., 2010; Hatami and Morcous, 2014; Reigle and Zaniewski, 2002). Once all costs have been identified, they are referenced to a point in time and the total is calculated. This total cost for an infrastructure's entire life span is the LCC, which can then be compared with the life-cycle cost of other designs for the same piece of infrastructure. LCCA becomes an effective way to compare designs and support the choice of a particular design as the most economically effective choice overall, even if its initial cost is high (Hatami and Morcous, 2014). This can be particularly helpful when talking to the public or working in public design and construction (Al-Wazeer et al., 2005).

Like any analysis process, LCCA is based on a couple of assumptions. Performing an LCCA assumes there are multiple designs for the same desired piece of infrastructure, whether bridge, building, or roadway, and that each of these designs can meet the needs and required performance capabilities. Additionally, it is assumed that each of these designs has varying initial, operating, and maintenance costs and can have varying lengths of life span (University, 2005). Therefore, these assumptions must be true and taken into consideration when performing an LCCA. If the case of several designs having different life spans is the case, they must be manipulated to have a common life cycle to compare them using an LCCA. For example, if design A has a life span of 25 years and design B has a life span of 50 years, then an analysis could assume that at the end of design A's life span, a second design A is built to have a life span of 50 years total. Then the combined consecutive construction of two design A's can be compared with design B using LCCA.

The LCCA process is laid out in Figure 2.6. Furthermore, designs with only one major component difference can be compared and the most cost-effective design type chosen using LCCA. This creates a simpler analysis where only a few variables are different between the two designs. Kang et al. (2007) utilize this approach by analyzing two designs for the same bridge, where the two designs use different superstructure components, e.g., using prestressed concrete beams versus prestressed box girders (Kang et al., 2007). For their LCCA, instead of analyzing the costs associated with every component of the bridge, they focus on only those associated with the superstructure, leading to a slightly simplified analysis.

However, LCCA is not limited to newly designed infrastructure. This analysis approach can also be utilized when looking at deteriorating infrastructure in need of maintenance, repair, and/or replacement. When looking at existing infrastructure, costs of maintenance, repair, and replacement (MR&R), along with costs to users due to inconveniences, are included in the life-cycle cost. These life-cycle costs can be

compared for different methods of MRR to determine the most economical long-term solution. After all, "one of the main aspects to be considered in LCCA of infrastructure is the anticipated maintenance and/or rehabilitation to be performed throughout the structure's life span" (Osman, 2005).

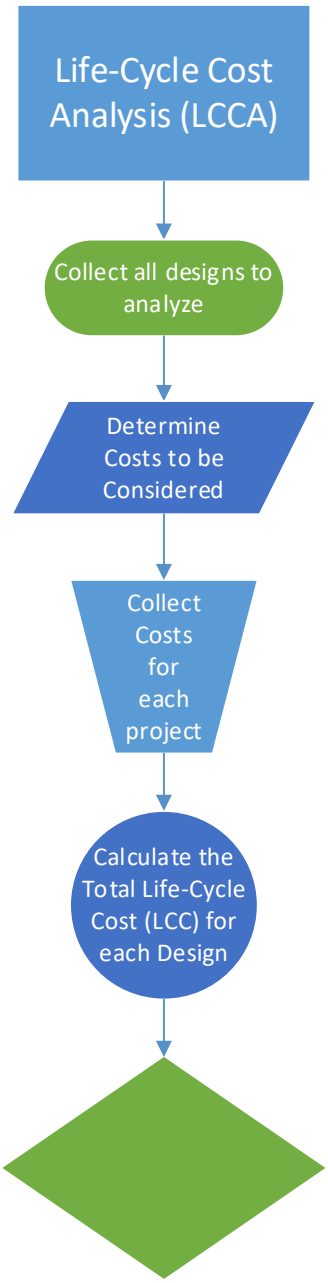

Figure 2.6 Life-cycle cost analysis process flow chart

Furthermore, there is more extensive application of LCCA to existing structures and relatively little application to new structures (Safi et al., 2015). This is despite the fact that LCCA applied to any structure will produce long-term savings, and if applied to a new structure it will produce the maximum savings because they were applied over the entire length of the structure's lifetime (Agency and Severn, 2000). However, an existing structure can also benefit from LCCA due to the structural system being composed of many smaller parts, and each of these has a different and likely shorter life span than the

overall system. Furthermore, these components are not usually easy or simple to replace; therefore, the costs associated with that replacement or repair can be critical (Riedel et al., 1998). This is not to say that designing a structure with these costs in mind at the beginning with an LCCA is not better in the long run, because it is; however, using LCCA in the continued maintenance is also beneficial.

There are several aspects that hinder the application of LCCA to new structures. One proposed by Safi et. al. that could be hindering the application of LCCA to new bridges in particular is the assumption that bridge management systems (BMSs) are completely separate from LCCA, when in reality much of the data used in BMSs could help determine an accurate LCCA (Safi et al., 2015). Another problem could simply be an incomplete understanding of LCCA benefits among implementers (Goh and Yang, 2014). Additionally, LCCA requires foresight, the funds to support a slightly more expensive design with long-term savings in mind, and time to perform the analysis. These deterrents are slowly becoming overwhelmed by the benefits of LCCA as they become better known and supported by federal agencies.

As the benefits of using LCCA in infrastructure analysis become common knowledge, it is suspected that more and more states will implement it as a regular practice. Utilizing LCCA can enable government and state agencies to make the most economical design and repair decisions regarding public infrastructure over the infrastructure's entire life span. This can lead to minimized MRR costs, as well as minimize delays and costs to users over the structure's lifetime.

All infrastructure is an investment. Public infrastructure is an investment of public funds; consequently, interest in the best use of funds for infrastructure maintenance is growing. According to Goh and Yang, before 1990 there was very little attention given to LCCA; however, in 1990, the Federal Highway Administration began to encourage its use in projects and later made it mandatory for projects of $25 million or more (Goh and Yang, 2014). Research and application have been increasing in all areas of infrastructure since this mandate. LCCA is becoming an integral part of design and maintenance of infrastructure and therefore should not be taken lightly.

2.10 Components of LCCA

Several components make up the costs analyzed in an LCCA. These components can mean slightly different things for different types of infrastructure, e.g., bridges versus buildings will have slightly different costs associated with them. Common cost components include initial/construction, operation, maintenance, renewal/replacement, cost of capital, and user (Board, 1998).

Figure 2.7 is a flow chart showing the components of each cost, followed by a general description of each main cost component related to LCCAs.

Initial cost is perhaps the simplest component of LCCA cost components. The initial cost is what the project will cost up front. This includes the costs of the design, contract, project management, construction, and the final inspection and certification, if necessary.

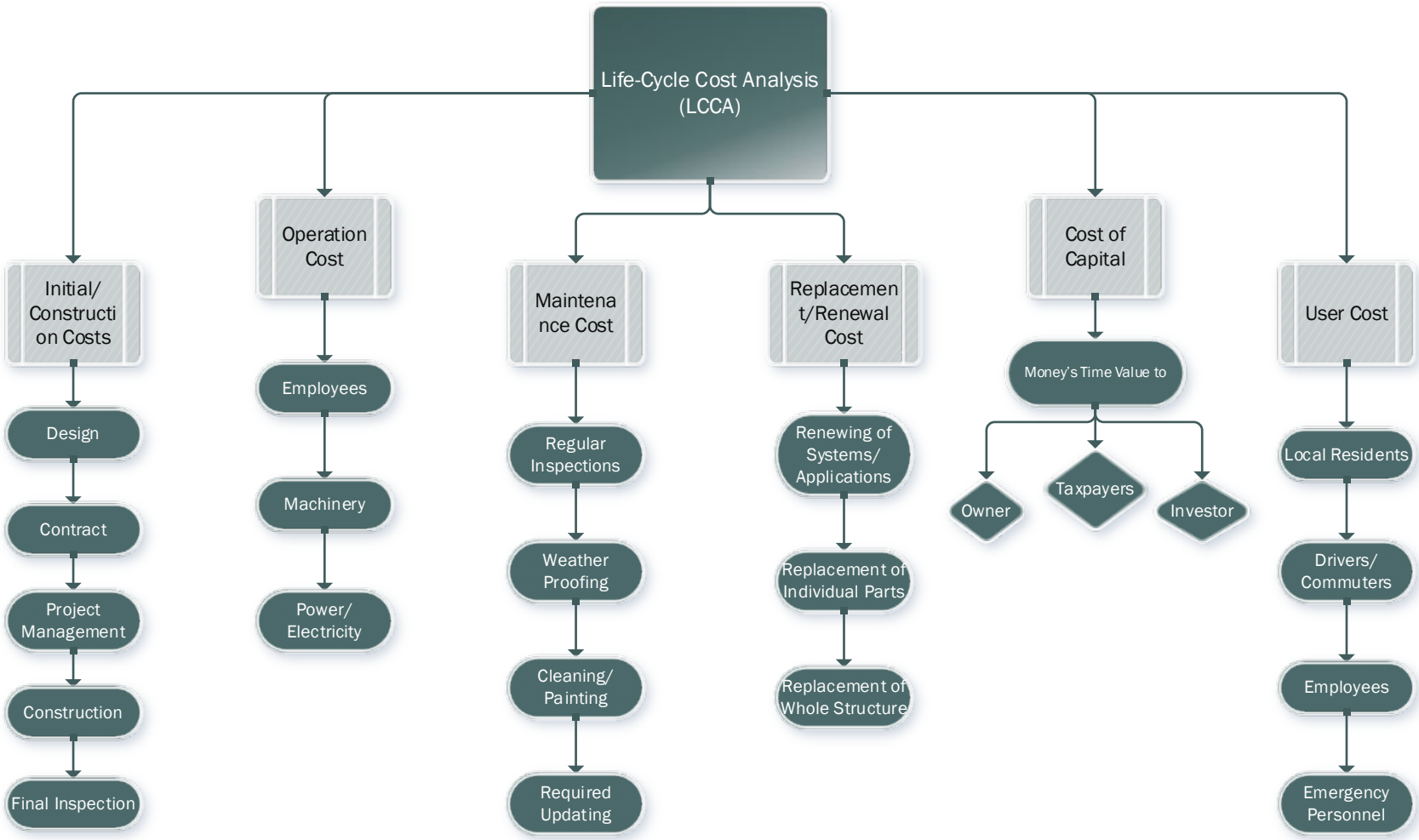

Figure 2.7 Life-cycle cost analysis costs flow chart

Initial cost is what has been traditionally used to choose which design to use for a project, independent of any other costs. The agency would traditionally receive several design bids and choose the lowest bid (Safi et al., 2015). The lowest bid procurement process does not account for any other cost components occurring throughout the structure's life. Instead of choosing the project with the lowest initial bid, the design could be chosen based on lowest LCC bid, which is what is proposed to the European Union Directive by Safi et al. (2015).

Operation cost is the cost needed to operate the infrastructure over its life span. This cost varies greatly depending on the infrastructure being analyzed. Some structures will have little to no operational costs, such as a simple bridge. However, other structures, such as buildings, drawbridges, or toll roads, will have various operation costs associated with employees and machinery. These costs could include employees to run the machinery or toll booths and electricity to power the structure.

Maintenance cost is the cost of maintaining the infrastructure in a safe, usable, and functional condition. Maintenance costs can include regular inspections, weather proofing, cleaning, painting, and any type of required updating. Depending on the structure, these maintenance costs could be as frequent as monthly or as infrequent as every few years. The importance of having funds to perform the maintenance is also going to depend on the structure. For example, the repainting of a steel bridge to prevent corrosion could have more importance than the repainting of a concrete building on schedule, because the steel bridge is typically going to be more immediately susceptible to deterioration than the building.

Renewal/replacement costs depend on the object of analysis, whether the objective is renewal of the structure or replacement of the structure in part or entirety. Renewal costs would be applicable to costs due to the renewal of software or electric systems; whereas, a replacement cost would apply to the replacement of anything connected to that piece of infrastructure or equipment. This could range from the replacement of a single element to the entire structure.

Cost of capital is money's time value to the owner, investor, or, in the case of public works, the taxpayers (Board, 1998). This cost adjusts for the fact that choosing a design using LCCA often means a higher initial cost compared with designs that do not use LCCA and would have higher maintenance and repair costs later. Therefore, the money's time value accounts for using that extra money to have a lower overall cost instead of using it to invest in something else.

User cost includes any costs to users of the infrastructure or system. This can include costs to drivers and passengers due to construction or traffic blocks for repair or replacement ("Life Cycle Cost Optimisation in Highway Concrete Bridges Management," n.d.). Another example of user costs could be due to relocation of employees in the case of a building's repair or maintenance.

2.11 Components and Parameters Related to Bridge Maintenance

Bridge design and MRR have specific costs within each general cost component of LCCA. Figure 2.8 is a flow chart for the LCCA costs specific to bridges. In order to compose a thorough LCCA for a bridge, each component of the LCCA must include all aspects that affect the bridge. In other words, the parameters must be tailored to the infrastructure and its environment, in this case a bridge and the outdoors (Hawk, 2003).

There are also parameters in addition to the cost components that need to be taken into consideration and have a particular application to bridges. These include the service life of the bridge and the analysis period of the LCCA. The service life is the time period over which the components of the bridge and the bridge itself are in serviceable condition based on the industry standard for acceptable condition limits. The service life does not always equal the design life, which might account for repair or replacement of some bridge's substructure parts. However, typical best management practices (BMPs) assume a service life between 70 and 100 years. On the other hand, the analysis period is the time span in which all costs in the LCCA are analyzed and brought to a total present value. This time period can be shorter or equal to the service life of the bridge, depending on the period the buyer wishes to analyze based on what years are of most importance. Typically, the analysis period is made equal to the service life in order to simplify the LCCA process (Hawk, 2003). However, if the analysis period is less than the service life, there is still value due to the remaining serviceable life of the bridge.

Initial and construction costs are some of the simplest components of an LCCA for bridges. Both are constant values, with little uncertainty associated with them because they are one-time costs at the beginning of the bridge's life. The initial cost is composed of the design and contractor costs, while the construction costs are those that cover construction materials, workers, and time, as well as any road closure costs due to the bridge's construction. This last aspect of construction costs affects user costs, as road or lane closures and/or detours will affect drivers in the area.

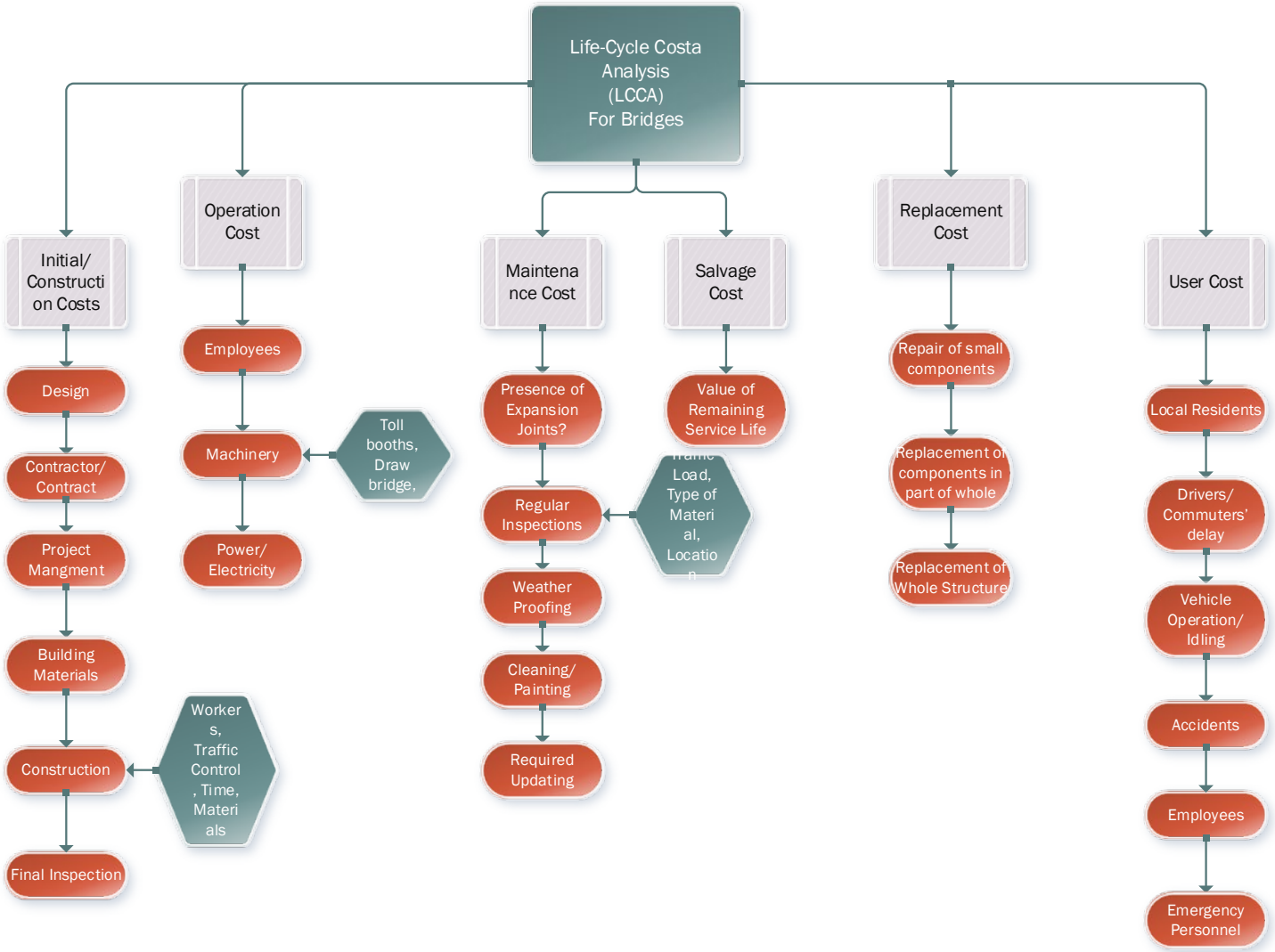

Figure 2.8 Life-cycle cost analysis costs flow chart for bridges

The maintenance costs for bridges depend on several key factors. The planned life span, the bridge structural material (i.e., steel or concrete), the anticipated traffic load, the environment, and whether or not preventative maintenance is included (Reigle and Zaniewski, 2002) all affect maintenance. Additionally, whether or not the bridge contains an expansion joint (and if it does, the type of expansion joint used) can also impact maintenance costs. In fact, when considering the LCCA of a bridge with expansion joints, they "should be considered a critical factor" (Savioz, 2014). Expansion joints are very susceptible to clogging, corrosion, and deterioration due to dynamic load impacts on their various components, which are more delicate when compared with a steel or concrete girder. Consequently, the probability of maintenance needed on the bridge will increase with the presence of an expansion joint. Furthermore, because they are a weaker bridge component that spans the width of the bridge, they can have significant impacts on other costs, such as user and replacement costs.

Repair and/or replacement costs for bridges are composed of the cost of repairing and/or replacing each component of the bridge with respect to that component's life span in comparison with the overall bridge's desired life span.

User costs for a bridge are composed of costs to the drivers and residents affected by the closing or limiting of traffic on the bridge due to maintenance, repair, or replacement. They are in some ways the most complex costs in an LCCA because they involve the public, which increases variability. These costs are due to delays experience by drivers, costs of vehicles idling in traffic, and accident rate increases related to road work (Kim et al., 2010; Reigle and Zaniewski, 2002). As such, they should be minimized by reducing the disruption caused by the repair or maintenance (Agency and Severn, 2000). This could be done by limiting the closure to one lane at a time and performing maintenance, repair, or replacement in stages/portions. These aspects can be categorized as three individual costs, the sum of which equals the user costs included in an LCCA. Kim et al. (2010) define these costs and formulate the following equations to use in an LCCA. The driver delay cost, vehicle operating costs, and accident costs are defined in equation form below, and all variables are listed in Table (Kim et al., 2010).

$$\text{Driver Delay Cost} = \left(\frac{L}{S_a} - \frac{L}{S_n}\right) \times ADT \times N \times w \quad \text{(Eq. 2.1)}$$

$$\text{Vehicle Operating Cost} = \left(\frac{L}{S_a} - \frac{L}{S_n}\right) \times ADT \times N \times r \quad \text{(Eq.2.2)}$$

$$\text{Accident Cost} = L \times ADT \times N \times (A_a \times A_n) \times c_a \quad \text{(Eq.2.3)}$$

Table 2.1 Parameters assumed for user cost computation (Kim et al., 2010)

Parameters	Symbols
Length of Affected Roadway (km)	L
Average Daily Traffic (ADT)	ADT
Normal Driving Speed (kmph)	S_n
Roadwork Driving Speed (kmph)	S_a
Normal Accident Rate (per million vehicles)	A_n
Roadwork Accident Rate (per million vehicles)	A_a
Hourly Driver Cost (US$)	w
Hourly Vehicle Operating Cost (US$)	r
Cost per Accident (US$)	c_a
Required Days for Repair	N_{repair}
Required Days for Replacement	$N_{replace}$

Each of the parameters in Table are used in the three user cost equations (Eq.2.1), (Eq. 2.2), and (Eq. 2.3). Furthermore, each is specific to that bridge. Therefore, the parameters in Table 2.1 are an example of parameters that might be used for an LCCA, and would need to be adjusted for a different specific bridge based on its location, current rates, expected traffic, dimensions, and any other available information.

2.12 Maintenance of Bridges with Expansion Joints

The MR&R procedures and the costs associated with them for bridges are critical to a bridge's LCCA. The MR&R are a substantial portion of the total LCC for a given bridge (Mao and Huang, 2015). They can be divided up as MR&R costs for each component of the bridge, such as the beams, columns, deck, and expansion joints (Kang et al., 2007). In fact, in 2002, a study showed that 20% to 50% of total infrastructure costs were due to MR&R in various countries (Mao and Huang, 2015). Therefore, the cost of MR&R is directly related and important to the overall LCCA. The many factors that influence MR&R costs for bridges are summarized in Figure 2.9. Traditionally, LCCA in general and MR&R costs specifically have been analyzed using statistical models and analyses, such as simple regression and overall trends, to calculate costs based on collected data (Mao and Huang, 2015). Furthermore, many traditional LCCA methods also neglect user costs and preventative maintenance benefits and costs due to a lack of data or the complexity of the calculations, which can affect all costs, including MR&R (Reigle and Zaniewski, 2002).

Most LCCA models do not give a specific approach for the maintenance costs, which can make it hard to determine that cost (Mao and Huang, 2015; Hawk, 2003). A more accurate and specific method would be to include probabilistic approaches, because "estimation depends on predicting how bridges deteriorate over time and what subsequent actions are taken" (Mao and Huang, 2015). These costs should then be based on those predictions. Mao and Huang (2015) conducted a study to estimate the MR&R costs of a bridge using a Monte Carlo simulation, applying probability distributions. They chose an expansion joint as their example bridge component; nonetheless, the analysis could be applied to any bridge component, thus the sum of all MR&R costs for each component would equal the total MR&R costs for the bridge.

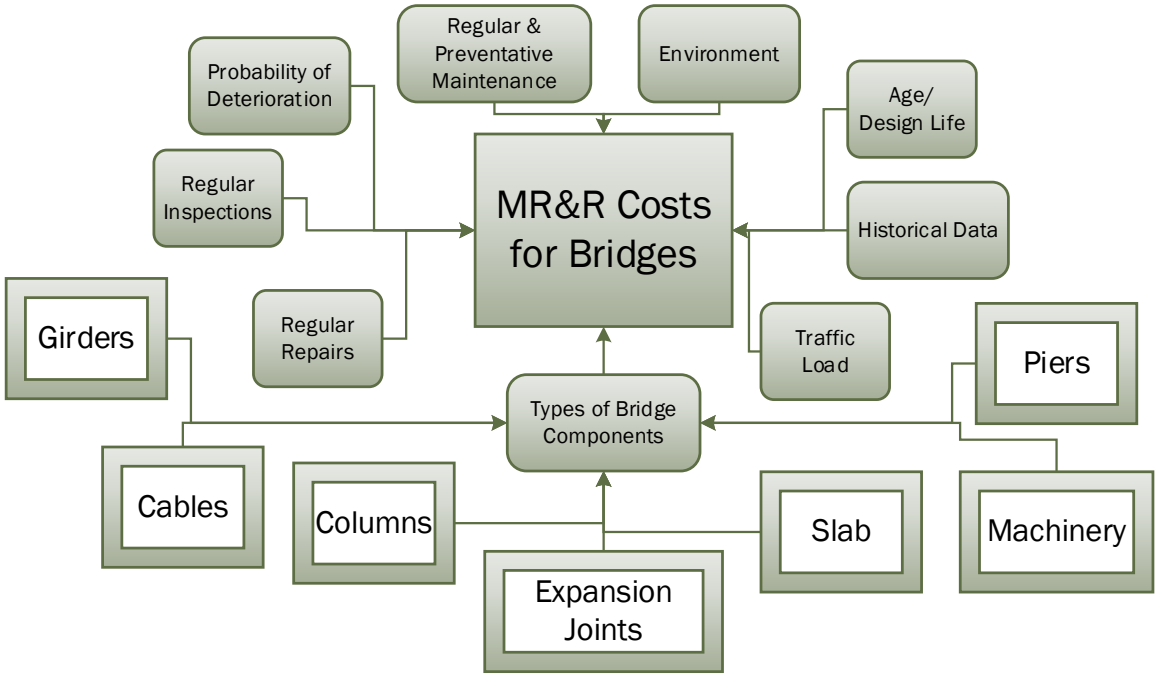

Figure 2.9 Factors affecting MR&R costs for bridges

However, using just a stochastic model utilizing probability of deterioration or defect and the probability that further deterioration will develop has limitations, too. For example, using a strict Markovian probability model might not account for unique factors affecting the current state of the bridge. The probability of transition from one form of deterioration to another requires sufficient observed data related to the specific bridge, which may not be available, especially for newer bridges (Mao and Huang, 2015). Furthermore, Huang and Mao argue that the future condition of the bridge is affected by its history, while Markov processes are, in part, defined by the fact that future conditions only depend on the current condition. While probability should be a key part of predicting defects and deterioration and thus MR&R costs, it should not be the sole source of that information. Other current and historical observations and the overarching deterioration processes should be used to enhance that prediction.

Typically, bridges are inspected visually for signs of deterioration and/or defects. While visual inspection can be subjective depending on the inspector, bridge, and governing guidelines or procedures, it still provides data for each aspect of a bridge. Furthermore, because bridges have been regularly visually inspected for the past 40 years in the United States, and for many years in other countries as well, there is a wealth of data and knowledge that, if made available, could be used as a basis for a deterioration model prediction and the evaluation of MR&R costs (Mao and Huang, 2015). These observations and archived data could be used to complement a probability matrix in order to predict the future MR&R needs for a bridge.

Furthermore, expansion joints are common in various forms in most bridges and are therefore a key, and at times critical, component for maintenance of a bridge, as well as a main component affecting costs in an LCCA. While most manufacturers will tout their expansion joints as having long service lives free of maintenance, this is seldom true in the field. In fact, the joints are commonly the first bridge components to need maintenance or repair (Lima and de Brito, 2010). This is because they experience millions of impact loads from vehicle wheels throughout their lifetime. These repeated impact loads can result in failure due to fatigue cracking (Savioz, 2014). Their deterioration can also be increased if water and/or debris are able to creep into the joint. Therefore, choosing the best type of expansion joint for the bridge and environment is critical to minimizing maintenance and replacement costs.

While joints are not an expensive part of the initial cost of a bridge, usually only about 1% of the total construction cost (Lima and de Brito, 2010), as discussed above, they can have a disproportionate effect on the maintenance/replacement costs over the life span of the bridge. A study in Portugal showed that over "the previous 3 years, more than 20% of the bridge conservation costs were related [to] the repair and replacement of expansion joints" (Lima and de Brito, 2010). However, some of the other cost parameters are indirect costs associated with expansion joints, such as costs to users due to limited or detoured traffic when conducting maintenance or repair.

As it relates to joint maintenance and repairs of defects, to minimize the damage and thus the cost, a preventative approach should be taken toward bridges and expansion joints rather than a corrective approach. A corrective approach only addresses the problem when it becomes so bad it threatens serviceability, whereas a preventative approach addresses the problem when it first begins to develop in order ensure it does not grow worse.

The first step in a preventative approach to maintenance and repair costs is choosing the right expansion joint type. The Colorado Department of Transportation (CDOT) typically uses a strip seal expansion joint, otherwise known as an elastomeric seal expansion joint. This type of joint uses an elastomeric "v-shaped" neoprene gland strip inserted into two parallel steel rails to seal the joint (CDOT, 2015). Figure 2.10 is a drawing of a strip seal, per CDOT standards. There is another variation on the strip seal, called a "hump seal," which adds a second layer of neoprene that humps up as the joint closes and stretches out as the joint opens. This humping up when the joint seals can serve to push out any debris or dirt that might have fallen into the joint (Savioz, 2014). The hump seal provides self-cleaning, which potentially can slightly decrease the frequency of maintenance inspections needed for the joint.

Another way to implement a preventative approach is by locating any defects in the expansion joint early in its development and fixing or correcting the issue to prevent degradation that might have otherwise been introduced by the defect (Lima and de Brito, 2010). What might start out as a small insignificant deterioration or defect could become a much larger problem if it is left to be subject to continued loading and environmental effects. This would exacerbate what started out as a small problem, cheap and simple to fix, turning it into a costlier operation that might also require a more extensive road closure, thus affecting user costs.

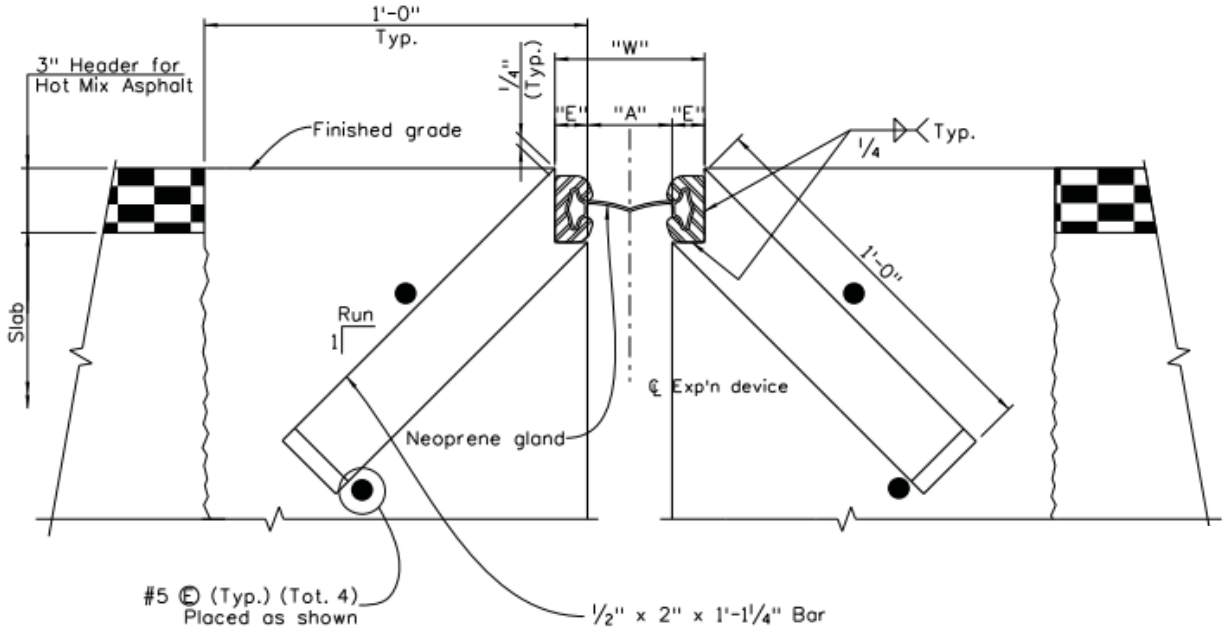

Figure 2.10 Section through strip seal bridge expansion device (CDOT, 2015)

Regular bridge inspections for maintenance are part of the maintenance costs in a bridge's LCCA. While joint inspections are included in regular bridge inspections, it is possible they need to be more frequent than the regular bridge inspection. This could be because the degradation rate of a joint is higher. A joint's degradation rate is affected by the type of joint, the volume of traffic experienced by the joint, and the environment in which the joint is located. Lima and de Brito (2010) categorize 12 different types of expansion joints from least amount of movement allowed to most, "open joints" to "preformed compression seal joints" to "multiple seal in metal runner joints." These types of joints are shown in Figure 2.11. Type 6 in Figure 2.11 is the elastomeric flexible strips, the same as the CDOT strip seal.

Each type of joint is susceptible to different types of degradation and defects and thus would affect the degradation rate. Additionally, each joint type would have different initial, maintenance, and repair costs (Kang et al., 2007). Similarly, depending on the bridge type and location, it will experience different traffic volumes, and a bridge with higher traffic volume will experience a higher rate of degradation (Lima and de Brito, 2010). Finally, the environment will affect the degradation rate, as a dry land-bound environment will cause less degradation than a wet coastal environment. Due to these many factors, Lima and de Brito (2010) recommend that the period between joint inspections should never exceed 15 months for a bridge with a high traffic volume.

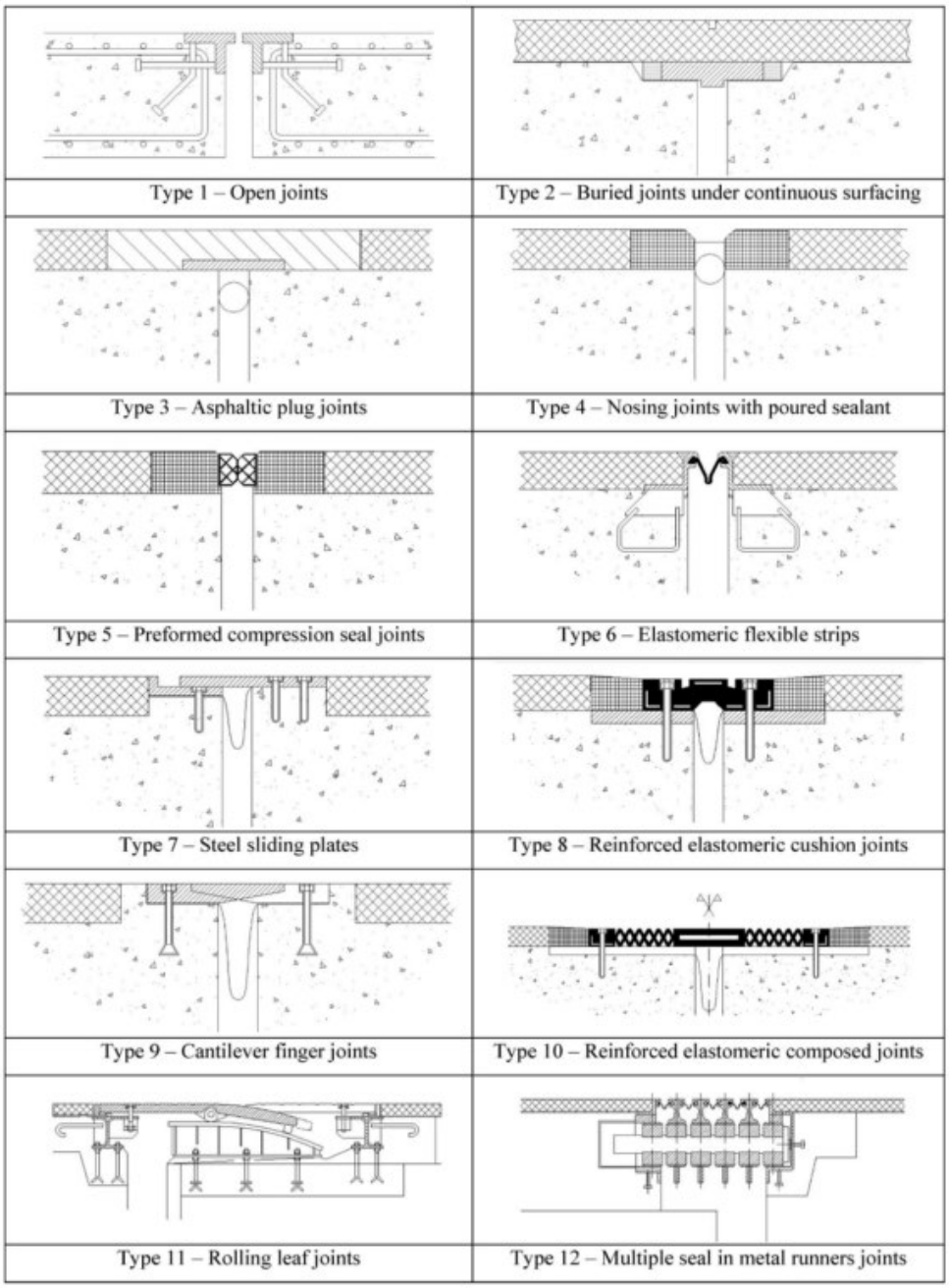

Figure 2.11 Types of Joints (Lima and de Brito, 2010)

Additionally, it should be noted that once one defect or type of degradation is detected, matrices can be used to determine the probability of other defects occurring due to association with the first defect (Lima and de Brito, 2010). This is additional support for approaching bridge maintenance with a preventative approach. These defects can be due to a variety of causes, as listed in detail by Marques Lima and De Brito; in general, however, they can be due to design errors, manufacturing defects, installation errors, a lack of maintenance, a sudden increase in traffic or use, a change in environmental factors, or sudden impact loads.

Lima and de Brito (2010) propose a rating system for defects in expansion joints. This system determines the rating in terms of the defect's severity and thus how detrimental it is to the service of the bridge. The rating system uses Equation (2.4).

$$P_i = 0.2I_{ext}\,(6I_tI_{loc}C_{vt} + 5I_c) + 2I_pC_{ep} \quad \text{(Eq. 2.4)}$$

Where P_i is the rating of the defect i. Each I is an index for defect extent, service life penalty, traffic penalty, defect location, structure potential penalty, and population penalty respectively, varying from 0 up to 5 depending on the index and based on increasing severity. The C's are coefficients for traffic volume and surrounding population, respectively. The numbers correspond to percent weights for the system such that if every index and coefficient where to be at critical the total rating would be 100. However, in reality, the highest rating would be 94, which concerns collapse or missing joints. Anything higher than 50 is considered very urgent and action should be taken immediately (Lima and de Brito, 2010). Similarly, if a joint is in perfect condition the rating should be equal to zero.

The total degradation of a joint can be classified as D_x, which is the sum of defect ratings, P_i, of all defects in the joint. See Equation (2.5).

$$D_x = \sum_{i=1}^{n} P_i \quad \text{(Eq. 2.5)}$$

This equation (0.5) would enable the comparison of multiple expansion joints in the bridge, therefore the most serious one could be repaired first.

Furthermore, when the expansion joint fails, comes to the end of its design life, or requires excessive and expensive maintenance and repair costs, the joint should be replaced (Savioz, 2014). This is a simple LCCA with fewer costs included; in it, the cost of continued maintenance is compared with the cost of replacement, and when the latter becomes the smaller number then replacement should occur.

The goal throughout all MR&R is to maximize the service life of the expansion joint while minimizing the cost. This fits directly into the objective of LCCA for bridges. Expansion joints are a significant part of bridge design. By increasing their life cycle while minimizing maintenance cost, the overall LCC can be decreased.

2.13 Current LCCA Models for Bridges

Over the last few decades, several LCCA models for bridges have been developed and redeveloped. Currently, there are three main types of LCCA models, deterministic, rational, and probabilistic, as seen in Figure 2.12. Each type has advantages and disadvantages depending on whether the bridge is new or old, and depending on the available practitioner experience in this area or access to archived observed deterioration data. Furthermore, each general model type has overlapping ideas and assumptions, as well as numerous variations developed by various researchers.

The simplest type of LCCA model is a deterministic model. Where each contributing cost constraint is identified, a corresponding cost value is found or estimated for each and the total is summed. The final LCC is a discrete deterministic result. This method produces an "acceptable range" but not a detailed or reliability based LCC (Basim and Estekanchi, 2015). This model type does not account for uncertainties, variations, or costs due to unexpected events affecting the bridge (Reigle and Zaniewski, 2002). The neglect of uncertainties in the deterministic LCCA approach can cause the results' validity to be questioned, because uncertainty is a part of any future value or cost. The cost components for costs over the life span of the bridge or structure might be the estimated median cost due to each component (Basim and Estekanchi, 2015), but an average does not account for probability due to different environments or events. The maintenance cost per year is often a rough estimate using a specified percentage of the construction cost if there are no historical data to use. Although if historical data are available, that value is preferred. Some costs that are hard to estimate or predict without data and probability are neglected, and these might include some or all costs associated with users (Kang et al., 2007).

Rational models for LCCA are a combination of deterministic and risk analysis. They primarily take a deterministic approach, but base the cost values on recorded data of similar bridges. These costs are based on the frequency of a certain cost affecting bridges in situations similar to the one being analyzed. Marques Lima and de Brito use a rational model for their LCCA, which is described for expansion joints above in section 2.4. Their model is primarily only for MR&R costs; however, the rational model could be expanded for whole bridge analysis. In general, their model uses a combination of matrices and tables that contain the various bridge or joint components, their respective rating, and maintenance cost (Lima and de Brito, 2010).

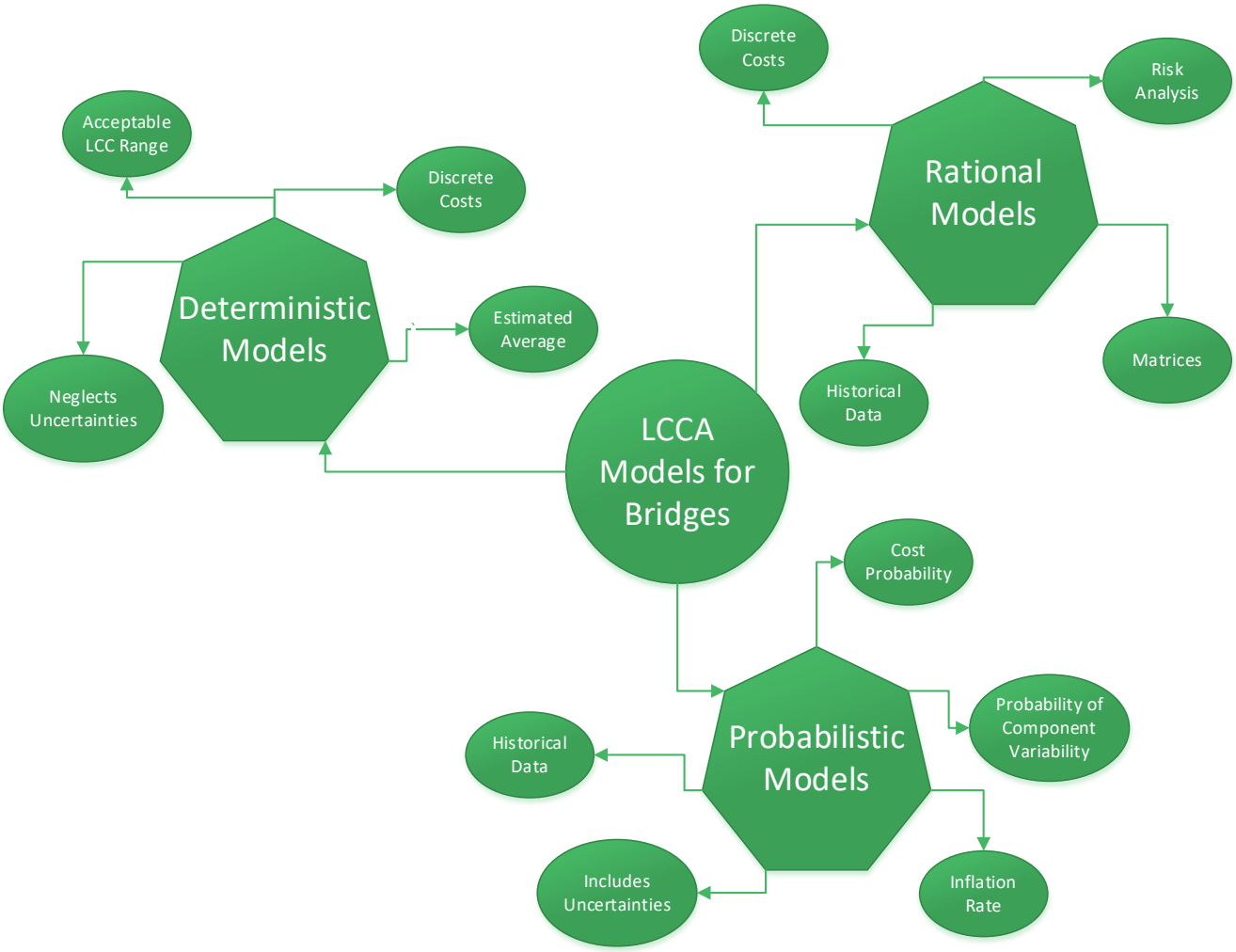

Figure 2.12 Life-cycle cost analysis models for bridges

Probabilistic LCCA models are based on the probability of each cost occurring, a risk analysis to determine the probabilistic risk associated with each cost, and the inflation rate over the life span of the bridge. This approach finds the variability associated with each cost component. If information and data are available, perhaps from the state highway associate or the local DOT, then it can be analyzed to estimate the probabilities associated with each parameter. The risk of each cost could then be modeled mathematically (Agency and Severn, 2000). However, if this type of data are not available or accessible then a qualitative risk assessment could be conducted (Agency and Severn, 2000). By including the uncertainty of the various cost components, the decision maker can take them into account when comparing different scenarios or designs (Reigle and Zaniewski, 2002). For most probabilistic LCCA models, probability distributions are used and all costs are brought back to a present worth value using basic net present worth analysis. Using a present worth analysis accounts for the monetary changes in a life cycle of various components and combining it with uncertainty analysis can provide a precise LCC (Girmscheid, n.d.).

While some probability analyses rely on analysis of bridge inspection data to form probabilities for the cost components, other LCCA models use predictive models (Reigle and Zaniewski, 2002). A probability or risk-based LCCA model creates a more universal model, because costs for each component are going to be similar for different bridges, however, the probability will change based on the environment, location, and conditions. Therefore, if probabilities are developed for the specific situation or design, then the LCCA can be conducted for that bridge.

In order to determine the probabilities for an LCCA, all possible "hazards and accidental load scenarios" must be identified before their probability can be found (Agency and Severn, 2000). If data are not available for analysis and calculation of probabilities, then a simple risk interaction matrix can be used. An example from Agency & Severn is below in Table 2.2. This matrix can then be used to analyze the hazards and risks associated with a given bridge. Agency & Severn took a 25-year-old existing bridge as an example and analyzed the risks with an interaction matrix, as seen in Table 2.3. However, if a risk interaction matrix were to be used in an LCCA, then the various classifications of severe, high, medium, low, frequent, occasional, remote, and improbable would need to have probabilities associated with their intersections: unacceptable, tolerable with precautions, and acceptable. Furthermore, the mitigation for each hazard would need to be quantified as a cost. These probabilities and costs could then be used in relation to the various hazards to determine the LCC in the LCCA.

Table 2.2 A risk interaction matrix (Agency and Severn, 2000)

Severity Category	Likelihood			
	Frequent	Occasional	Remote	Improbable
Severe	U	U	U	U
High	U	U	U	T
Medium	U	T	T	T
Low	T	T	A	A

A = Acceptable T = Tolerable with precautions U = Unacceptable/undesirable

While Agency & Severn's solution to a lack of reliable data, described above, is workable, it is not as ideal or precise as analyzing real inspection data for probabilities. Osman, in his report on "Risk-Based Life-Cycle Costs," discusses this need for reliable inspection data as one of the disadvantages of probabilistic LCCA. He cites the need for large amounts of reliable cost and performance-related data, simulation capability, and statistical manipulations as a hindrance to probabilistic analysis (Osman, 2005). However, this is a limitation for him because he is focused on private sector design and building.

Federal and state agencies, such as state DOTs, have access to all of their previous bridge inspections and performance data for various types of bridges in different types of locations. Therefore, if an LCCA is being carried out in the public sphere by either the state highway association or local DOTs or another company contracted by one of them, the data should be available for probabilistic analysis.

A newer bridge will have a higher probability of the "do nothing" action (the least severe action) being chosen, because most of its deterioration is minimal and non-serious with respect to the serviceability of the bridge. The converse would be true of an old bridge, which would have a higher percent of severe deterioration, and thus a higher probability of needing repair or replacement. As the bridge ages and begins to exceed 30 years in service, the probability of replacement quickly increases to 100% (Mao and Huang, 2015). Therefore, these probabilities can be used to determine the LCC for MR&R costs for a bridge based on its current age and for the rest of its life cycle.

Table 2.3 Risk interaction matrix for example (Agency and Severn, 2000)

Hazard	Likelihood	Severity	Initial Risk	Mitigation	Residual Risk
Overload	Remote	High	U	Bridge was designed to British Standards, carry out assessment to Eurocodes. From past data and bridge location, review the possibility of abnormal vehicles	T
Disproportionate and progressive collapse	Remote	High	U	Assess the effects of failure of parts, such as bearings or bolts. Confirm that structure has sufficient redundancy and that requirements of Eurocode 1 are met.	T
Vehicle Impact	Occasional	Medium	T	Bridge was designed with standard UK aluminum parapet. Carry out assessment to Eurocodes and using local UK risk assessment methods for parapets.	T
Corrosion	Occasional	Medium	T	Review previous inspections. Carry out further inspections at time intervals specified in local UK requirements. If there is corrosion, determine likely loss of section for use in assessment.	A
Flooding to beam level	Remote	High	U	Bridge originally designed for flood flows. Review historical river flow data. Assess structure for debris loads and water pressures if required.	T
Scouring Foundations	Remote	High	U	Review previous inspections. Carry out further inspections at low flows.	T
Settlement of foundations	Occasional	Severe	U	Bridge originally designed for significant movements from ground settlement from mineral extraction. Review extent of current extraction and future extraction; assess effects on structure (bearings and joints in particular)	T
Seismic Effects	Remote	Medium	T	Bridge not designed for seismic loads, review local UK requirements. Review robustness of structure and beam seating requirements in particular	A
Fire	Remote	Medium	T	Review likelihood of storage of hay or other flammable material under structure	A

A = Acceptable. T = Tolerable with precautions. U = Unacceptable/undesirable

The probability for each component based on deterioration and the age of the bridge can be combined to form the many MR&R costs included in the LCCA (Mao and Huang, 2015). Therefore, for any bridge components, the MR&R costs should be correlated to the age of the bridge, and the fact that their probability will increase as the bridge ages should be taken into consideration in any LCCA. The costs can be brought to a present value that includes this probability with respect to age.

Another one of the current LCCA approaches was developed for the National Corporative Highway Research Program (NCHRP). The bridge life-cycle cost analysis (BLCCA) methodology was described in a 2003 report by Hugh Hawk. When it was written, many states had not yet implemented any form of LCCA. The report was aimed to help more states implement LCCA approaches in their decision processes. While more states today are using LCCA in their decision making, the report still provides an excellent description of a general model for LCCA of bridges. Furthermore, the NCHRP model for BLCCA could provide a

useful starting guide for developing an LCCA model for expansion joints in bridges. NCHRP's BLCCA model is described below.

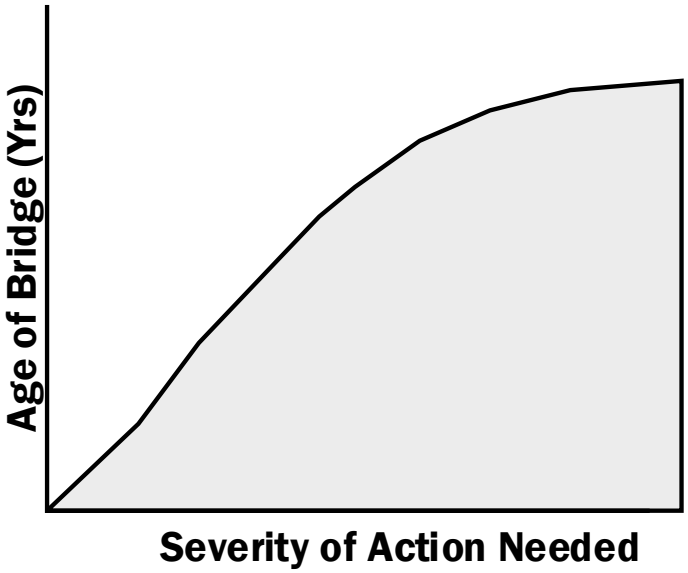

Figure 2.13 MR&R Action Severity vs Bridge Age

First, risks and vulnerabilities must be determined for a bridge location, and each of those risks assigned a cost based on the probability of it occurring and consequent costs caused by the risk. These risks and vulnerabilities could be due to overloads of traffic or equipment on the bridge, seismic events, bridge scour, partial failure, and other factors. (Hawk, 2003). Other costs should be estimated as well. Hawk describes agency costs as those including maintenance, rehabilitation, and replacement. Each agency cost is affected by material type, condition, environment and location, average daily traffic, element types, and frequency of maintenance and inspection, among other fators (Hawk, 2003). User and operation costs are also directly related to agency costs and should be analyzed and determined. User costs were discussed in detail in Section 2.3.

The general form of the BLCCA equation is

$$LCC = DC + CC + MC + RC + UC + SV \quad \text{(Eq. 2.6)}$$

Where:

LCC = life-cycle cost,
DC = design cost
CC = construction cost
MC = maintenance cost
RC = rehabilitation cost
UC = user cost
SV = salvage value

The BLCCA model's costs that occur in the bridge's future are brought to a present worth value using net present value formulas for uniform series, one-time series, gradient series, or combinations depending on the nature of the cost. This would produce the present LCC for each alternative. In the BLCCA model, Hawk describes predicting the distant future as impractical. Instead he proposes that a specific sequence of maintenance and rehabilitation be analyzed for LCC; he then suggests that, for analysis purposes, this sequence continuously repeats itself. Eventually, the bridge is replaced and the whole LCCA is repeated. This perpetuated bridge maintenance and rehabilitation is due to most bridge design life spans being 50 years or more (Hawk, 2003). Furthermore, while using probability and data for determining the components

of the BLCCA equation, it is not appropriate to assume complete accuracy when approaching the end of the life span of the bridge, but by using the most current data available, an acceptable confidence level might be reached.

2.14 Conclusion

LCCA is critical for cost-effective bridge and expansion joint design, with cost components ranging from initial cost to maintenance and replacement costs. While there are so many factors affecting the LCC of a bridge, there are many ways to calculate that cost and perform an LCCA, from a strictly determinate analysis to one based on probabilities. Each model, as discussed above, has advantages and disadvantages. However, by taking the best parts of the various models and building a more comprehensive model for expansion joints based on determinate costs of each component and a probability of that cost being applied over the life span of the bridge, then a realistic LCC might be reached. This approach can be used to form an LCCA equation for expansion joints in bridges; however, it can also be used to form an LCCA equation for replacing expansion joints with a continuous connection. With these two equations, for an expansion joint that has reached the end of its life span and needs to be replaced, the LCCA can be compared for replacing the joint with a second expansion joint or for retrofitting the joint to be continuous. The more economical solution can be chosen based on these LCCs. The equations for each scenario are shown below as Eq. 2.7 and 2.8.

Proposed LCCA model

$$LCC_{EJ} = f\left(C_i + C_c + C_o + C_m P_{m+} C_r P_r + C_{cc} P_{cc} + C_u P_u + SV\right) \quad \text{(Eq. 2.7)}$$

$$LCC_{RC} = f\left(C_i + C_R + C_o + C_m P_{m+} C_r P_r + C_{cc} P_{cc} + C_u P_u + SV\right) \quad \text{(Eq. 2.8)}$$

Where:

LCC_{EJ} = Life Cycle Cost of Expansion Joint

LCC_{RC}= Life Cycle Cost of Retrofitted Continuous replacement of joint

C_i = initial cost, fixed cost

C_c = construction cost, fixed cost

C_R = retrofitting cost for continuous, fixed cost

C_o=cost of operation, fixed cost (only applicable for toll draw bridges)

$C_m P_m$=cost of maintenance (function of temp) = ($C_{mH} P_{mH}$ if Temp > 32 ˚F;
$C_{mC} P_{mC}$ if Temp < or = 32 ˚F)

$C_m P_m$= composed of maintenance costs of each part of the expansion joint

$C_r P_r$ = replacement cost (function of temp) = ($C_{rH} P_{rH}$ if Temp > 32 ˚F;
$C_{rC} P_{rC}$ if Temp < or = 32 ˚F)

$C_r P_r$ = composed of replacement costs of each part of the expansion joint

$C_{cc} P_{cc}$ = cost of capital

$C_u P_u$ = user cost = $C_d P_d + C_v P_v + C_a P_a$

$C_d P_d$ = driver cost

$C_v P_v$ = vehicle operation cost

$C_a P_a$ = accident cost

The probabilities, P, for each cost would come from an analysis of the respective DOT's bridge inspection data. The costs, C, for each component would come from the respective DOT's data, typical industry standard costs, related articles, other LCCA models, and costs for similar products or projects. These probabilities and costs could then be input into Eq. (2.7) and (2.8) to calculate the LCCAs for each case.

The LCCA for both expansion joints and for retrofitted continuous joints could be determined and the most cost effective solution chosen for any bridge scenario. While these equations are primarily designed for analyzing the LCC of joints for existing bridges, the model equations could easily be adjusted for use on new bridges. The costs and probabilities for each component would have to be adjusted for the whole bridge rather than only the joint.

This would expand the number of components within each overarching cost component; however, the overall process and overarching cost components would remain the same.

3. BRIDGE SELECTION AND FIELD INSTRUMENTATION PLAN

3.1 Introduction

In collaboration with the Colorado Department of Transportation (CDOT), multiple bridges were considered for instrumentation to investigate thermal loading and the implications of deck joint elimination. To correlate the movements detected by the instrumentation as much as possible due to those thermal effects, specific geometries and characteristics of candidate bridges were desired. The bridges selected for modeling needed to possess at least one deck joint and simply supported structural elements that frame into the deck joint. Safe access to bridges for instrumentation purposes was also an important factor considered when assessing bridge candidates. Bridges with minimal skew, horizontal curvature, and vertical curvature were sought.

As discussed in Section 2, skew and curvature have an effect on the movements of bridges under thermal loading. However, this study focuses primarily on the vertical thermal gradient. In order to truly assess how a vertical thermal gradient manifests itself in bridge movement and performance, it was necessary to minimize the effects that other bridge characteristics would have on the sensors' measurements. Therefore, bridges possessing minimal to no skew and curvature were considered for model calibration and deck joint performance assessment.

One concrete and one steel bridge were chosen for field testing and for numerical modeling in CSi Bridge, a finite element software produced by the maker of SAP2000. An instrumentation plan was developed to capture the thermal loading throughout the superstructure depth at the expansion joint and the structural response. Therefore, temperature, strain, and displacement sensors were used on the bridges selected for fine instrumentation. Details of the instrumentation plans for the two bridges chosen to be finely instrumented are discussed further in Subsection 3.4.

An additional 16 bridges were chosen to be instrumented across Colorado with scratch gauges, which are displacement sensors developed by CDOT and manufactured at the Structural Engineering Laboratory at Colorado State University (CSU). It is a non-electronic displacement sensor developed to assess the influence of regional variations on expansion joint movement. Further details on the scratch gauge configuration are discussed in Subsection 3.4.

3.2 Steel Bridge (B-16-FM)

The steel bridge selected for the study, B-16-FM, is located approximately 10 miles north of Fort Collins, CO, and allows County Road 58 to pass over Interstate 25. The proximity to CSU will give future researchers access to the bridge to troubleshoot any difficulties with the data acquisition system (DAQ) and/or instrumentation sensors. Figure 3.1 shows an aerial view of B-16-FM.

Figure 3.1 Plate Girders for Bridge B-16-FM (Google Maps Image)

The bridge possesses three steel plate girders with varying flange thicknesses, bearing and intermediate stiffeners, and steel diaphragms. Traffic crosses the bridge through one eastbound and one westbound lane. Figure 3.2 shows the superstructure from under the west abutment of the bridge.

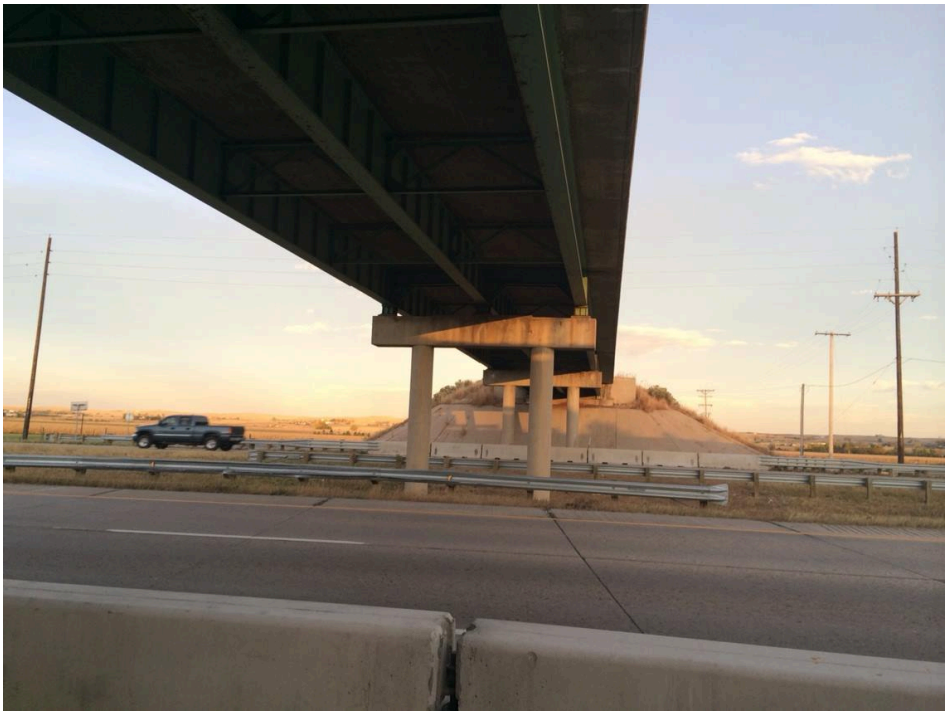

Figure 3.2 B-16-FM Superstructure from the West Abutment (photo by authors)

The bridge consists of four spans (three steel spans and one short concrete approach span). The three steel spans are 74’6” in length, simply supported, and separated by expansion joints. Figure 3.3 shows another view of the superstructure and piers. Finger joints, a common type of expansion joint, shown in Figure 3.4, are in place over the expansion joints to allow thermal movement. The spans are supported on rocker bearings that transfer the loads to the piers.

Figure 3.3 View of B-16-FM from east abutment (photo courtesy of CDOT)

Figure 3.4 Finger joint clogged by debris on B-16-FM (photo courtesy of CDOT)

The bridge superstructure was instrumented at the centermost pier, labeled pier 3 by CDOT nomenclature. Thermocouples, strain gauges, and linear potentiometers were used to collect information about temperature, strain, and displacement, respectively. In addition to instrumenting the joint with sensors, an additional strain gauge was placed at the bottom of the web of the plate girder at mid-span of an adjacent span to validate the finite element model. Data used in calibration were obtained using control load testing. The test was conducted using a truck with known dimensions and axle weights, which was provided by CDOT. More information about the control load testing can be found in Section 5.

3.3 Reinforced Concrete Bridge (C-17-AT)

A three-span, five-girder traditionally reinforced concrete bridge was chosen for the study. C-17-AT carries northbound Interstate 25 over a gravel service road, and is shown in Figure 3.5 and Figure 3.6. The bridge is located approximately 30 miles south of CSU. The proximity to CSU will give future researchers access to the bridge to troubleshoot any difficulties with the DAQ and/or instrumentation sensors.

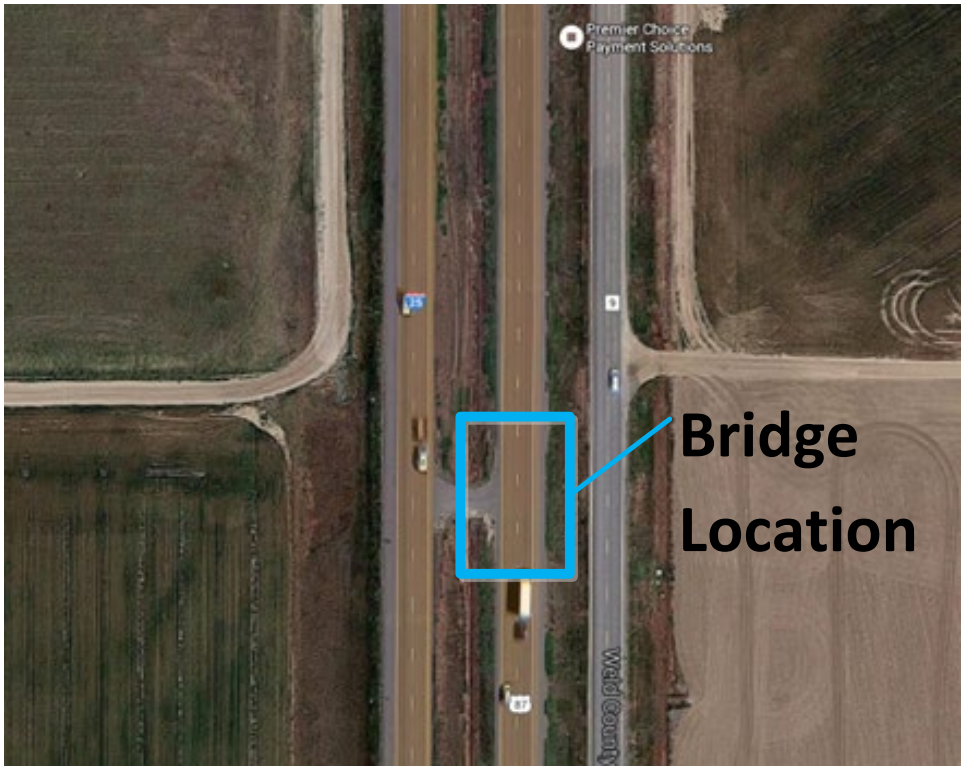

Figure 3.5 Aerial view of C-17-AT (photo courtesy CDOT)

Figure 3.6 C-17-AT (photo courtesy CDOT)

The concrete girders are traditionally reinforced, the spans are simply supported, and two expansion joints separate the three spans. Extensive corrosion and damage are observable below the deck joints. Figure 3.7 shows the discoloration of the pier caps, which are directly below the expansion joints.

Figure 3.7 Discoloration under expansion joint on C-17-AT (photo courtesy CDOT)

3.4 Field Instrumentation

Since the process of field instrumentation is general for both bridges, the logistics for Bridge C-17-AT only are discussed. C-17-AT is a three-span (with two expansion joint), five-girder, traditionally reinforced concrete bridge, which carries northbound I-25 over a gravel access road that connects frontage roads. These can be seen in Figure 3.8 and Figure 3.9. Located approximately 30 miles south of CSU on I-25, the bridge is close enough to provide easy access for field implementation and for researchers in the event of repairs or remediation needed by either the DAQ or the sensors.

The spans are each approximately 31 ft. long and 42 ft. wide, with expansion joints separating the three spans. See Appendix A for drawings. Each of the five girders, as well as the deck, are traditional reinforced concrete and simply supported. Pier caps and columns are also reinforced concrete. Furthermore, extensive damage and corrosion and leakage from the expansion joint can be seen on the underside of the girders and expansion joints. See Figure 3.10.

The expansion joints are simple joints with a rubber silicone seal; however, the seal was cracked and the joint was clogged with visible clogging and deterioration on the ends. See Figure 3.11 and Figure 3.12 showing the clogging present in the expansion joint at the time of instrumentation.

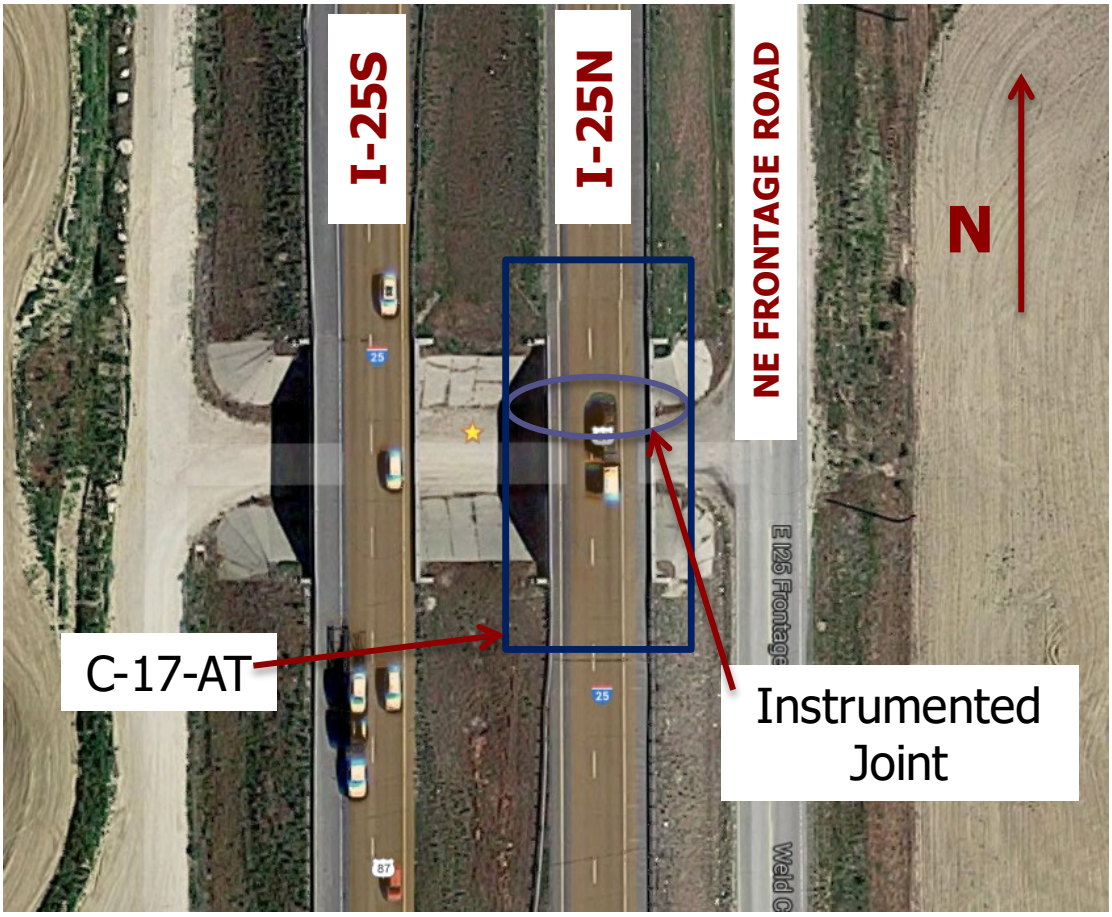

Figure 3.8 C-17-AT overview

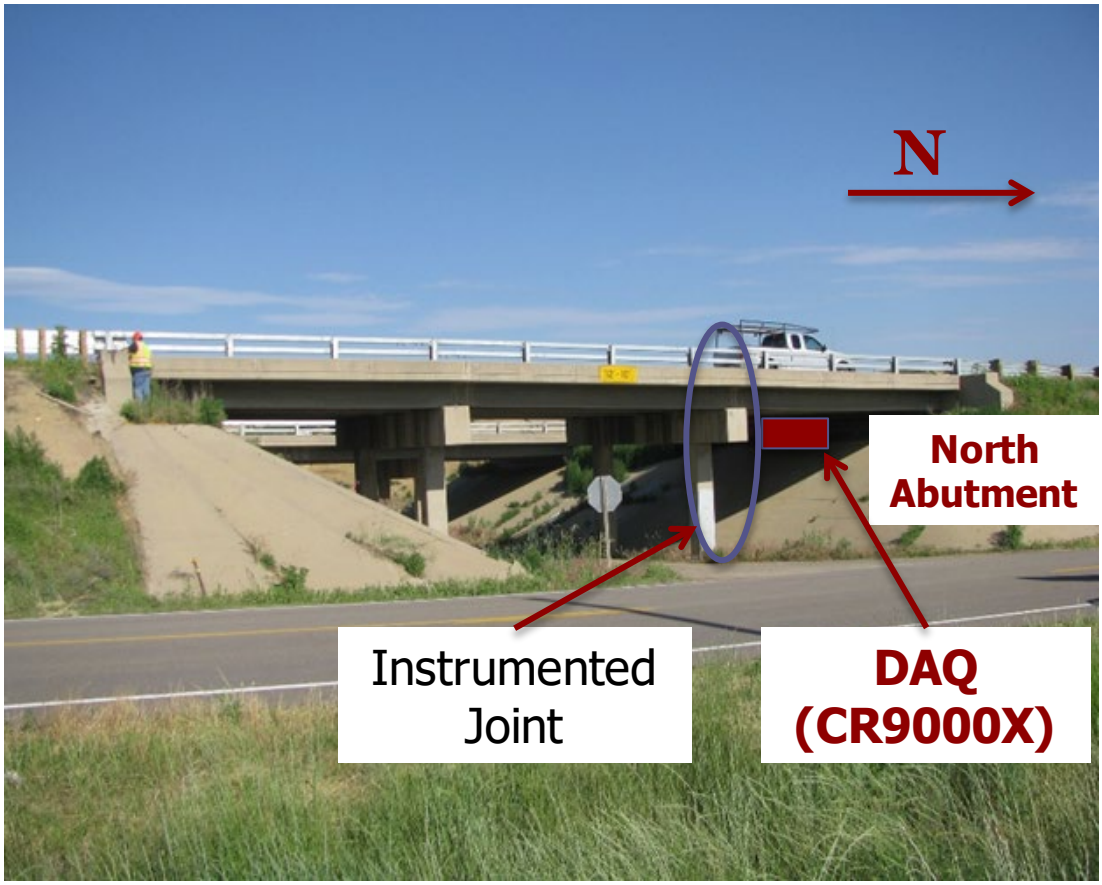

Figure 3.9 C-17-AT sideview

Figure 3.10 C-17-AT underside – corrosion and leakage

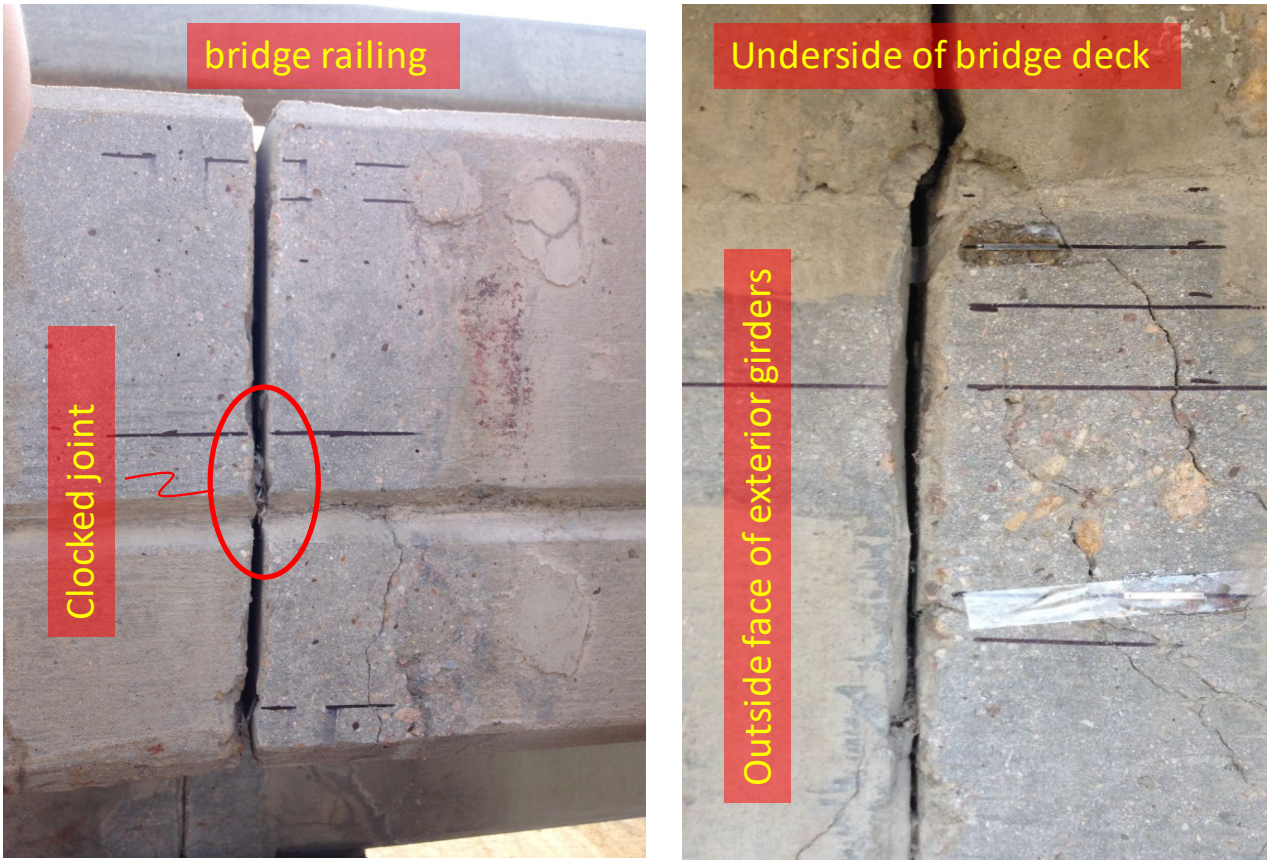

Figure 3.11 C-17-AT expansion joint clogging

The northernmost expansion joint was selected for instrumentation, as seen in Figure 3.8 and Figure 3.9. The eastern facing side of the north expansion joint was selected for the instrumentation to prevent the effects of shadowing from the southbound bridge directly to the west of the northbound bridge. By choosing the eastern facing side of the joint, there is nothing blocking the sunrays from hitting the sensors on the joint, and will therefore provide the most uninterrupted thermal behavior for the sensors. Three different types of sensors were used to monitor the thermal gradient along the depth of the joint as well as the structure behavior due to thermal gradients and vehicle traffic loading on the joint. Strain gauges were used to measure the strain (and by relation, the stress), thermocouples were used to measure the thermal gradient, and linear potentiometers were used to measure displacement (both expansion and compression) along the depth of the joint. The placement of these sensors on the joint can be seen in Figure 3.13 (See Appendix B for more details), and their details are discussed in Sections 3.2.1, 3.2.2, and 3.2.3, respectively.

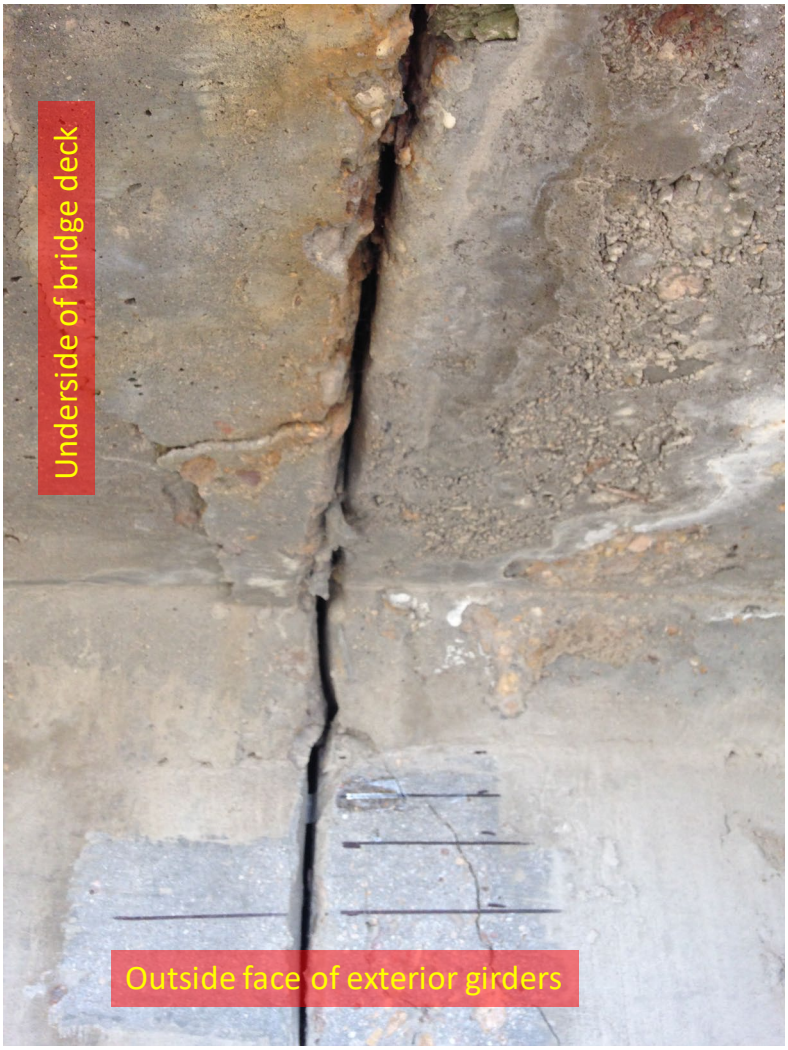

Figure 3.12 C-17-AT expansion joint deterioration

The bridge was instrumented August 22−24, 2016. The overall instrumentation process was smooth, with only minor adjustments needed in the field, such as running the wires along the bridge railing instead of along the bottom of the girder. Because the bridge carries northbound I-25, running wires along the railing was done at night, 9 p.m. on August 23, 2016, in order to utilize a nighttime construction lane closure.

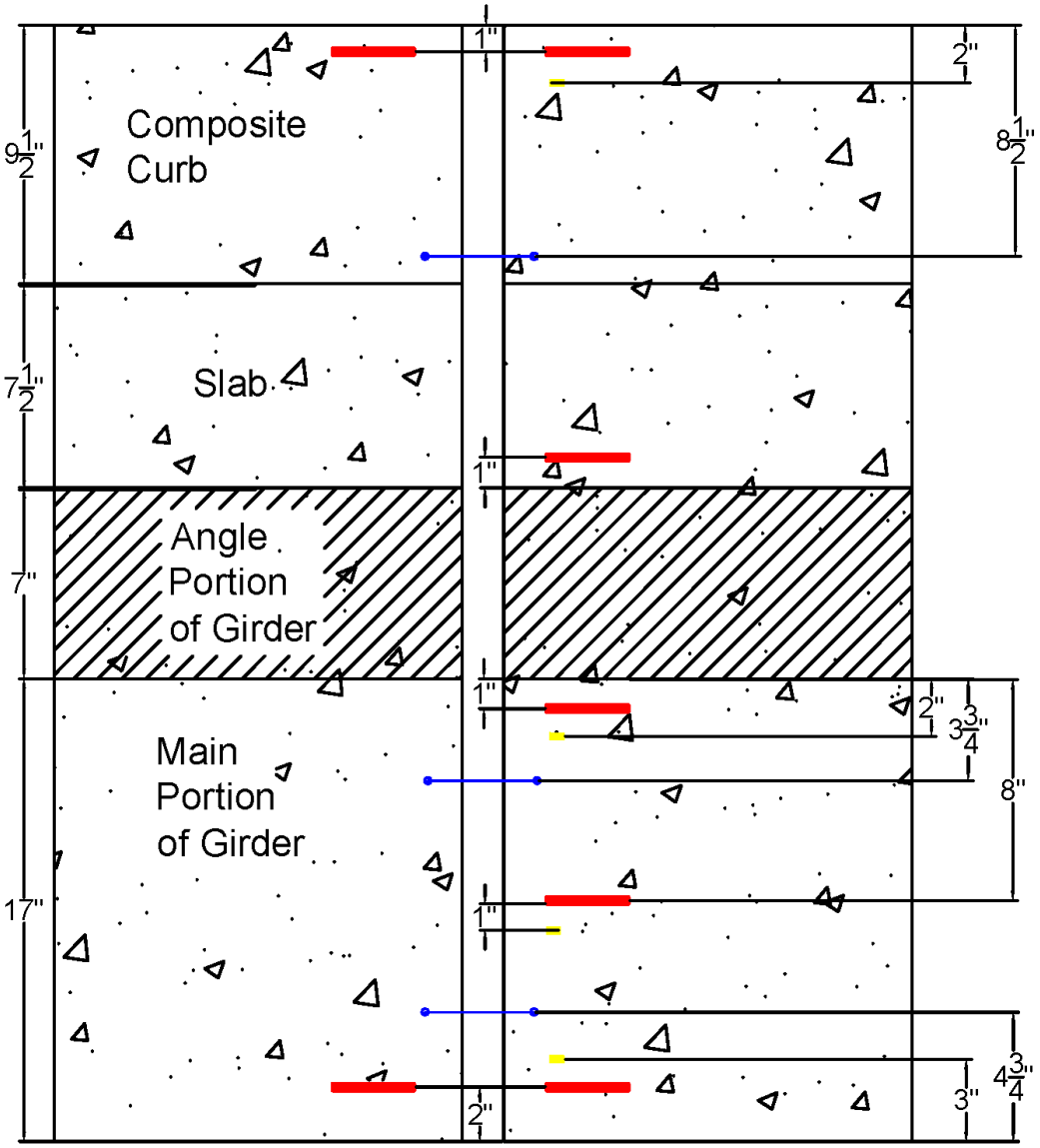

Figure 3.13 C-17-AT expansion joint sensor placement

3.4.1 Strain Gauges

In order to monitor the stress and strain experienced by the joint due to both thermal and vehicle loading, seven strain gauges were placed along the depth of the joint. However, due to the nonhomogeneous nature of concrete long (30 mm) 350 ohms Omega strain gauges were used for C-17-AT. See Figure 3.14. The length of the gauge is designed to account for variability in the material's response through averaging of the measurement along the gauge length, and thus provides a more representative strain reading.

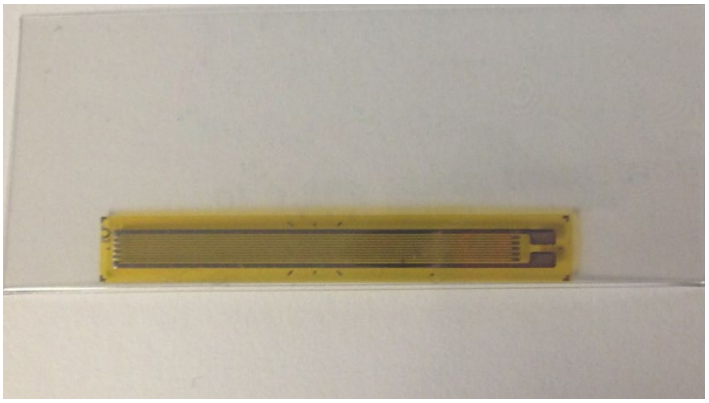

Figure 3.14 Concrete strain gauge

Two strain gauges were placed approximately one inch from the top of the slab on either side of the expansion joint to provide redundancy. One was placed approximately one inch above the bottom of the slab on the north side of the joint. One was placed on the girder approximately one inch below the slab on the north side of the joint. A fifth was placed halfway down the girder on the north side of the expansion joint. The two final gauges were placed on either side of the joint approximately one inch above the bottom of the girder. These can be seen in Figure 3.13.

The concrete was ground smooth with a grinder before the strain gauges were applied to the concrete of the slab and girders with strong epoxy glue. The smooth surface provided by the grinder ensures full contact between the sensor and the concrete. Once glued to the slab and girders, the strain gauges were soldered to their corresponding labeled wires. Soldering was done in the field due to the length of the strain gauges. With shorter/smaller strain gauges, soldering can be completed in the lab and the gauges can be brought to the field already connected; however, the longer strain gauges needed for the concrete are more bendable and fragile than smaller ones used for steel. Thus, soldering before application introduces an unreasonable risk of damage to the strain gauge. This application process can be seen in Figure 3.15 and Figure 3.16. Once the strain gauge was soldered to the wires in the field, the resistance at the other ends of the wires was tested to ensure proper connection to the strain gauge. Extra strain gauges were available in the event that soldering was improper and unfixable, in which case a new strain gauge would have been applied and soldered and tested. Once the strain gauges were fully installed and tested, they were covered by an adhesive rubber protective cover that was additionally caulked along the edges to ensure protection from the elements.

Figure 3.15 Strain gauge application

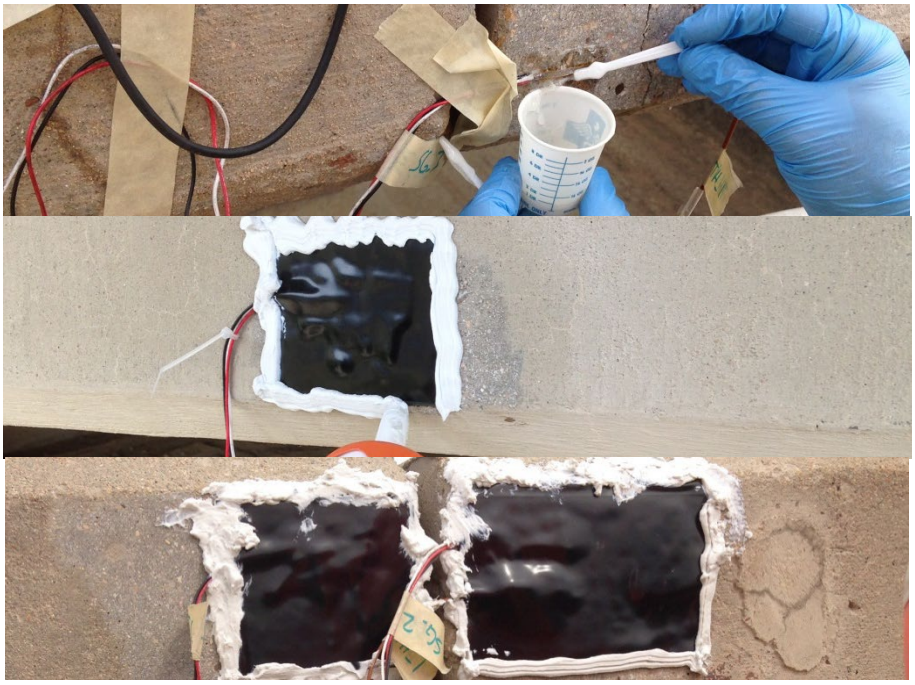

Figure 3.16 Strain gauge protection

3.4.2 Thermocouples

Thermocouples were used to monitor the thermal distribution throughout the depth of the expansion joint. Omega type K thermocouples were chosen; they are self-adhesive and designed to resist the outdoor elements. Their flexible design allows for full contact with the material and a large temperature range of -58°F to 392°F. These are the same thermocouples used for bridge B-16-FM, and have provided consistent data for that bridge, thereby supporting the decision to use the type of thermocouples for bridge C-17-AT.

Four thermocouples were used along the depth of the expansion joint to record and monitor the thermal gradient along the joint. One thermocouple was placed approximately two inches below the top of the slab, or approximately one inch below the strain gauge on the north side of the joint. A second one was placed approximately two inches below the bottom of the slab on the girder (about one inch below the strain gauge). A third thermocouple was placed at mid-depth on the north girder approximately one inch below the mid-depth strain gauge. A final thermocouple was placed approximately two inches above the bottom of the north girder, about one inch above the bottom strain gauge. Their placement can be seen in Figure 3.13.

The concrete was also ground smooth with a grinder before the thermocouples were applied by peeling off the protective cover and pressing the adhesive side to the concrete, as shown in Figure 3.17. Once the thermocouple was firmly attached, the wires were connected using thermocouple wire connection plugs, which were prewired to the thermocouple and the shielded wires before instrumentation. These connection plugs are specific to type K thermocouples and provide a fully secure, protected, and complete connection between the thermocouple and the wire and thus the DAQ. These connectors, seen in Figure 3.18, help ensure accurate data are recorded.

Figure 3.17 Thermocouple Application

Figure 3.18 Thermocouple connectors

3.4.3 Linear Potentiometers

Measuring the displacement of the joint in both directions, expansion and contraction, is the primary indication of how critical the expansion joint is to the bridge, as well as the effects of clogging and thermal gradient changes on the bridge. To measure these displacements, Celesco model CLP 50 linear potentiometers were chosen. These linear potentiometers can measure up to one-inch extension and one-inch compression, for a total of two inches of displacement. The linear potentiometer in Figure 3.19 is shown extended to its full two-inch extension. This model has a life expectancy of 25 million repetitions and is designed to resist environmental elements, including a temperature range of -40˚F to 212˚F and up to 20,000 Hz of vibration. These were the same linear potentiometers used on B-16-FM, and have provided consistent and continuous displacement data from that bridge.

Figure 3.19 Extended linear potentiometer

Three of these linear potentiometers were used on the north joint of C-17-AT. The first was placed across the joint at mid-depth on the slab, approximately 3.75 inches below the top of the slab. The second linear potentiometer was placed across the joint on the girders, approximately 3.75 inches below the bottom of the slab. The last linear potentiometer was placed across the joint on the girders, 3.75 inches above the bottom of the joint. Their placements can be seen in Figure 3.13.

In order to ensure full extension and compressibility of the linear potentiometers across the joint, the linear potentiometers were mounted on mounts made of a Plexiglas square with a bolt through the middle, which was then ran through the ring on the end of the linear potentiometer and secured with a nut (see Figure 3.20). The concrete was ground smooth with a grinder before the mounts were glued to the girder with the same epoxy used for the strain gauges. When mounting the linear potentiometers, measurements were made and marked on the concrete before the mounts were glued in placed. The epoxy takes only a couple minutes to harden, and once hardened the linear potentiometers were attached and bolted in place, as seen in Figure 3.21. Finally, the linear potentiometer was covered with half of a PVC pipe to protect the sensor from

weather. The PVC pipe was attached on only one side of the joint to ensure free movement of the joint and sensor. The PVC covered linear potentiometer can be seen in Figure 3.22.

Figure 3.20 Linear potentiometer mount

Figure 3.21 Linear potentiometer in place on joint

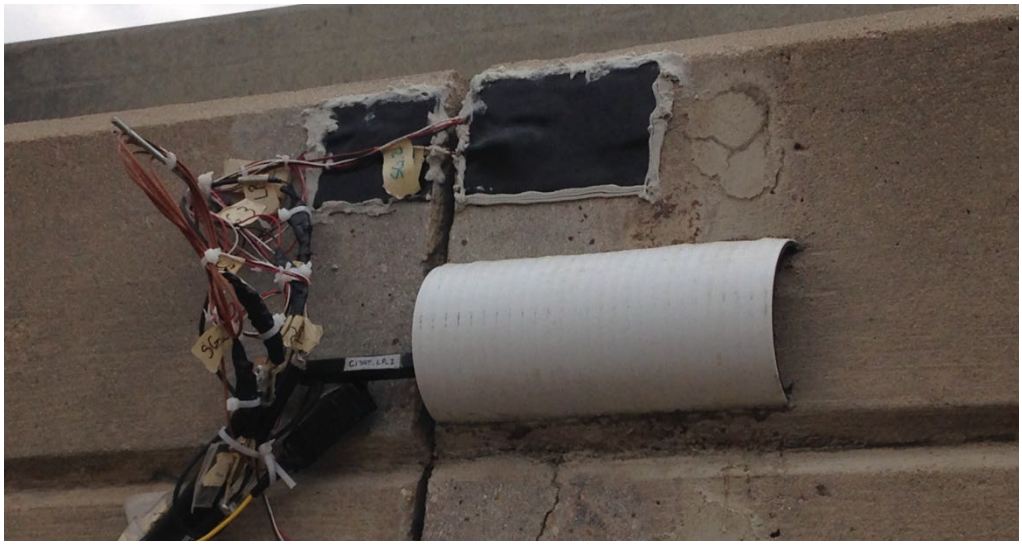

Figure 3.22 PVC covered linear potentiometer

3.4.4 Wires

Shielded wires were used for all sensors to protect the data from the elements and minimize noise in the data collected. Two types of shielded wires were used. Thermocouples wired over distances greater than a few feet require shielded thermocouple wires that will transmit the temperature over longer distances and protect them from the elements. Thus, Type K Omega extension thermocouple wires were used. These wires have a polyvinyl shield, a max temperature of 221˚F, and solid No. 6 AWG wires, as seen in Figure 2.23.

Figure 3.23 Shielded thermocouple wire

For the strain gauges and linear potentiometers, shielded wires from Allied Wire and Cable were chosen, including the FR-EPR/CPE instrumentation cable with individual and overall shielded pairs. These wires have AWG No. 18, with two pairs of wires. The wires have copper drain wires that were grounded to minimize noise, ethylene propylene rubber (FR-EPR) insulation, and shields of aluminum with overall covers of chlorinated polyethylene (CPE). They have a maximum temperature of 194˚F and voltage of 600V. These double shielded wires are shown in Figure 3.24.

Figure 3.24 Double shielded wire

3.4.5 The Data Acquisition System

For the collection of data from the sensors, a Campbell Scientific CR9000X Data Logger was chosen as the data acquisition system (DAQ). The CR9000X is a multiprocessor, high-speed, 16-channel system, including digital and analog filters to eliminate noise and provide clear signals. With a measurement rate of 100,000 Hz, the CR9000X provides high-speed sampling capabilities that are ideal for this project, in which measurements from the sensors are recorded every five seconds. Furthermore, data can be collected directly or remotely (with the addition of a wireless modem) from the DAQ. This allowed us to connect the DAQ to a laptop computer in the field and monitor the data as soon as the sensors were in place and wired to the DAQ. Monitoring the data on-site ensured that the sensors were operating correctly and allowed for an immediate review of the response of the bridge.

On-site, the CR9000X data logger was enclosed in a large steel weatherproof job box. The job box with the DAQ inside was placed on the north abutment of C-17-AT, as seen in Figure 3.25, and was chained to the bearing. Figure 2.26 shows the DAQ inside the job box.

Figure 3.25 Job box on north abutment

Figure 3.26 DAQ in job box

The wires were run from the sensors on the north joint along the top of the bridge to the job box. The wires were connected to the railing along the west edge of the bridge using zip ties and protected by halved PVC pipes to provide uniformity and security. The wires were then run through a gasket on the side of the job box and connected to the CR9000X data logger inside. The wires running along the bridge are shown in Figure 3.27.

Figure 3.27 Wires along railing

The DAQ system is powered by a size 27 deep cycle marine battery charged by a 70-watt solar panel. The battery is stored inside the job box next to the CR9000X, as seen in Figure 3.26, and connected via wires to the positive and negative terminals in the CR9000X. The solar panel was installed a month and a half after sensor installation due to shipping time. During the interim period, the battery was charged about once each week. The solar panel, installed on the west side of the north abutment, was placed at a 45-degree angle to maximize sunlight exposure throughout the year. The solar panel was wired to a charge controller, which was then connected to the battery. The charge controller prevents the battery from becoming over-charged. The solar panel installation is discussed in Subsection 3.5.

3.5 Remote Data Collection

Two methods were available for data collection from the CR9000X. The DAQ stores data on a 2 GB memory card, which can hold several months of data. The first method of collection would be to go out to the bridge periodically for collection by hardwiring a laptop to the DAQ and downloading the data from the memory card. The second option would be connecting a wireless modem to the CR9000X data logger and then downloading the data remotely from the DAQ to an office computer using a static IP address.

The second method was chosen as more convenient and economical. Not only would a wireless connection to the DAQ make data collection easier, it would also allow the researchers to check on the sensors remotely. This would ensure that sensors are working properly, thus allowing researchers to easily see when a sensor might need attention or mediation in the field.

The Campbell Scientific RavenXTV modem was chosen for wireless data collection. This modem is designed to work with the CR9000X data logger and a Verizon IP address. A static IP address was chosen to provide easier access to the data. Once the Verizon static IP address was set up and assigned to the modem, the modem was configured using provided software and plugged into the CR9000X data logger on-site. Figure 3.28 shows the modem connected to the data logger and Figure 3.29 shows the modem's antenna attached to the side of the bridge. For collection, the software RTDAQ was used to connect remotely to the CR9000X via the modem and IP address. Once connected, data can be downloaded and saved as .csv files and analyzed. Data were collected, downloaded, and converted once a week to minimize any backup of data and streamline the analysis process discussed in Subsection 3.6.

Figure 3.28 RavenTXV modem

Figure 3.29 Modem antenna

3.6 Solar Panel Installation

The location of bridge C-17-AT does not provide access to electricity; consequently, alternative sources of energy for powering the CR9000X system were considered. First, rechargeable batteries were considered. These would be switched out and recharged by either CSU or CDOT personnel. The second option considered was a rechargeable battery charged by a solar panel attached to the abutment. This second option proved to be both more cost and time effective because it would not require regular trips to the bridge. The cost of the solar panel proved to be comparable to a second rechargeable battery and would significantly cut maintenance hours. The battery chosen was the Diehard Group 27M deep cycle, 12-volt marine battery. The solar panel chosen was a Newpowa 70-watt panel with a 12-volt solar charge controller to prevent over-charging of the battery. The solar panel weighs 13 pounds and is 30.48 in. x 26.57 in. x 1.18 in., and is shown in Figure 3.30.

Figure 3.30 Solar panel, 70-watt

A frame to hold the solar panel at a 45-degree angle against the abutment was built of 2x4s. Positioning the solar panel at a 45-degree angle allowed for maximum sunlight ray absorption throughout the calendar year based on sun ray angles. The framed 2x4s were connected to the solar panel using screws and brackets, as seen in Figure 3.31. The ends of the frame were attached to brackets, which would be attached to the concrete abutment using screws. The in-place solar panel is shown in Figure 3.32 below.

The solar panel was installed on October 8, 2016. The panel was installed after the rest of the instrumentation due to shipping time constraints. During the interim between instrumentation and solar panel installation, the battery was picked up once every eight days to be charged and then returned to the site. The panel was installed by using a pachometer to detect rebar in the abutment. The locations of the screws were then marked and holes drilled into the concrete. The solar panel was then put in place and the frame screwed into the concrete. Once in place, the solar panel wire was connected to the charge controller and to the battery providing power to the DAQ.

Figure 3.31 Solar panel frame

Figure 3.32 Solar panel attached to abutment

4. CONTROLLED LOAD TEST MODEL VALIDATION

4.1 Introduction

In order to validate the finite element model of the bridges, a static control load test was performed following the completion of the field instrumentation. The test was performed by parking a truck with known dimensions and axle weights on the bridge and strain data were collected. The test was performed in two parts: first with the front axle directly above the mid-span strain gauge, and second with the back axles centered above the mid-span strain gauge. The same truck loads were placed on the finite element model and the two responses were compared.

4.2 Test Vehicle Information

An Aspen Aerials A-40 Bridge Inspection Unit truck, provided and operated by CDOT personnel, was used for the control load test. This was the same truck used for sensor installation on the bridge. The axle weights and dimensions for the A-40 truck can be seen in Figure 4.1. These axle weights are for when the inspection bucket arm is fully contracted and stowed on the bed of the truck. These axle weights are accurate to within +/- 2% of the exact weight, according to the manufacturer. The position shown, with bucket arm fully contracted, is how it was parked on the bridge for the test.

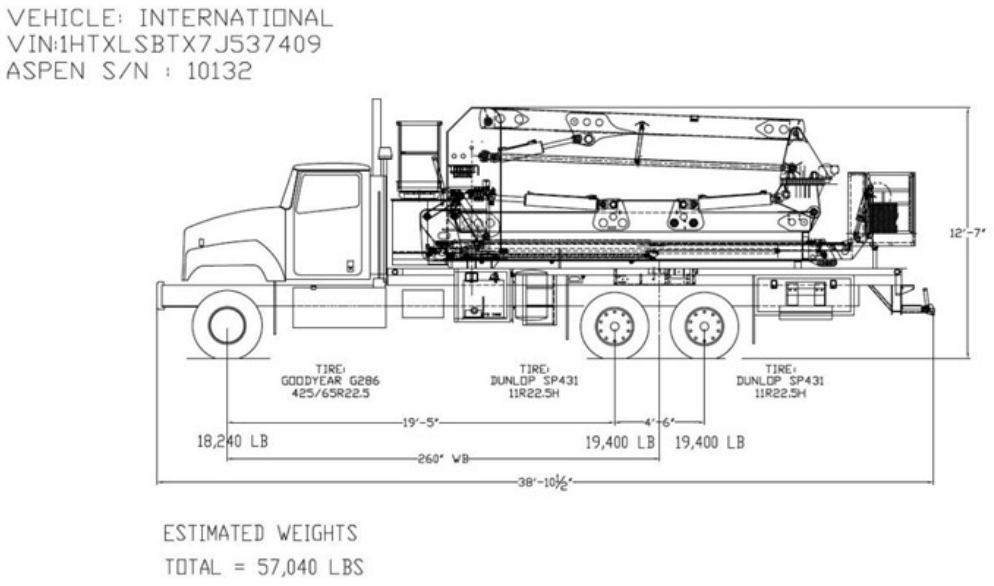

Figure 4.1 Aspen Aerials A-40 truck with dimensions and axle weights

4.3 Model and Predictions

The effect of the Aspen Aerial A-40 truck was included in the finite element model of bridge by inputting the axle weights as point loads representing the tires in the same location as in field test scenarios. Two scenarios were considered: 1) when the truck was parked with its front axle at the mid-span location and 2) when the truck was parked with its two back axles over the mid-span location.

The strain gauge at mid-span, for both bridges, was monitored during the truck load tests and used for validating the numerical model. For the reinforced concrete bridge, this strain gauge was installed about two inches above the bottom of the outside west girder at mid-span. For the steel bridge, the gauge was installed on the centermost girder.

For the concrete bridge, the first scenario in the finite element model, where the front axle is above mid-span, gives the stress at the bottom of the girder at mid-span to be 0.146 ksi. The second scenario, when the back axles are centered above mid-span, gives the stress at the bottom of the girder at mid-span to be 0.349 ksi. For the steel bridge, when the front axle is located at the mid-span of the bridge in the finite element model, the stress on the top of the bottom flange at mid-span is 1.39 ksi. When the back axles are split across the mid-span, the model predicts the stress on the top of the bottom flange at mid-span to be 2.20 ksi.

4.4 Results and Comparison with the Finite Element Models

4.4.1 C-17-AT

Each of the two scenarios of the control load test was performed for approximately one to two minutes. During each of these tests the data were collected in the field at five-second intervals from the strain gauge at mid-span. Collecting several data points over the span of the test allowed for a moving average to be applied to the data. These average strains were then converted to stress and compared with the corresponding finite element model stresses. Figure 4.2 and Figure 4.3 show some of the data collected for the front axle test and for the back-axle tests, respectively.

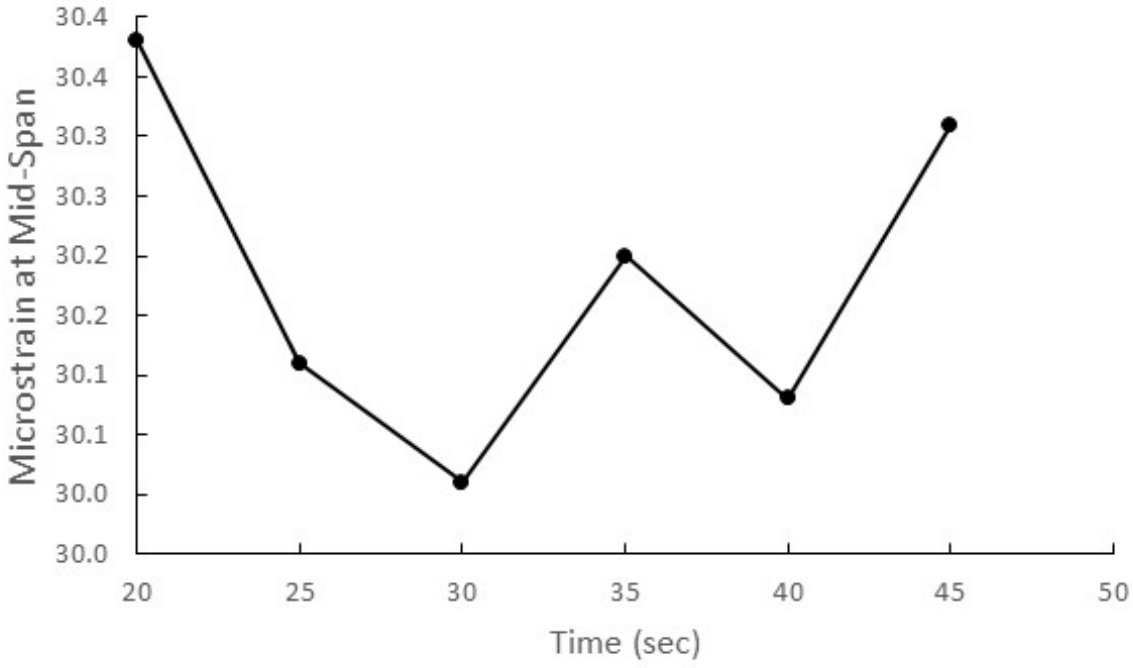

Figure 4.2 Front axle control load test data

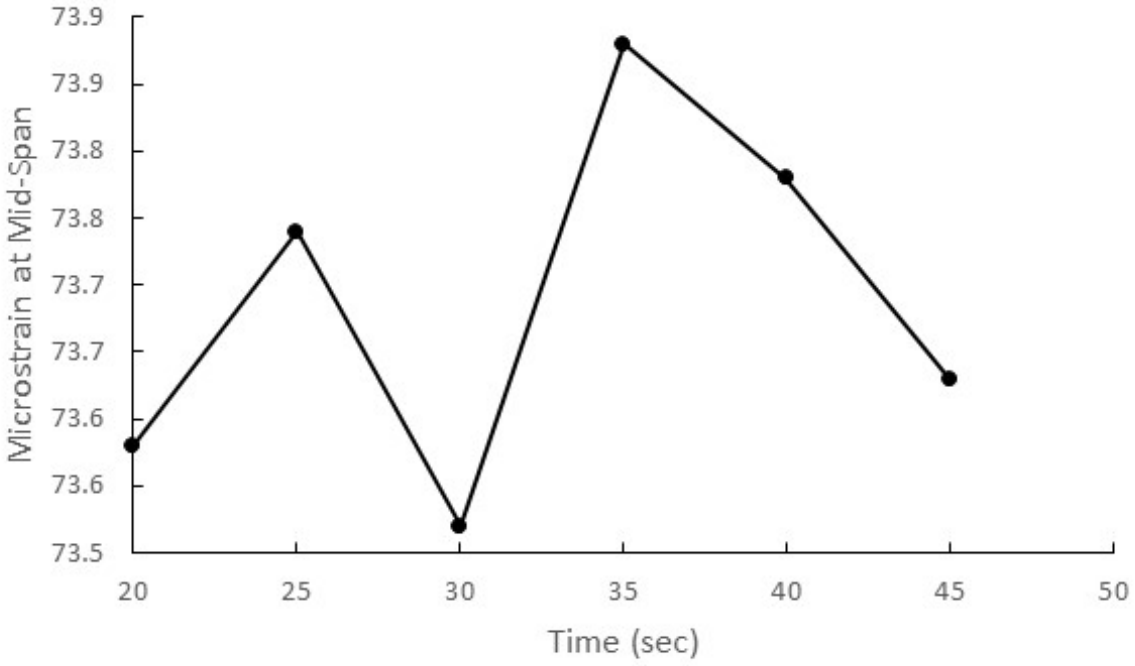

Figure 4.3 Back Axle Control Load Test Data

An average of the data collected during the field test was used to calculate the average microstrain for each of the two scenarios. The front axle scenario gave an average microstrain at mid-span of 30.18. The back axles gave an average microstrain at mid-span of 73.69. These microstrains were converted to stresses using the modulus of elasticity of the concrete, 3604 ksi. Table 4.1 shows both the predicted stresses from the numerical model and the measured field response stresses. Table 4.1 also shows the calculated percent difference between the predicted and measured stresses. A percent difference less than 20% was considered good, and as shown, good agreement was achieved between the field test and the numerical model.

Table 4.1 Comparison of field stress and model stress predictions

	Front Axle at Mid-span	**Back Axles at Mid-span**
Predicted Stress (ksi)	0.146	0.349
Measured Stress (ksi)	0.109	0.266
Percent Difference (%)	11.5	9.74

4.4.2 B-16-FM

Control load tests were performed with the front axle at mid-span and again with the rear axles at mid-span to match the scenarios that were modeled. During each test, the data from the mid-span strain gauge were collected in the field at five-second intervals for approximately one minute. Some noise in these data was expected due to the length of the wires being approximately 240 ft. Collecting several data points allowed a moving average to be applied to the data to determine the actual strain. Figure 4.4 shows the microstrain at mid-span when the truck was parked with its front axles at mid-span. Figure 4.5 shows the microstrain at mid-span when the truck was parked with its rear axles at mid-span.

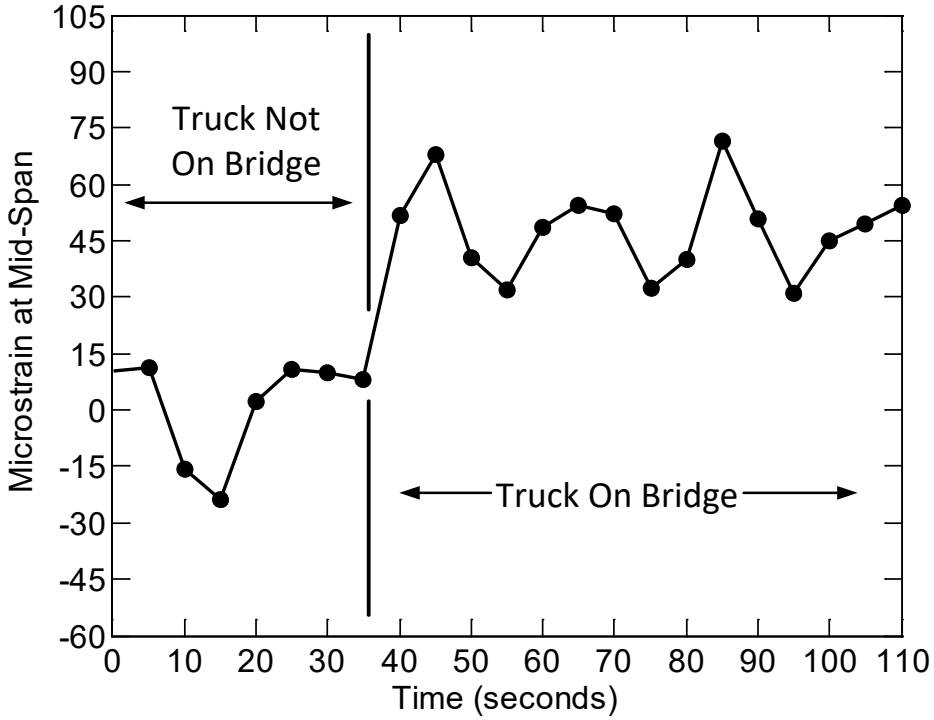

Figure 4.3 Field control load test with front axle of A-40 truck at mid-span

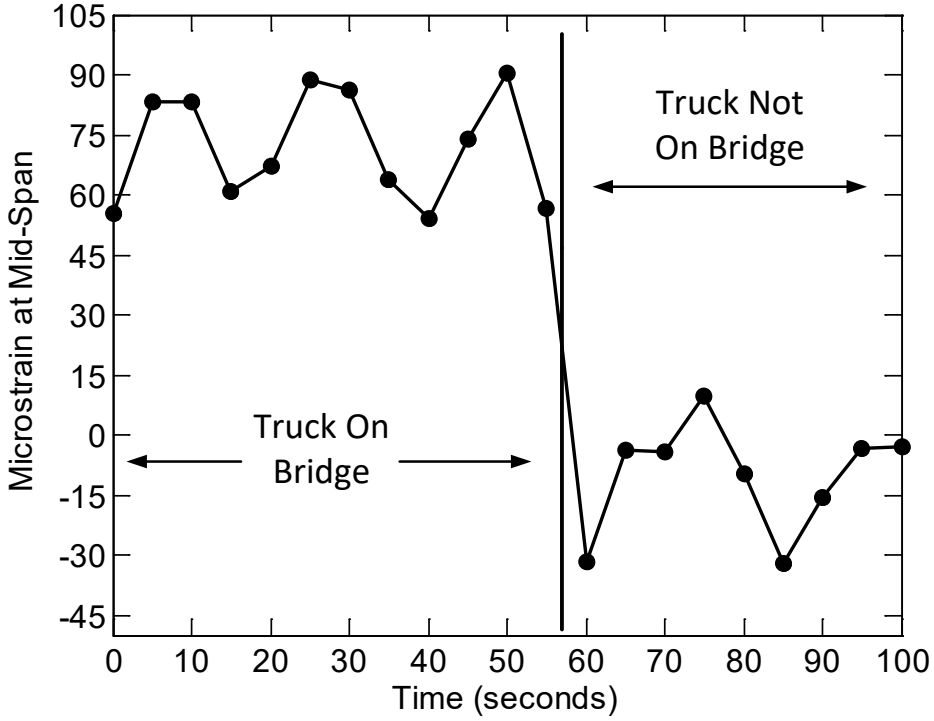

Figure 4.5 Field control load test microstrain with back axles at mid-span

A simple average of the data collected was used to determine the average microstrain for each scenario. The average microstrain when the front axle was located at mid-span was 47.36, while the average microstrain when the back axles were located at mid-span was 71.99. The microstrains were converted into stress using the modulus of elasticity. Table 4.2 shows the comparison of the model predictions to the measured field response. As shown in the table, excellent agreement was achieved.

Table 4.2 Comparison of field stress to modeled stress predictions

	Front Axles at Mid-span	**Back Axles at Mid-span**
Predicted Stress (ksi)	1.39	2.20
Measured Stress (ksi)	1.37	2.09
Percent Difference (%)	-1.22%	-5.10%

5. DATA ANALYSIS FOR BRIDGE C-17-AT

5.1 Introduction

The data from the bridge were downloaded weekly and a brief analysis performed using an analysis and plotting code written in RStudio (2016). The data were visualized and analyzed to determine patterns and correlations between the thermal, displacement, and strain/stress data. The analysis was conducted in order to discern how much movement, stress, and temperature change the bridge was experiencing. This knowledge was used to enhance understanding of the expansion joints on the bridge's overall health and LCC. The correlations and patterns were used to draw conclusions about the impact of the clogged joint and of the thermal gradients through the depth of the bridge. The thermal gradients measured were also compared with standard thermal gradients for further analysis. This data and analysis were finally used to form recommendations for joint removal and retrofitting.

5.2 Analysis Plotting Code

The analysis code for the C-17-AT and B-16-FM data was written in RStudio in order to provide easy comparison and visualization of the data. The code was divided into three sections. The first section provided a general analysis and comparison of the sensors' data by producing a three-part graph. The second section provided a comparison of the maximum temperature difference and the stress by producing a two-part graph. The third section calculates the minimum, average, and maximum thermal gradients through the depth of the bridge and plots them next to each other on a three-part graph for comparison with the standard temperature gradients of AASHTO and New Zealand.

The data were downloaded from the DAQ through the wireless RAVEN XTV modem as .dat files. These .dat files were then converted to .csv files and both saved and backed up. The code works by reading in the appropriate files as .csv files. The user then selects the date range, desired sensors, and sets the plotting parameters. Next, the code was run and the plots simulated. Finally, the plots were saved and analyzed.

5.3 Sensor Correlation and Patterns

Due to bridge C-17-AT's location in Colorado where there is a large range of temperatures, a maximum range of 140℉ (60℃) over the course of the year, the bridge is likely to experience significant differences in temperature (AASHTO, 2012). Thermal gradients are usually most uneven at times of heating or cooling of the bridge, especially during times of direct sunlight. Heat transfer due to direct radiation from the sun, conduction, or convection occurs every time the ambient air temperature varies – typically every morning and evening. Multiple parameters affect how evenly the bridge loses and gains heat, including bridge orientation, length of concrete overhang, depth of girders, height of concrete slab, and girder spacing (Chen, 2008).

The coefficient of thermal expansion, commonly expressed as μ or α, describes the increase in length of a material for a given increase in temperature. A negative result for the change in length corresponds to a shortening of the material and, conversely, a positive value corresponds to an increase in material length. Bending stresses can develop through the depth of the bridge due to the presence of thermal gradients causing the concrete deck and girder to expand at different rates.

The five months in which data had been collected to date on the C-17-AT bridge provide a foundation for preliminary conclusions about temperature's effect on the expansion joint and allows for comparison with theoretical expectations. The displacement experienced by the expansion joint should be closely correlated with the effective temperature experienced by the joint. This was found to be true in the research monitoring conducted by Y. Q. Ni et al. (2007) on the Ting Kau Bridge. It was also found that the correlation could be predicted using a linear regression model (Ni et al., 2007). However, only the effective temperature, which is the weighted average temperature throughout the depth of the bridge, was considered, rather than the exact temperature at each point through the depth of the bridge. The study also did not include monitoring of stress and strain at the expansion joint. When evaluating the data from C-17-AT over the course of these first five months, similar correlations were seen between the temperature, stress and displacement. Figure 5.1 shows a two-week span of the C-17-AT data at the end of October and indicates a distinct converse pattern between the temperature data plotted in (a) and the displacement data plotted in (b). As the temperature increased the displacement decreased, i.e., the girders expanded and the joint closed; conversely, as the temperature decreased, the displacement increased, i.e., the girders contracted and the joint opened farther. This behavior of the joint, in conjunction with the temperature, confirms that the joint was directly affected by the changing temperature. A fainter pattern can be determined between the stress (from the strain gauges) in (c) and the temperature and displacement data. During the first half of the data set, the temperatures show a greater range (about 15°) and higher average compared with the second half. Also during the first half, the stress data show more variance and during the second half are more constant. Additionally, the displacement changes less during the second half as well, showing that the greater the range of temperature experienced in a short time period the greater the displacement changes and the larger the effect on the stresses in the bridge.

The impact of the daily temperature range can be further seen by looking closer at the data during a smaller range period and a larger range period. Figure 5.2 shows data from C-17-AT from November 30 through December 2, and Figure 5.3 shows data from October 15 through October 18. In Figure 5.2, the temperature range is only approximately 10° and the displacement in (b) shows minimal change, a maximum of 0.05 inches of change in displacement. The stress also shows very little change in (c). On the other hand, looking at Figure 5.3, the temperature range is around 15° and the displacement (b) shows a little more change, a maximum of about 0.09 inches, and the stress (c) shows some variance. All of which indicates the importance of the temperature range on the joint and bridge's overall health.

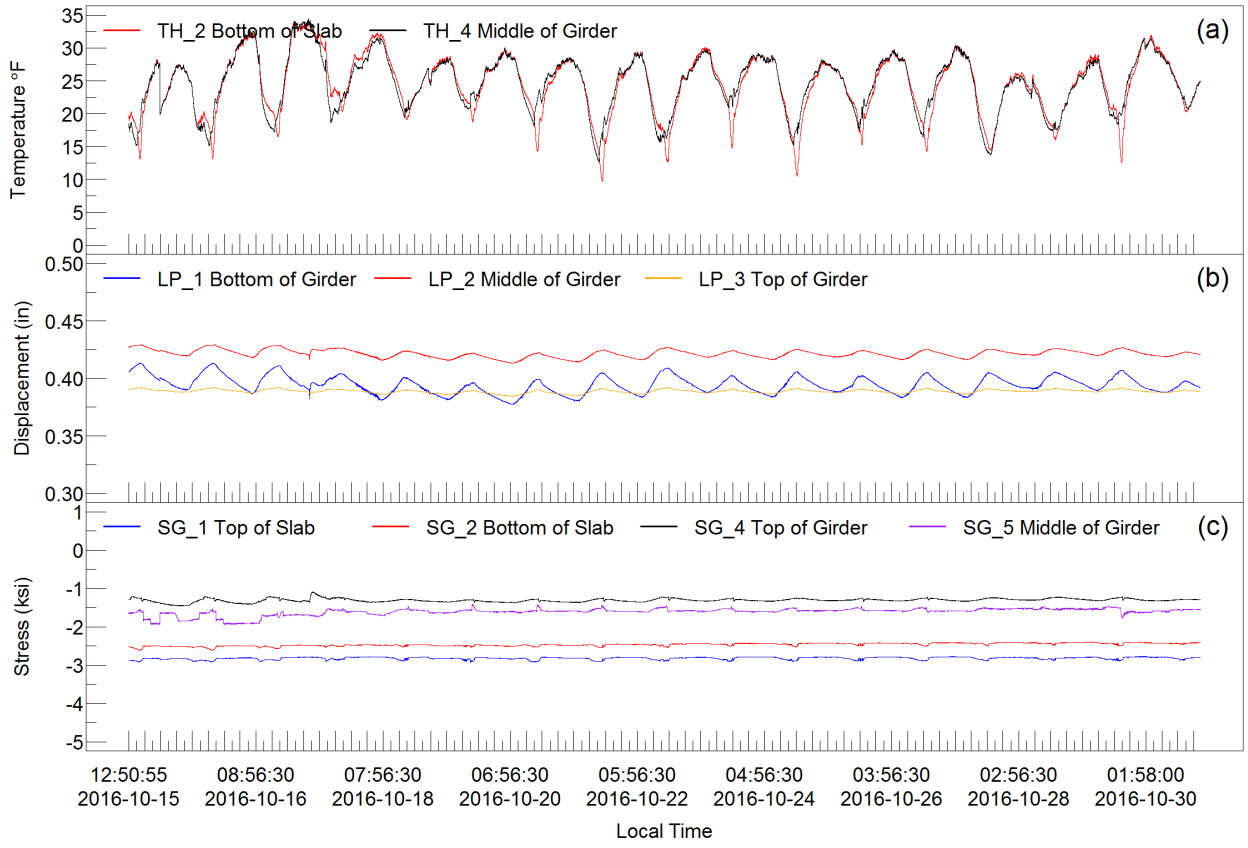

Figure 5.1 C-17-AT bridge sensor data October15 through October 30, 2016
(a) Thermocouple Data, (b) Linear Potentiometer Data, (c) Change in Stress Data.
Note: ℃ = (℉ – 32)/1.8; 1 in = 25.4 mm; 1psi = 6.89 kPa

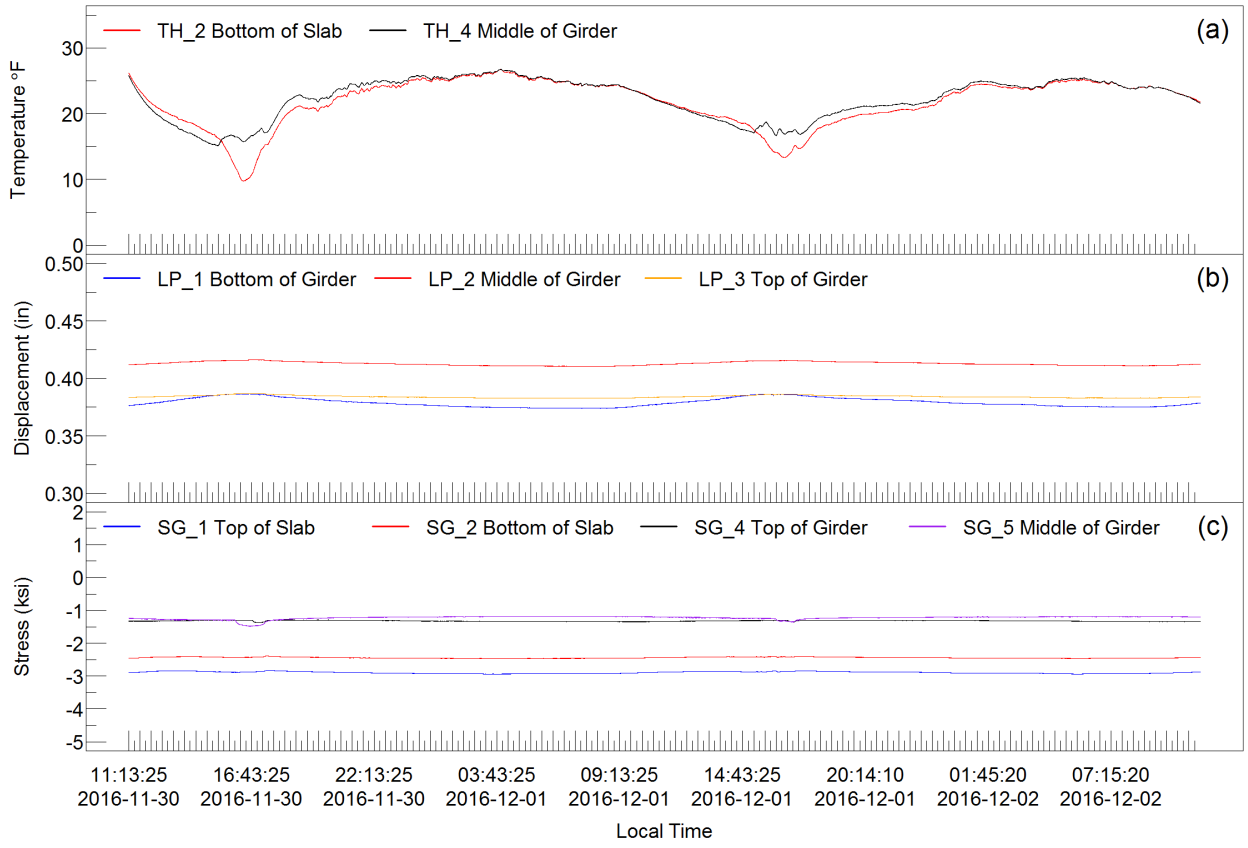

Figure 5.2 C-17-AT bridge sensor data November 30 through December 2, 2016
(b) Thermocouple Data, (b) Linear Potentiometer Data, (c) Change in Stress Data.
Note: ℃ = (℉ – 32)/1.8; 1 in = 25.4 mm; 1psi = 6.89 kPa

Furthermore, these patterns and relationships between temperature and joint displacement and stress can be seen more distinctly in data from the steel girder bridge, B-16-FM. The B-16-FM bridge's data show these relationships more clearly for two reasons: The first is because of the data being collected during times of greater temperature ranges, and second is due to the nature of the bridge, because in B-16-FM the girders are steel and on rollers, the bridge is under more direct sunlight, and the joint is more severely clogged. Figure 5.4 shows some data from B-16-FM that confirms the same relationships seen in C-17-AT's data above. When evaluating the middle portion of Figure 5.4, one can see that the temperature varies very little, as are the displacement and stress compared with either end of the data where significantly greater temperature ranges and variance in displacement and stress are observed.

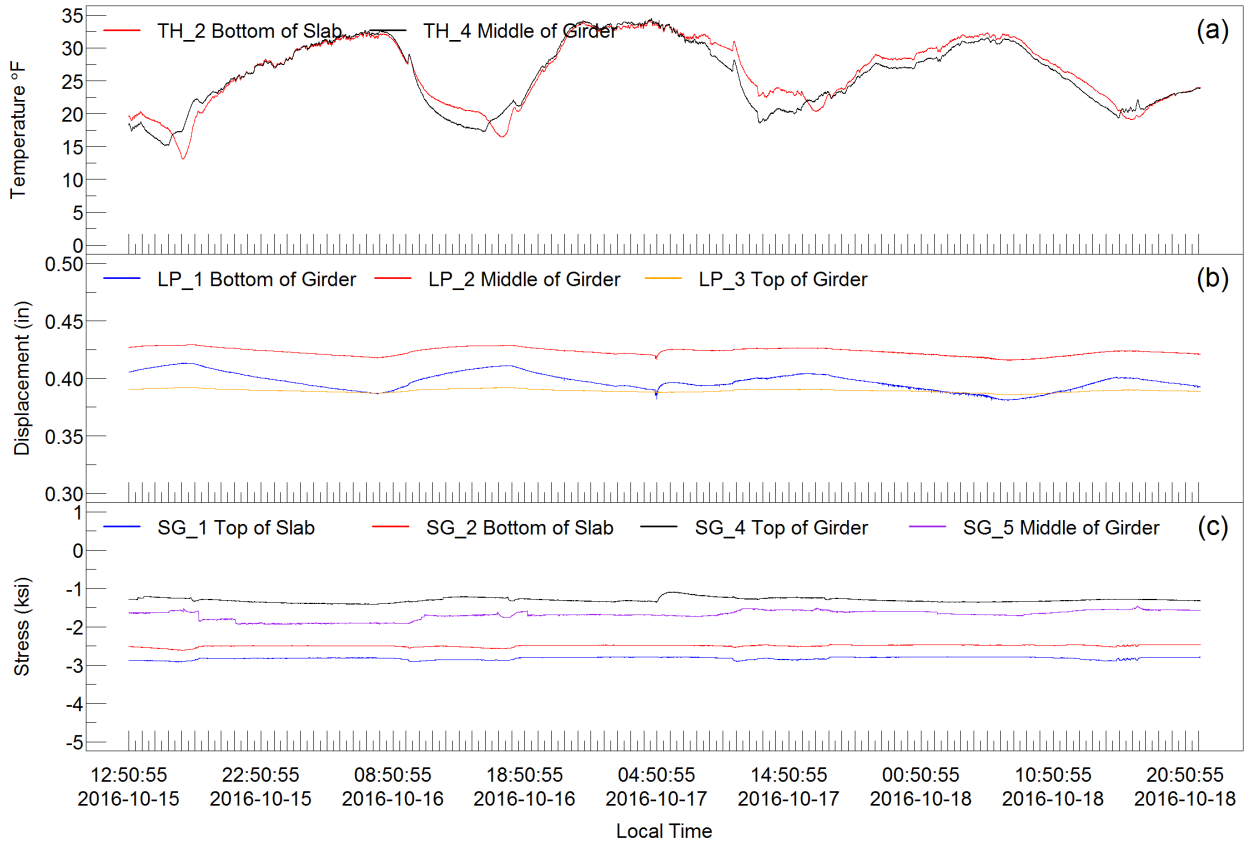

Figure 5.3 C-17-AT bridge sensor data October 15 through October 18, 2016
(c) Thermocouple Data, (b) Linear Potentiometer Data, (c) Change in Stress Data.
Note: ℃ = (℉ – 32)/1.8; 1 in = 25.4 mm; 1psi = 6.89 kPa

From these initial correlations, it can be concluded that not only is the temperature change affecting both the expansion joint's movement but also the stress experienced in the vicinity of the joint. When the temperature has a similar daily variation of about or less than 10°, the average stress varies by less than 0.25 ksi for the concrete bridge and 3 ksi for the steel bridge, and displacements vary by about 0.02 in. and 0.5 in., respectively. However, when the daily temperature range changes from day to day and is larger (15° or more), the joint experiences larger stress and displacement shifts. These larger daily temperature shifts cause stresses to vary by 0.25 -0.5 ksi and 5 - 7 ksi (34450 - 48230 kPa), respectively, and displacements by about 0.05 - 0.09 in. and 0.5 in. (14 mm), respectively. While these values are still not large, they should be considered carefully when discussing the possible removal of the expansion joint. Additionally, for the reinforced concrete bridge, C-17-AT, the data collected so far is for small temperature ranges and the stresses and displacements are likely to increase as the temperature range increases through the changing seasons. This is also indicated by the CSiBridge model parametric study and parts of the LCCA discussed below in Sections 6 and 7, respectively.

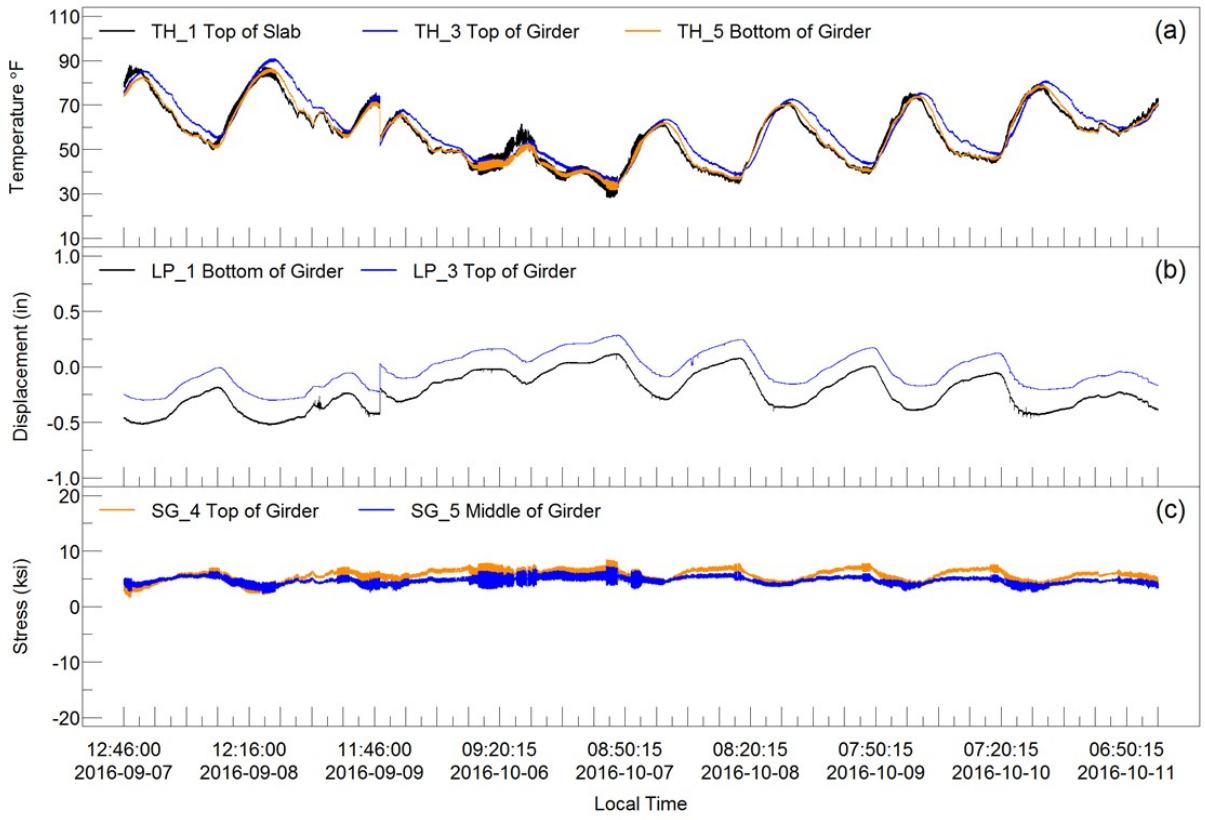

Figure 5.4 B-16-FM bridge sensor data September 7 through October 11, 2016
(d) Thermocouple Data, (b) Linear Potentiometer Data, (c) Change in Stress Data.
Note: ℃ = (℉ – 32)/1.8; 1 in = 25.4 mm; 1psi = 6.89 kPa

A concept worthy of recognition is the difference in timing between critical thermal movements and critical thermal stresses. The maximum bridge expansion and contraction occur at the joint during the warmest days in summer and the coolest nights in winter, respectively. However, the maximum thermal stresses due to the presence of thermal gradients through the depth of the superstructure occur during the warming of the bridge in the early afternoon or the cooling of the bridge in the evening rather than that in the morning (Moorty, 1992). Verification of this concept and further understanding of the heating and cooling cycles on Colorado bridges can be further understood with temperature data from instrumentation of in-service bridges, such as C-17-AT and B-16-FM.

Although current AASHTO provisions only require consideration of total longitudinal thermal movement based on average bridge temperatures, stresses due to temperature differentials in the cross section were shown to commonly be above +/- 5 ksi (34450 kPa) in steel box girder bridges in Texas (Chen, 2008). Although different girder material, widths, depth, and bridge location would change the value of these stresses, as shown above, it is clear that the significance of these stresses is worth analyzing in Colorado's reinforced concrete and steel bridges.

The significance of the thermal gradient across the depth of the bridge is justified not only through the correlation between the temperature measurements and corresponding stresses, but also by calculating and comparing the maximum temperature difference. The maximum temperature differential through the depth of the bridge was calculated from the thermocouple data and compared with the stresses experienced by the bridge, as seen in Figure 5.5. The peaks in stress correlate with the larger magnitude temperature

differences. Furthermore, the warmer the season becomes the greater the maximum difference in temperature across the girder's depth and the greater the stresses experienced.

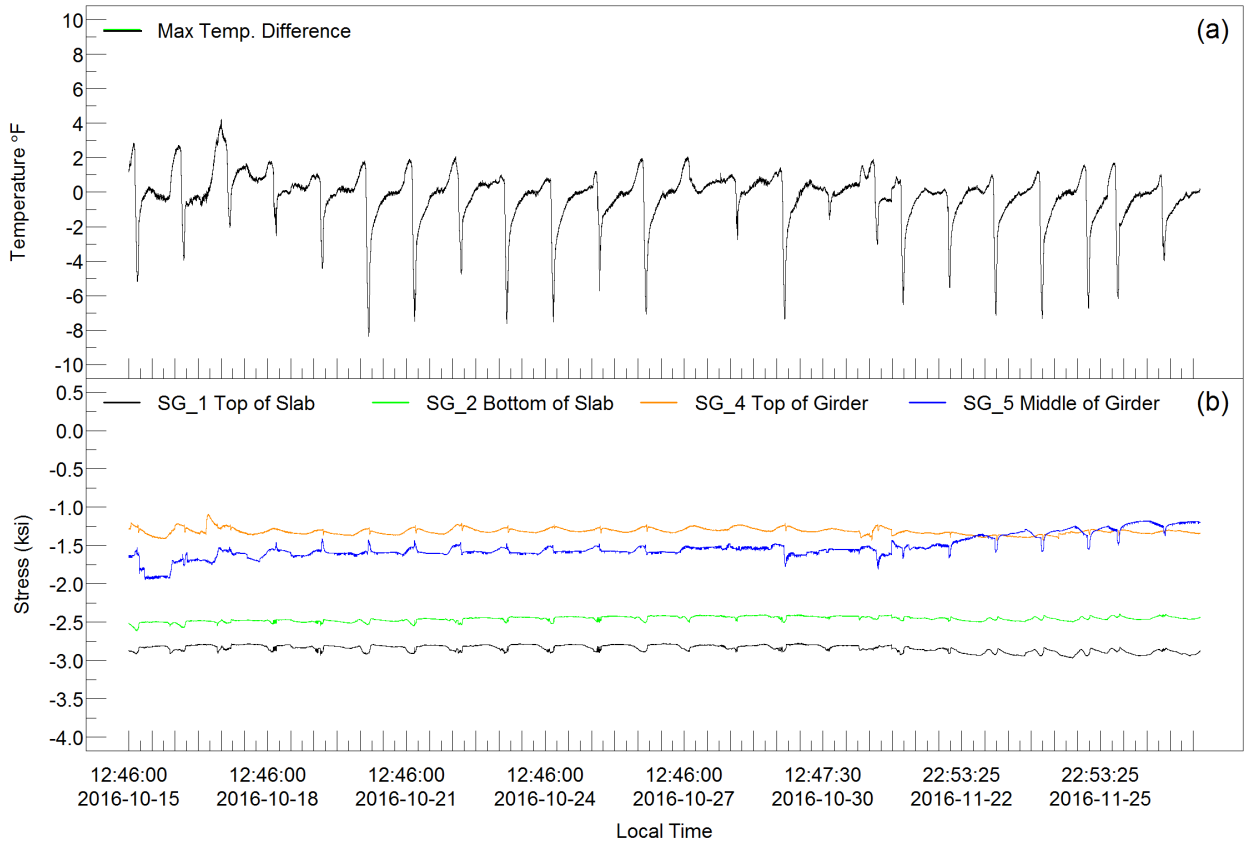

Figure 5.5 Maximum temperature difference through depth vs. stress data
(a) max temperature difference, (b) change in stress data
Note: ℃ = (℉ – 32)/1.8; 1 in = 25.4 mm; 1psi = 6.89 kPa

5.4 Thermal Gradients and Bridge Deterioration

The next step is to compare these thermal gradients through the depth of the joint with standard design gradients. First, the temperature gradient with the minimum temperature and the average of the temperature gradients in the 10th percentile of measured temperature and, second, the temperature gradient with the maximum temperature and the average of the temperature gradients in the 90th percentile of measured temperature were plotted to see what shape the thermal gradient formed on the joint, as seen in Figure 4.6 (c) below. The standard thermal gradients were also plotted on the depth of the girder for full comparison. What is initially apparent is that the minimum and maximum gradients have opposite shapes, as seen in Figure 4.6 (c), although the maximum temperature gradient has a more gradual slope when compared with the minimum. Nonetheless, when compared with the shape of the New Zealand and the AASHTO standard temperature gradients, as shown in Figure 5.6 (a) and (b), respectively, they do not match (AASHTO, 2012; New Zealand, 2013).

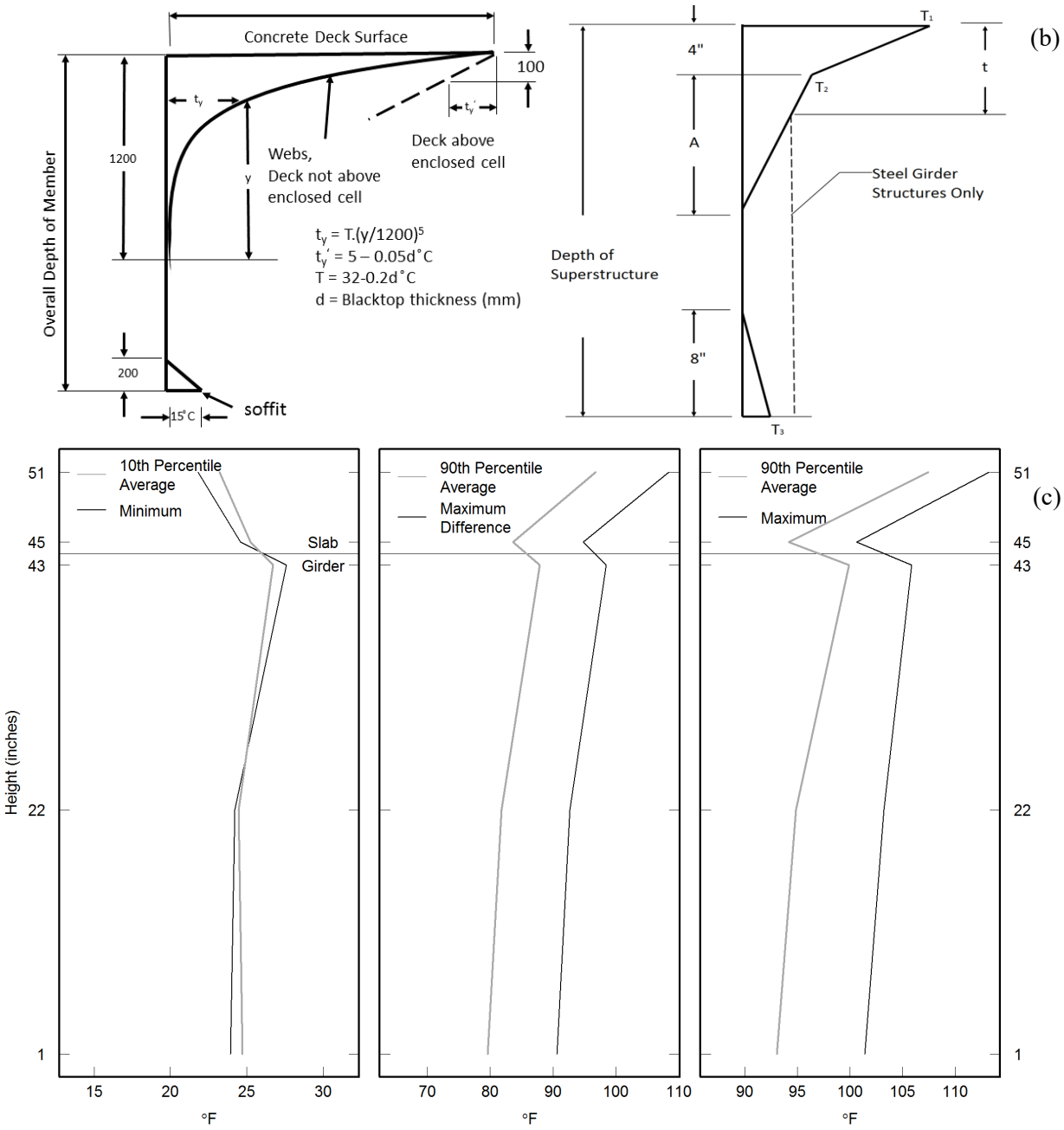

Figure 5.6 Design standard vs. measured temperature gradients. (a) New Zealand (mm) (17), (b) AASHTO (in) (1), (c) measured temperature gradients
Note: ℃ = (℉ – 32)/1.8; 1 in = 25.4 mm

The maximum gradient is the most similar to the AASHTO standard with its positive slope in the top half. The bottom half is still, however, different than the standard. Furthermore, neither of the two gradients matches the New Zealand standard, which has a more parabolic shape and a varying slope. Neither standard appears adequate for either a maximum or minimum temperature gradient on C-17-AT. This implies a need for further research into the accuracy of these temperature gradient design standards and modification for more accurate predictions. However, the comparison does indicate that the standards are in some ways conservative given that they appear to predict a higher temperature then the actual temperature being experienced by the joint.

Finally, it should be noted that the standard temperatures are to be applied on top of the temperature at which the bridge was built, while the gradients shown from the measured data are just the raw temperatures experienced by the bridge, and these gradients are only for the winter months due to limited C-17-AT data. This does not impact the ability to compare shapes of the gradients and if anything shows that the standard gradients might be aimed at summer temperature gradients. However, even in the summer, they may prove too conservative given the current observations.

While conservatism is beneficial in providing safety factors, economical design should also play a role. Furthermore, an economical design and solution is what many DOTs are most interested in when considering bridge expansion joints. Furthermore, when instrumenting bridge C-17-AT and bridge B-16-FM, the severe clogging of the joints and associated deterioration in the surrounding decking and abutments was noted. The deterioration at the joints and abutments can be seen in Figure 5.7 and Figure 5.8 for Bridge C-17-AT and Bridge B-16-FM, respectively. Perhaps the greatest insight from these data is the consequences of the partially locked joint, as evident by the present stresses shown above with their correlation to the temperature experienced and the deterioration shown below. This type of deterioration, cracking and spalling, is likely in part due to the clogged joints inducing stress when the bridge tries to expand. If the joint was fully functioning, little to no stress would be present in or around the joint. The joint is not fully locked, as shown by the linear potentiometers measuring displacements. While movement can initially be seen as good because it proves the joint is not fully blocked, this, in combination with the present changes in stress, indicates the potential for fatigue and deterioration.

Figure 5.7 Deterioration of C-17-AT abutments and joints

Figure 5.8 Deterioration of B-16-FM abutments and joints

With this in mind, the measured thermal gradients were utilized for the analysis of temperatures impact on abutments, assuming clogged joints, as were seen in the field. In order to perform this analysis, the maximum and minimum temperature gradients measured for each bridge were applied to that bridge's CSiBridge model. This created four models, and each was run and the forces at the ends of the girders due to the thermal loading were recorded. The average force for each case and the average temperature for each gradient was calculated, as seen in Table 4-1 below. These average values were used to find a linear equation relating force to temperature for each bridge, and the equations are shown below. The relationships these equations represent, while they are approximate due to the need to use averages for simplicity, show a direct relationship between the stresses experienced by the bridge and abutments due to temperature and clogged joints. The equations differ by a magnitude of 10. This could be partially due to the steel data, and thus thermal gradients having six months of data that span winter and summer, compared with the concrete bridge, C-17-AT, with only three months of winter data to utilize. The limited amount and type of data available for the concrete bridge C-17-AT is likely causing it to have a significantly smaller slope due to less variance in temperature limiting the simulated relationship. This is further supported when comparing the average maximum and minimum temperatures for the two bridges. C-17-AT had significantly, and unrealistically, low average temperatures with a max at only 24℉. However, until further data are obtained, the thermal gradients were assumed to uniform so that a greater range of temperatures could be analyzed in the models and a more realistic equation could be determined. This process is discussed and utilized in Section 7 as part of the LCCA for bridges with expansion joints. The analysis includes the impact of clogged joints on their abutments.

Table 5.1 Temperature and force for C-17-AT and B-16-FM

Variable	B-16-FM	C-17-AT
Average Force – Max Temp. Gradient	31.8 ksi	1.6 ksi
Average Force – Min Temp. Gradient	7.6 ksi	0.75 ksi
Average Temperature – Max Temp. Gradient	102.8℉	37.75℉
Average Temperature – Min Temp. Gradient	23.75℉	15.25℉
Equation	Y=0.306*T	Y=0.038*T

5.5 Summary and Preliminary Conclusions

The impact of temperature, thermal gradients, and overall shifts in temperature due to changing seasons has a significant effect on bridge expansion joints in Colorado. The potential for 0.01 in. of movement and 0.5 ksi in. stress increase on concrete bridges regularly, and 0.5 in. movement and 5 ksi stress on steel bridges regularly is not negligible. Furthermore, these preliminary data on concrete bridge C-17-AT only accounts for mid -winter and does not account for the hottest or coldest days of the year, which can cause the greatest movement in the expansion joint. This fact should be kept in mind when considering these preliminary findings and their application. However, these limited observations do imply that if CDOT is interested in removing an expansion joint, the bridge superstructure and retrofit option would need to support the movement of the bridge at the abutment and the potential for abutment stresses due to movement. These displacements do not appear so great as to require the use of an expansion joint. On the other hand, more data at different times of the year are needed for a more definite recommendation.

Removing the joint would eliminate the concentrated stresses that could prevent possible fatigue cracking at joints. This would not eliminate the stresses introduced at the abutment and could introduce more. In the event of joint removal, the abutments would need to be analyzed and reinforced to support these stresses due to the temperature gradients and thermal contraction and expansion. Nonetheless, the impact and potential benefits of constructing a bridge without deck joints or bearings, or eliminating all deck joints and bearings by retrofitting an existing bridge, is significant. The behaviors of interest and parameters influencing them are numerous and vary for new construction and existing bridges. These parameters and costs are analyzed further in Chapter 7. Additionally, based on the comparison of thermal gradients with standard gradients, further research is needed to determine a more accurate standard for temperature gradient prediction. This would not only help predict stresses around a joint due to thermal gradients, but also benefit abutment design for continuous or retrofitted bridges. All of which could potentially lead to a more economical and safe design. Finally, more scientifically verified information on the response of reinforced concrete and steel bridges and development of well-understood replacement connections would assist in furthering the concept of deck joint replacement and, therefore, decrease maintenance costs and increase the durability of bridges' superstructures.

6. PARAMETRIC STUDY FOR C-17-AT

6.1 Introduction

Described below is the numerical model and parametric study performed using the CSiBridge three-dimensional numerical C-17-AT model, which was validated using the control load test discussed in Section 4. The objectives of the parametric study were to consider the different code-based thermal gradients and the effects of these thermal loads on the joint and bridge performance. The behavior of the bridge under different amounts of joint clogging while under thermal loads was also examined. Different joint elimination scenarios were also examined to provide DOT engineers with the implications of different joint removal alternatives. Three joint removing connections, three thermal load scenarios, and three joint clogging scenarios were analyzed.

6.2 CSiBridge Finite Element Numerical Model

The finite element software chosen was CSiBridge, which is used by many practicing engineers. The software was created by the same developers as SAP2000 and was chosen by CDOT due to its heavy presence in private consulting.

The finite element model was built using thin shell elements for the girders and slab, as seen in Figure 6.1. The thin shell elements were assigned dimensions and area section properties to match the properties of bridge C-17-AT. Rebar was included for both compressive and tensile reinforcement in the girders and for two-way slab action in the concrete deck. For concrete properties, the compressive strength of 4000 psi concrete was defined along with a modulus of elasticity of 3604 ksi. The shell elements were meshed at six-inch intervals to provide uniform response and minimize computational time.

Composite action was obtained using short frame elements connecting the girders to the slab. These short frame elements were assigned Grade 50 steel properties with a modulus of elasticity of 29000 ksi. These elements represented the shear studs used in traditional reinforced concrete construction to connect girders to slabs. The stiff links are shown as blue lines connecting the node on the girder to a node on the slab in Figure 6.2. These stiff link shear studs were sized so that their cross-sectional area matched that of the shear connectors detailed in the construction documents in Appendix A.

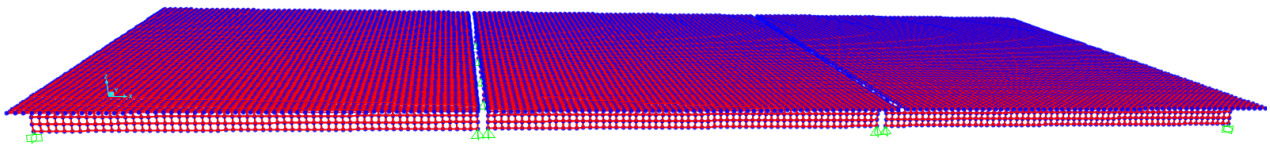

Figure 6.1 C-17-AT finite element model

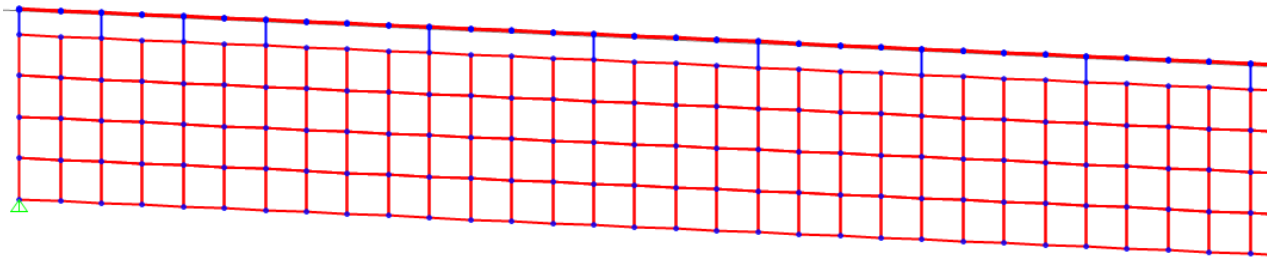

Figure 6.2 C-17-AT finite element model ties between girder and slab

Several loading scenarios were analyzed. Self-weight dead loads, point loads, and uniform loads were applied for the first verification stage. Theoretical calculations were also made using these same loads and composite beam theory in order to perform the initial verification. The second verification stage, discussed in Chapter 4, used a CDOT A-40 truck's axle loads on the instrument bridge and in the finite element model. The strong agreement between the theoretical calculations (within 10%) as well as the field tests (within 15%), and the CSiBridge finite element model, provide the confidence needed for the parametric study to be completed.

The boundary conditions for the bridge were fixed at the abutment ends because of bridge C-17-AT being monolithic with the abutment. At the pier caps, due to the presence of bearing pads, the connection is not a true pin. Instead, the bearing was retained as a spring boundary connection fixed in the vertical direction and with a spring stiffness value of 45 kip/in. due to friction in the horizontal and transverse directions. The friction resulted from the interaction between the concrete girders and the neoprene bearing pads on the pier caps.

6.3 Joint Retrofitting Options Analyzed

There are multiple alternatives for connecting two spans after the removal of a joint. This parametric study focuses on past alternatives that have been considered and utilized by transportation agencies. This allows for the results to be related to typical field practices among DOTs. The three connection types chosen were 1) deck only, 2) girder only, and 3) deck and girder full-moment splice. Localized stresses in the girder and deck were examined for each connection type.

To model the deck only connection, the slab was connected in the finite element model using the same slab type of shell elements. The girder was connected similarly by connecting the girder sections with the same shell elements. The full moment splice was achieved by connecting the slab and girders with their respective shell elements.

In order to assess the superstructure's response to different thermal loading scenarios in the modeled bridge, while also looking at the effects of removing joints, three vertical thermal distributions were utilized. Two of these distributions had a gradient through the depth of the bridge while the third had a uniform thermal distribution. The first thermal gradient considered was adopted from the AASHTO LRFD Bridge Design Specifications, and the second thermal gradient considered was based on the New Zealand bridge design code. This New Zealand code was selected because a previous study conducted by French et al. (2013) showed reasonable agreement between this fifth order gradient curve and the field-measured thermal loading on the bridge studied. Finally, a uniformly distributed temperature change of 50°F was applied. The uniform temperature distribution entailed an increase of 50°F, which was applied to the entire cross-section along the length of the spans in order to determine how thermal stress from a uniform thermal gradient compares with varying vertical thermal gradients. An increase of 50°F was chosen because all bridges in Colorado experience this temperature change over the course of a year. The AASHTO and New Zealand thermal gradients are shown in Figure 6.3.

The temperatures were applied to the bridge model using a piece-wise thermal gradient method modeled after an example, "Temperature Changes and Fabrication Errors," in the textbook *Matrix Analysis of Structures* by Aslam Kassimali (2012). The piece-wise approximation divides the girder and slab into elements and each element is assigned a single temperature based on the equivalent piece-wise distribution of the thermal gradient. For the model of C-17-AT, the bridge's depth is divided into five shell elements, including the slab thickness. The piece-wise approximations for the AASHTO, New Zealand, and uniform thermal gradients are shown below in Figure 6.4.

(a)

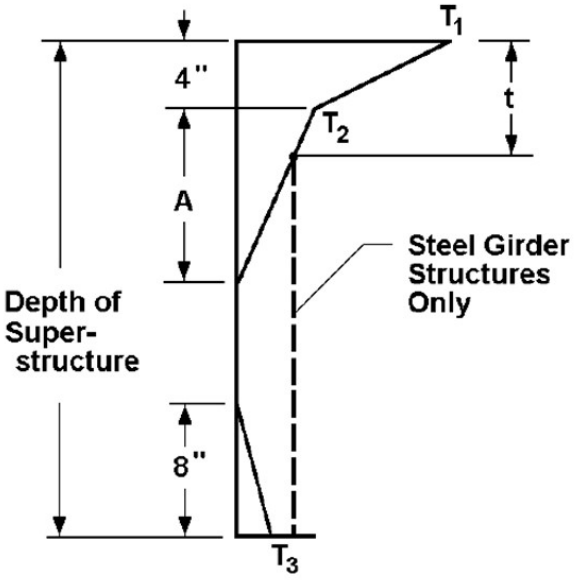

(b)

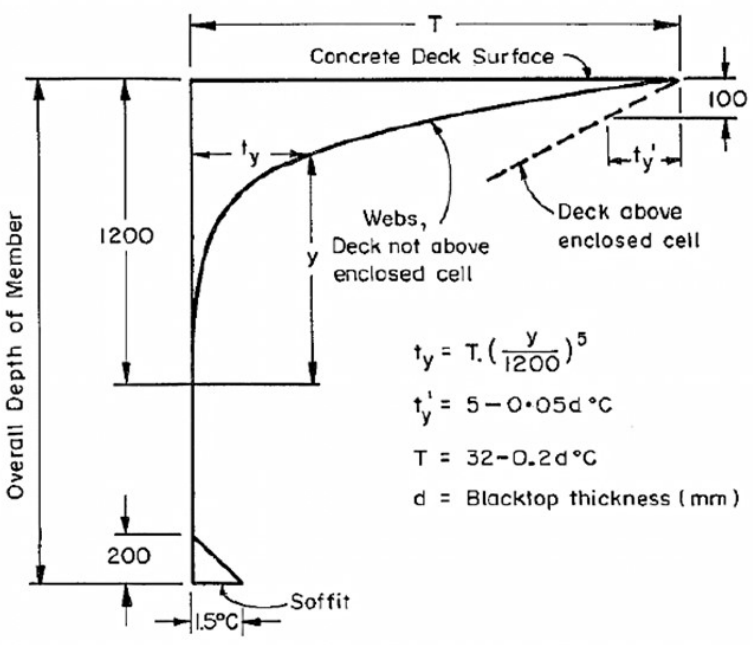

Figure 6.3 (a) AASHTO thermal gradient, (b) New Zealand thermal gradient

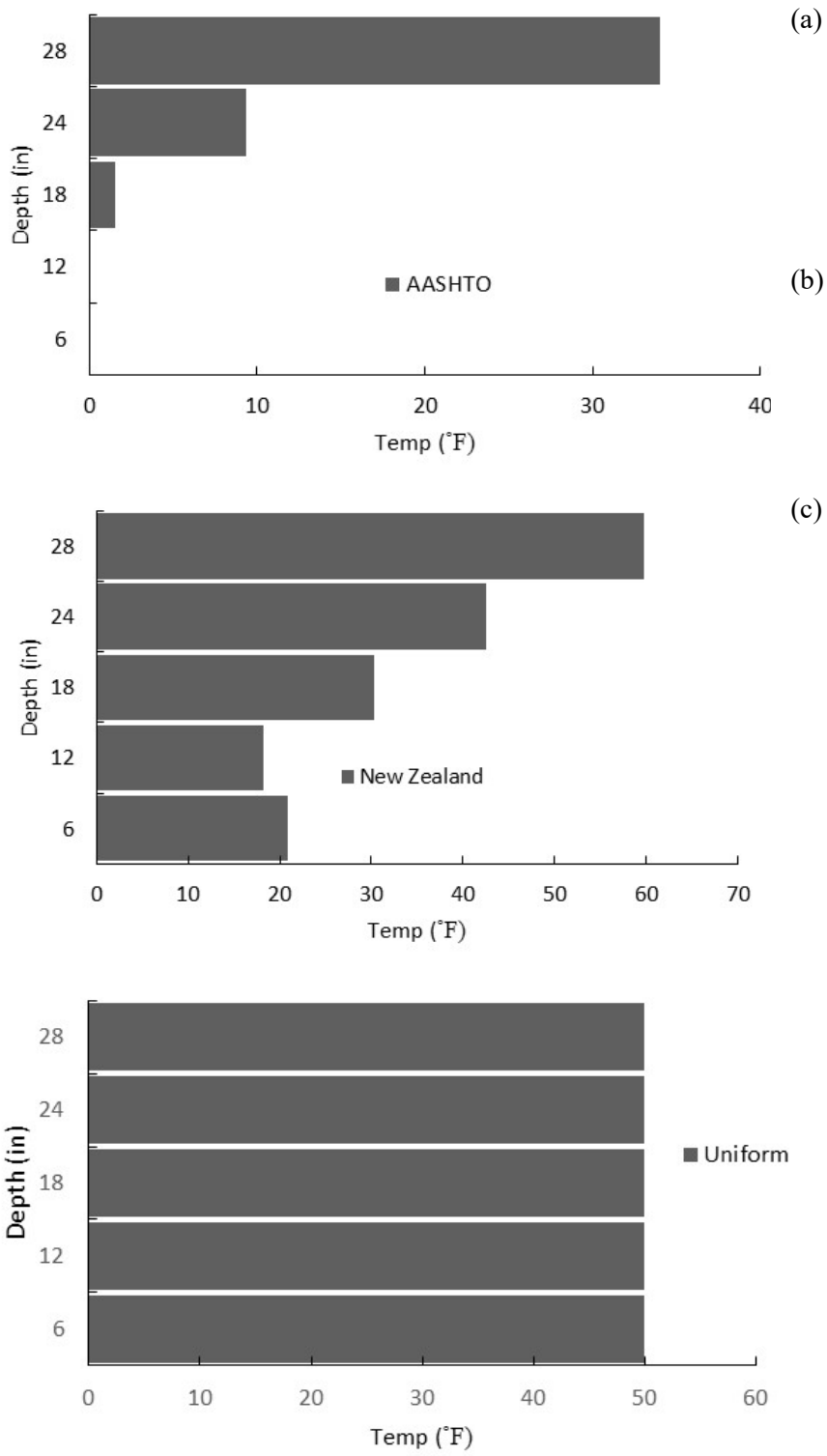

Figure 6.4 Piece-wise approximation: (a) AASHTO thermal gradient, (b) New Zealand thermal gradient, (c) uniform gradient

6.4 Joint Clgging Stiffness Considered

Past research has determined that joints are often clogged with debris soon after being placed into service (Chen, 2008). In order to model this clogging in CSi Bridge, axial stiffness coefficients were assigned to links connecting the slabs across the joints. These axial stiffness coefficients were calculated based on the moduli of elasticity of soil types that commonly clog joints, primarily sand and gravel. Stiffness values (k) are typically calculated as EA/L, where E is the modulus of elasticity, A is the area, and L is the length of the element.

The soil volume clogging the joint is the structural element considered for the axial stiffness. Gravel has a typical modulus of elasticity of 22 ksi (150 MPa) and sand has a modulus of elasticity of 7 ksi (50 MPa) (Briaud, 2013). The length of the clogging debris was taken as the joint opening, which was 0.125 inches (L), as measured in the field. Axial stiffness was determined for each soil type and a blend. The stiffness placed evenly across the joint by placing links every six inches in the transvers direction. This assumes that the joint is evenly clogged along its length, and consequently assumes no torsional effects. The axial stiffness coefficients were taken as 30 kip/in. for gravel filled joints, 10 kip/in. (~1751 kN/m) for sand filled joints, and 20 kip/in. (~3502 kN/m) for a joint that is clogged with a mixture of gravel and sand. The same methodology was used in analyzing the steel bridge, as outlined in Rager (2016).

6.5 Parametric Analysis Matrix

The effects of the different combinations of connection type, clogging material, and thermal gradients on local and global performance were examined using a parametric study matrix, as shown in Figure 6.5. The two types of joint alterations, clogging and connection type, were analyzed with each of the three thermal gradients. All analyses were conducted using the finite element model of C-17-AT, and the results are discussed in Subsection 6.6.

Thermal Gradients	Stiffness of Clogging Links Across Joints			Connection Retrofit	
	10 kip/in	20 kip/in	30 kip/in	Deck only	Deck and Girder
AASHTO	x	x	x	x	x
New Zealand	x	x	x	x	x
Uniform (+50˚F)	x	x	x	x	x

Figure 6.5 Parametric study matrix

6.6 Analysis Results and Implications

The results and implications of the parametric study analysis are divided into two sections: those associated with clogged joints and those associated with the retrofit connection types. The results from the clogged joints are presented as line graphs, because the stiffness values assigned to the two-joint links are continuous quantitative variables. However, the retrofit connection types are discrete qualitative variables, and are therefore presented as bar charts for comparison.

In order to analyze the different connection types and clogged joint stiffness and their effect on global and local bridge behavior, three different load scenarios were examined: thermal gradient load only, truck load only, and thermal gradient and truck loads combined. The truck load used was an AASHTO HS2044 truck, as shown in Figure 6.6.

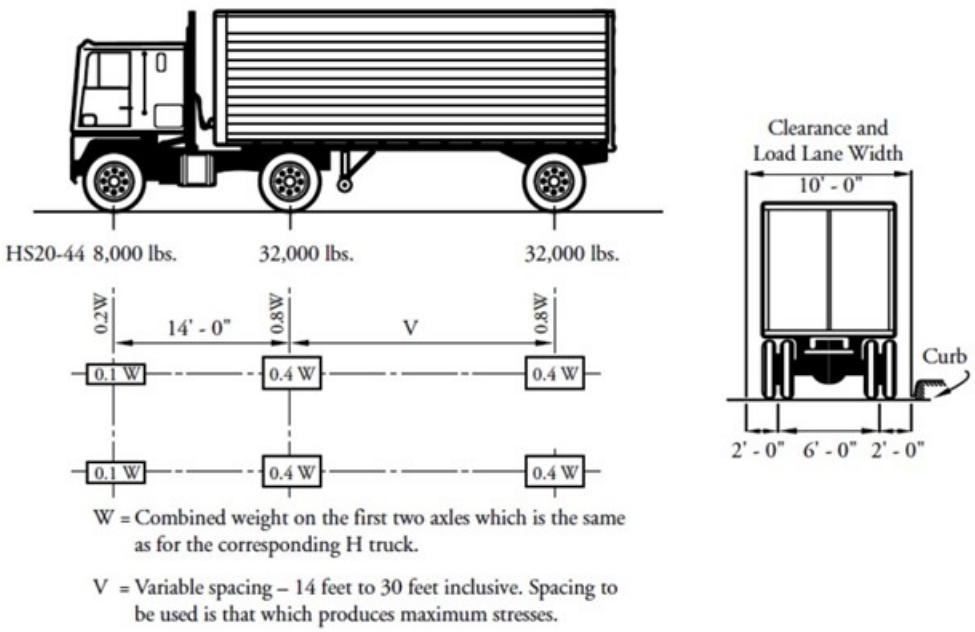

Figure 6.6 AASHTO HS20-44 truck (Precast/Prestressed Concrete Institute, 2003)

The location of the truck was determined by performing an influence line analysis to find the location that produced the maximum moment demand. This location was found to be where the front axle is over the bearing near the beginning of the span, and the back two axles are placed 14 feet apart (V=14 feet). In the remainder of the chapter, truck loading refers to this location of the AASHTO HS20-44 truck on the bridge.

6.6.1 Clogged Joint Results and Implications

The effects of clogged joints in the parametric study on the bridge are analyzed using the truck loading, thermal gradients, and values for link stiffness (k = 10 kip/in., 20 kip/in., 30 kip/in.) described above. The analysis was performed considering only the thermal and truck loads; the dead load due to self-weight of the bridge was neglected.

First, the maximum stress in the bottom of the girder at the ends and at the mid-span due only to each of the three thermal gradients was determined for each of the three link stiffness values. Figure 6.7 and Figure 6.8 show these results for the girder ends and girder mid-span. The model experienced a maximum compressive stress of 0.217 ksi in the girders at mid-span, with a 10 kip/in. link stiffness and under the AASHTO thermal gradient load. The maximum tensile stress in the bottom of the girders was 0.026 ksi in the girders at mid-span, with a link stiffness of 30 kip/in. and under the uniform thermal gradient load.

The maximum loads experienced in the girders due to all thermal gradient loads occur at mid-span. At the bottom ends of girders, the AASHTO thermal gradient is the most conservative with compressive stress at around zero due to no temp load applied at the base of this gradient. On the other hand, the AASHTO thermal load gives the largest compressive stresses at the girder bottoms at mid-span due to the larger moment induced by the gradient. New Zealand is the middle loading gradient with the uniform thermal load behaving conversely to the AASHTO gradient, giving the largest compressive stress at the bottom of the girder ends and the least at mid-span.

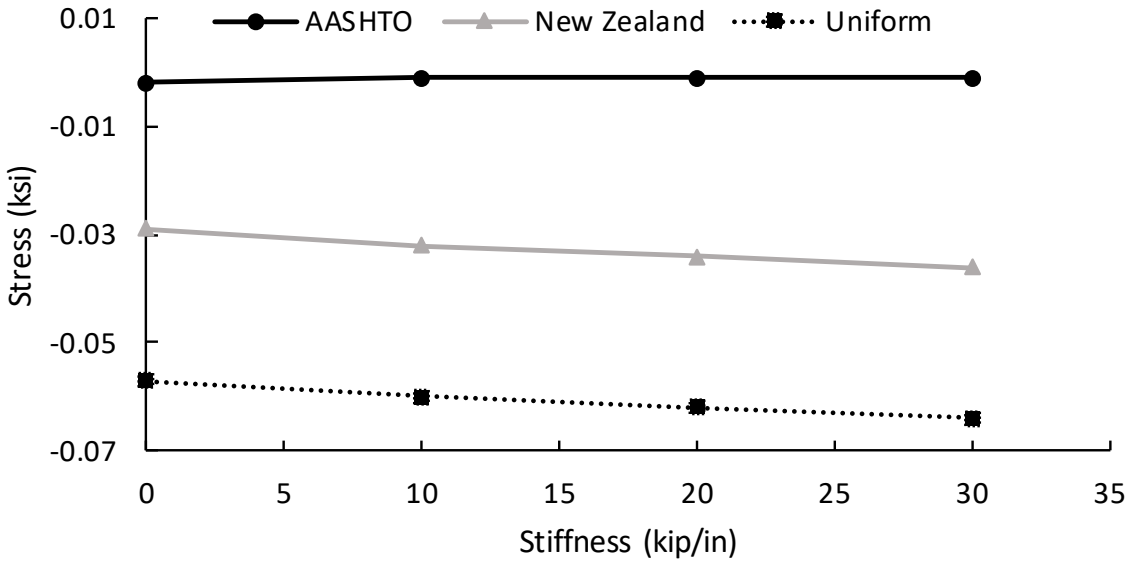

Figure 6.7 Maximum stress in bottom of girder at end

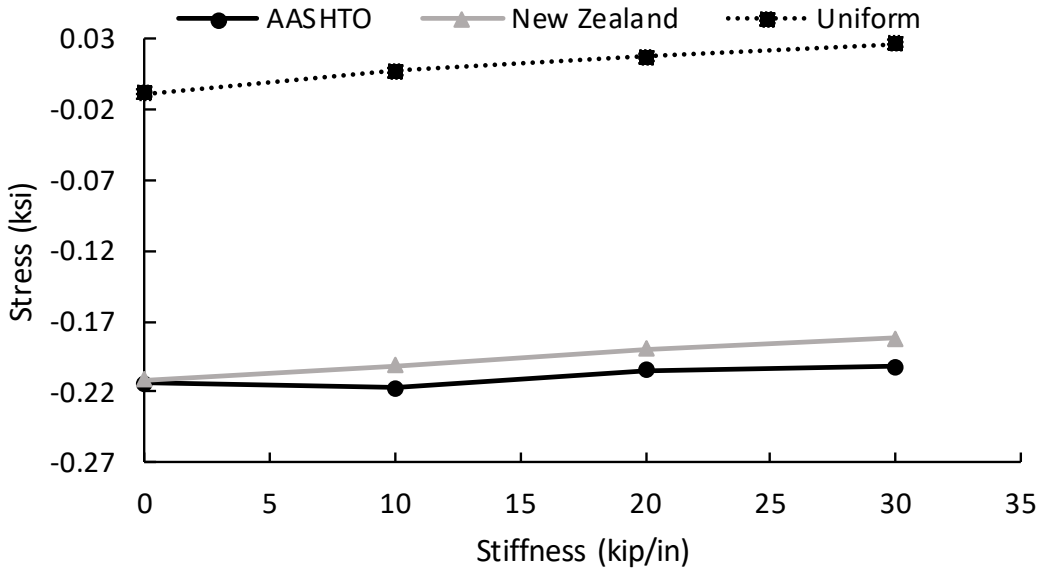

Figure 6.8 Maximum stress in bottom of girder at mid-span

The maximum in the top of the girder was also analyzed at both mid-span and at the ends due to each of the thermal gradients for each of the link stiffness values, as shown in Figure 6.9 and Figure 6.10. The maximum tensile stress for each link stiffness value was produced due to the AASHTO thermal gradient load-induced moment at mid-span in the top of the girders. This is expected since AASHTO had the highest temperature load difference between the top and bottom of the girder. The maximum tensile stress at each of the link stiffness values was produced by the uniform thermal gradient load in the girder at mid-span. Overall, comparing the two standard thermal gradients, AASHTO appears to have the more conservative gradient due to the larger difference in temp between top and bottom despite New Zealand applying a greater maximum temperature at the top.

In all four figures, the clogged joints, symbolized by the link stiffness values, do not show a significant impact on the global or local demand on the bridge superstructure. Both the stresses at the top and bottom of the girders showed relatively small changes in compressive and tensile stress under each thermal gradient load as the stiffness increased. The maximum stress range on the girders for the different stiffness values were 0.02, 0.05, and 0.06 ksi for AASHTO, New Zealand, and uniform thermal gradients, respectively, all less than 0.1 ksi difference.

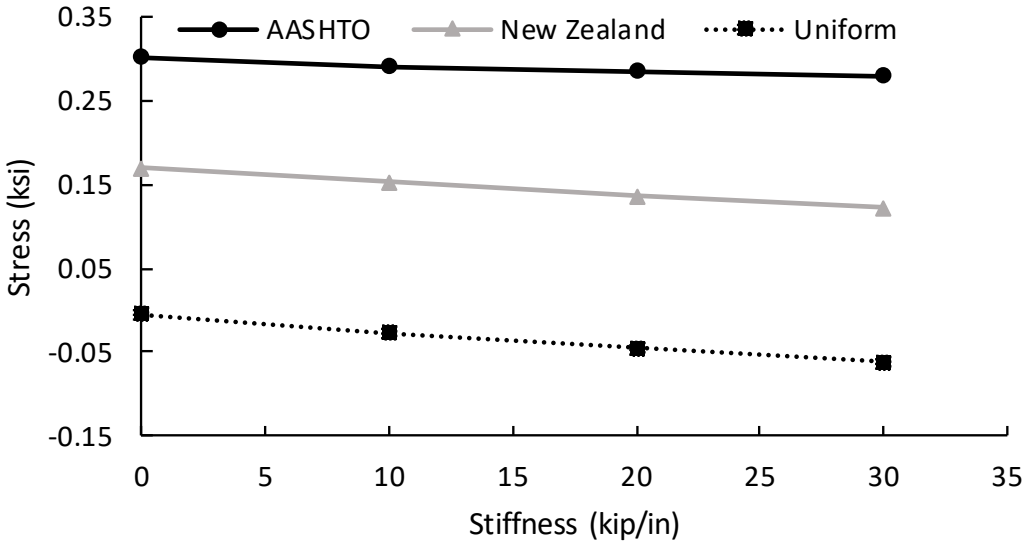

Figure 6.9 Maximum stress in top of girder at mid-span

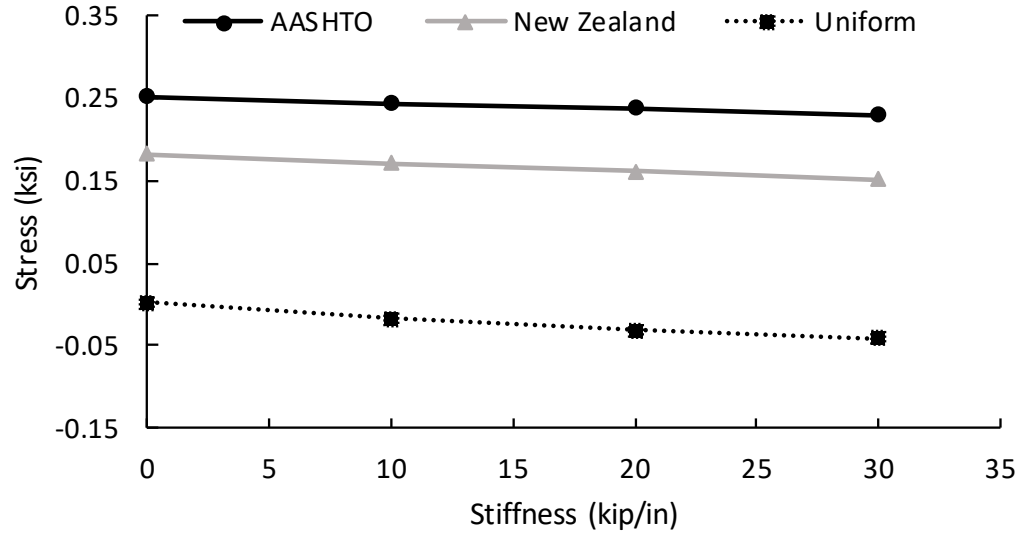

Figure 6.10 Maximum stress in top of girder at the ends

With the clogging stiffness established as not having significant impacts on the bridge's behavior, a truck load was added to the analysis. The HS20-44 truck was examined, first with only the truck, and the second combined with the thermal gradient loads. Figure 6.11 show the results of the model with the truck loading and clogging stiffness. The truck load's moment demand on the bridge decreased slightly due to the clogged joints modeled by the link stiffness values, because the simulated clogged joints hold the concrete in a negative moment region. Consequently, some moment is transferred in this negative moment region, and the positive moment region's moment demand will decrease slightly, unlike in an unclogged joint. This overall decrease is only about 0.0257 ksi, which is only 0.4% of the moment demand with an unclogged joint and as such is insignificant, reinforcing the insignificance of the stiffness of the clogged joint.

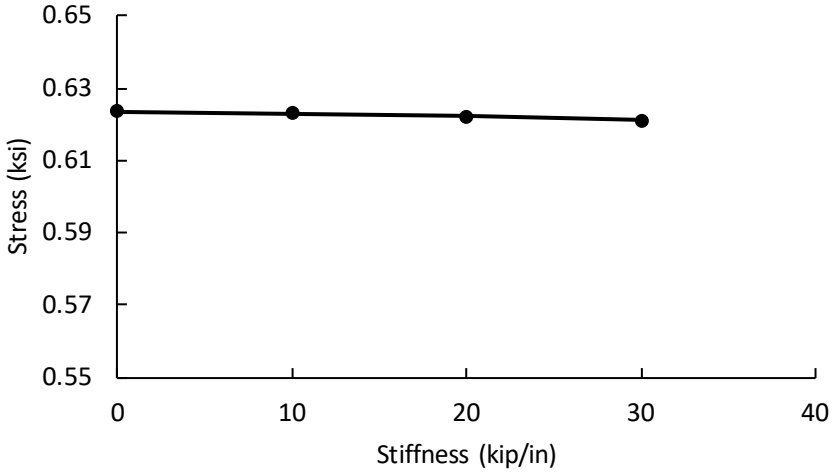

Figure 6.11 Stress demand in bottom of girder at mid-span due to moment resulting from the truck load

Next, the analysis of the thermal and truck loading combined was conducted, and the results are shown below in Figure 6.12. The uniform thermal gradient showed the most obvious change between just the thermal load and the thermal load and truck load, with an increase of about 0.6 ksi. This is likely because the uniform gradient had almost no stress at this location by itself, and thus the addition of the truck load was close to total. The New Zealand and AASHTO gradient moved from compression to tension with an average stress change of about 0.6 ksi as well, moving from about -0.22 ksi to 0.38 ksi. The results indicate that the truck load counteracts the thermal load on the bridge.

Additionally, similar to when examining the thermal gradient loads only, the combined loads showed negligible changes in stress relative to the increase in clogged link stiffness. The maximum stress ranges on the girders for the different stiffness values were 0.012, 0.026, and 0.03 ksi for AASHTO, New Zealand, and uniform thermal gradients, respectively.

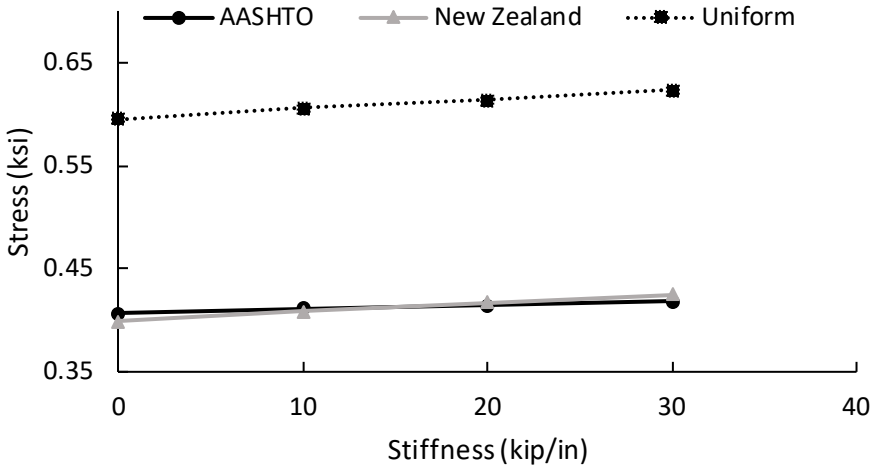

Figure 6.12 Moment demand due to thermal and truck load in bottom of girder at mid-span

6.6.2 Joint Retrofit Connection Results and Implications

First, the maximum stress at the bottom of the girders near the bearings caused by the thermal gradients only was determined for each connection type. Figure 6.13 shows these stress values. The stresses induced by the AASHTO recommend that thermal gradient is a lower tensile stress when compared with the New Zealand gradient; whereas, the uniform thermal gradient gives the largest compressive stresses. This is to be expected because the uniform thermal gradient is a uniform temperature increase of 50°F throughout the depth of the structure. Therefore, the temperature load at the bottom of the girder for the uniform gradient of 50°F is significantly larger than the 20.82°F and 0°F for the New Zealand and AASHTO recommended thermal gradients, respectively. This larger temperature load will cause greater thermal expansion of the concrete and consequently greater compressive stresses. Conversely, the AASHTO recommended thermal gradient has the lowest temperature load at the bottom of the girder; therefore, it is reasonable to conclude it should produce lower compressive stresses than when the bridge is exposed to only the thermal loads with the two retrofit options. The deck only connection produces lower stresses than the full moment splice connection for all three thermal gradients. The significant difference is likely due to the boundary conditions on the bridge; the abutment connections for the superstructure are fixed conditions. Thus, when the deck is connected, the joints are now transferring a little of the moment capacity contained in the fixed ends through to the center span. However, when the deck and girders are connected in a full moment splice, that entire moment can be carried throughout the length of the bridge and across all spans, significantly increasing the moment capacity. This allows a negative moment region across the supports, and increases the moment capacity and thus the stress in the girders. For the AASHTO and New Zealand thermal gradients, the full moment splice increases the tensile stress significantly. This is likely due to the lower temperature loads at the bottom of the girder when compared with the top. The difference of 30° to 40°F creates significantly greater compression in the top versus the bottom and induces a moment that the full moment splice allows to be carried, increasing the stress.

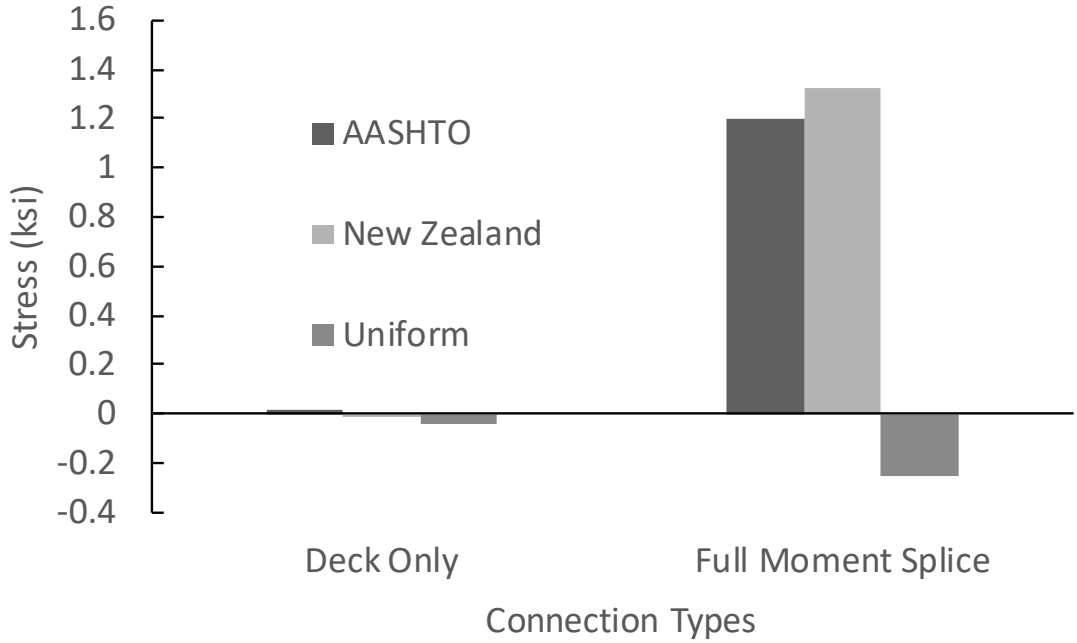

Figure 6.13 Maximum stress at bottom of girder due to thermal gradients only

In order to fully evaluate a potential increase in the span's moment capacity for the two retrofit connection types considered, the analysis was performed for only the truck load with each of the connection types. The stress values due to the truck loading are shown below in Figure 6.14. The maximum stress at the bottom of the girders near the bearings was measured to gauge the moment demand for each connection type. When the deck only connection was examined, the truck load induced a tensile stress in the girders of 0.06 ksi, whereas when the full moment splice was examined the truck load induced a greater compressive stress of 0.46 ksi. This change from tensile to compressive stress indicates an increase in moment capacity of the superstructure, corresponding to a 75% decrease in moment demand.

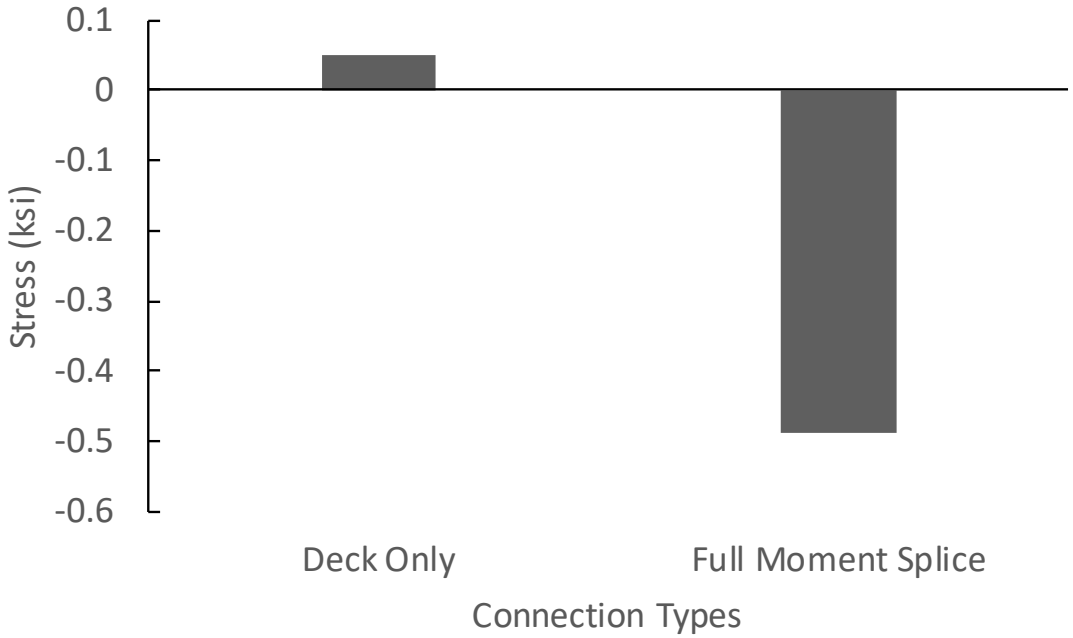

Figure 6.14 Maximum stress at bottom of girder due to truck loading only

Once thermal gradient loads and truck loading scenarios were analyzed separately, analysis was completed for combined thermal and truck loading for both connection types. The stress at the bottom of the girders near the bearings due to both loads is shown in Figure 6.15. Comparing Figure 6.13 and Figure 6.14 with Figure 6.15, it is evident that under the stresses increased in tension with the "deck only" connection. Under the uniform thermal gradient and deck only retrofit connection, the truck load caused the stress to switch from compressive to tensile. On the other hand, the truck load in the full moment splice connection decreased the tensile stress under the AASHTO and New Zealand thermal gradients, and increased the compressive stress when the uniform thermal gradient was applied. This change in stress illustrates how the connection type for joint retrofitting influences global moment demand on the bridge when considering thermal gradients. The truck load counteracts the thermal loads once again, and the full moment splice increases the bridge's moment capacity significantly compared with the deck only connection.

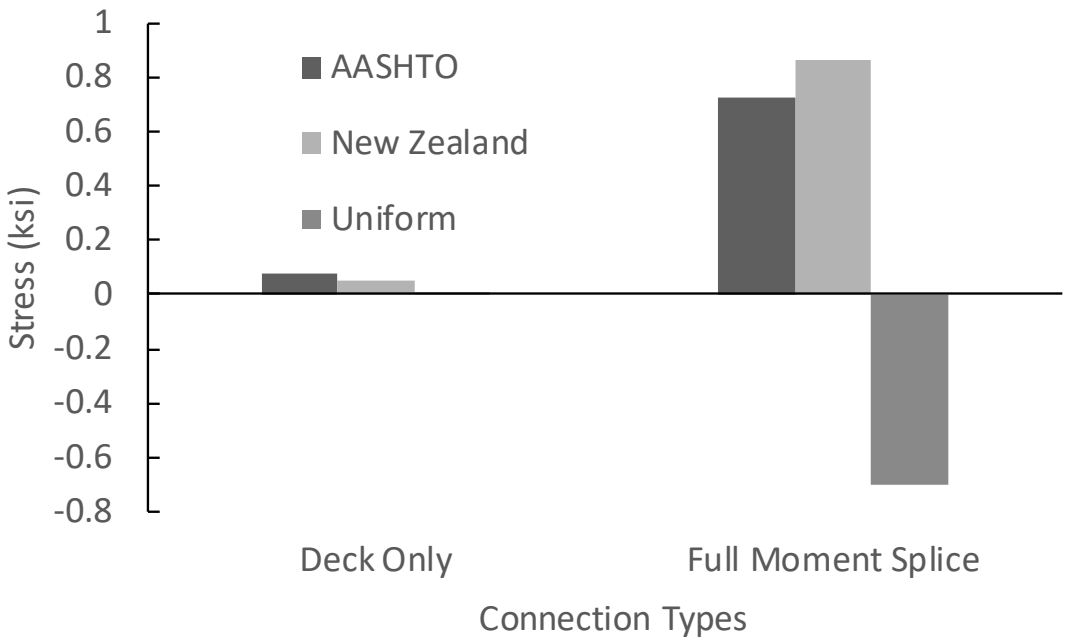

Figure 6.15 Maximum stress at bottom of girder due to thermal gradients and truck load combined

6.7 Conclusion

These parametric study results illustrate the differences between the thermal gradients and joint retrofit connection types considered. The thermal gradients, when subjected to different joint clogging stiffness values, showed relatively little change in stress as the stiffness increased. At mid-span, the AASHTO thermal gradient showed the greatest stresses, while at the girder ends the uniform thermal load showed the greatest stress. Applying a standard truck load to the bridge counteracted the stresses and moments induced by the thermal loads.

When applied to the different connection types, the thermal gradients and truck load's impact on the bridge's moment capacity was examined. The New Zealand thermal gradient showed the greatest difference in stress load for the two different connection types. This can be attributed to the fact that the New Zealand thermal gradient has the greatest temperature at the top of the gradient, creating a difference of about 40°F between top and bottom, and inducing significant expansion at the top with the potential for moment transfer when fully connected. A decrease in moment demand was observed when the full moment splice connection was used under only truck loading. However, the moment capacity and demand increased when the truck load was combined with the AASHTO and New Zealand thermal gradients and a full moment Splice was utilized. This increase in demand is influenced by the fixed ends of the bridge at the abutments, which allow for moment transfer throughout the length of the bridge when a full moment splice connection is used. With the full moment splice connection giving the greatest increase in moment capacity, the full moment splice will be assumed for the retrofit to continuous analysis in the LCCA in Section 8.

7. PARAMETRIC STUDY FOR B-16-FM

7.1 Introduction

One of the primary objectives of this study was to establish a finite element model to assess thermal movements, thermal stresses, and joint removal retrofit options. The developed design and assessment procedures were developed with the intent to be used in industry for eliminating bridge joints. Therefore, choosing a finite element software widely used by practicing engineers is vital to correct implementation of the developed procedure. CSi Bridge software (same developers as SAP2000) was chosen by CDOT due to its prevalence of use in private practice. This chapter focuses on the model for the steel bridge, B-16-FM. Theoretical calculations were performed using composite beam theory in order to verify the finite element model.

Multiple loading scenarios were considered. Dead loads due to self-weight, uniform loads, and point loads were considered first during the verification process. Then, live loads were applied using the AASHTO HS20-44 truck and a CDOT A-40 snooper truck. Agreement among the CSi Bridge model, the theoretical calculation, and field measurements was found to be very good. The strong validation of the finite element models solidified confidence in the results of the parametric study discussed in Section 6.

7.2 B-16-FM: Steel Plate Girder Bridge with Concrete Slab

Geometric and structural properties specific to B-16-FM and the modeling techniques are discussed in this section. The structural information and dimensions were obtained from the construction documents provided by CDOT. The bridge is described in Section 3.2 with photos from the site. Steel plate girders support three spans with a length of 75 ft. (~23 m) each, and one shorter approach span (44 ft. [~13.4 m]) at the end of the bridge is supported by concrete girders. The steel span's superstructure consists of three plate girders spaced at 10 ft. (~3 m) on center in the transverse direction.

The top and bottom flange thickness of the plate girders varies along the length. The flanges nearest to the vertical supports are 5/8 in. thick. The thickness of the flanges increases to 1¼ in. (31.75 mm) after a distance of 11 ft. (~3.35 m) from the supports is reached. Finally, for the central 32 ft. (~9.75 m) of the girders, the flanges are 1¾ in. (44.45 mm) thick. Figure 7.1 shows the layout of flange variance in one girder that is typical for all three steel spans.

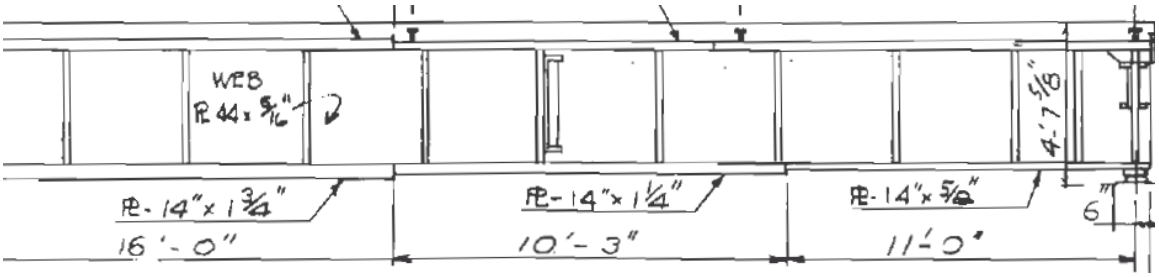

Figure 7.1 Plate girders in construction documents for bridge B-16-FM (courtesy CDOT)

Intermediate stiffeners are located along the length of the plate girders and bearing stiffeners are located near the supports. The web is 5/16 in. thick and 44 in. high. The diaphragms between girders were excluded from the model. The main function of the diaphragms is to tie the girders together during construction, so their absence in the finite element model is moot. In the case of bridge skewedness or curvature, torsional stresses could develop, which would require that the diaphragms are kept in place. Since this bridge does not possess any skew or curvature (no torsion-induced loading), the diaphragms are

excluded from the finite element model. Figure 7.2 shows the extruded view of the plate girders with the intermediate and bearing stiffeners. The slab is excluded from this view to better show the girders.

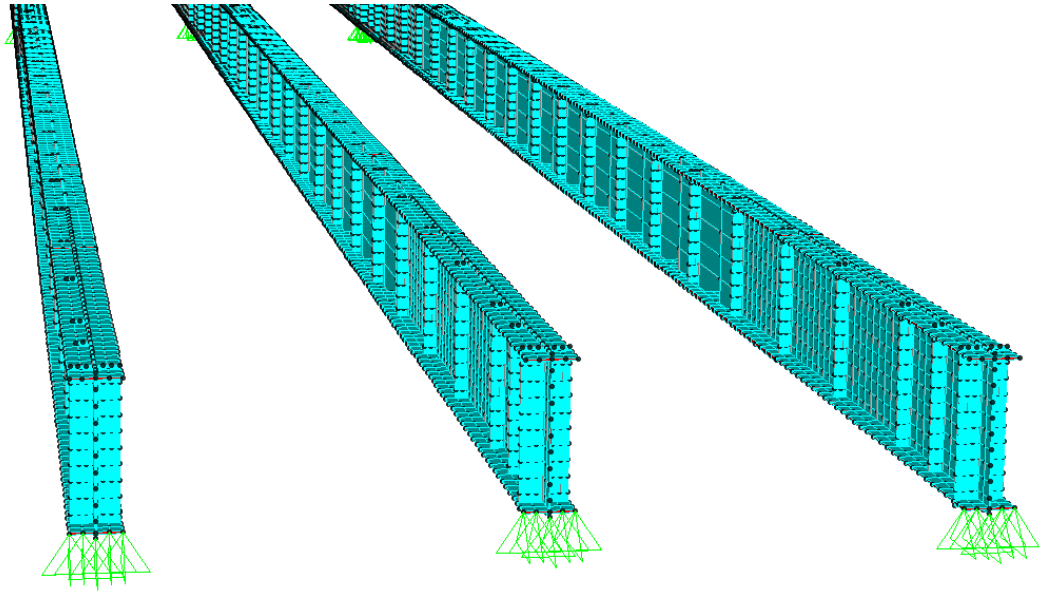

Figure 7.2 Plate girders for bridge B-16-FM

The slab was modeled considering the super-elevation described in the construction documents. The high point of the slab is along the centerline of the roadway and a slope of 0.015 ft./ft. downwards exists on each side until the centerline of the outside girders. The slab then ceases to change elevation. This results in an elevation at the edge of the deck that is 2.4 in. lower than at the centerline. Figure 7.3 shows the slab geometry in the construction documents, and Figure 7.4 shows the slab geometry in the finite element model.

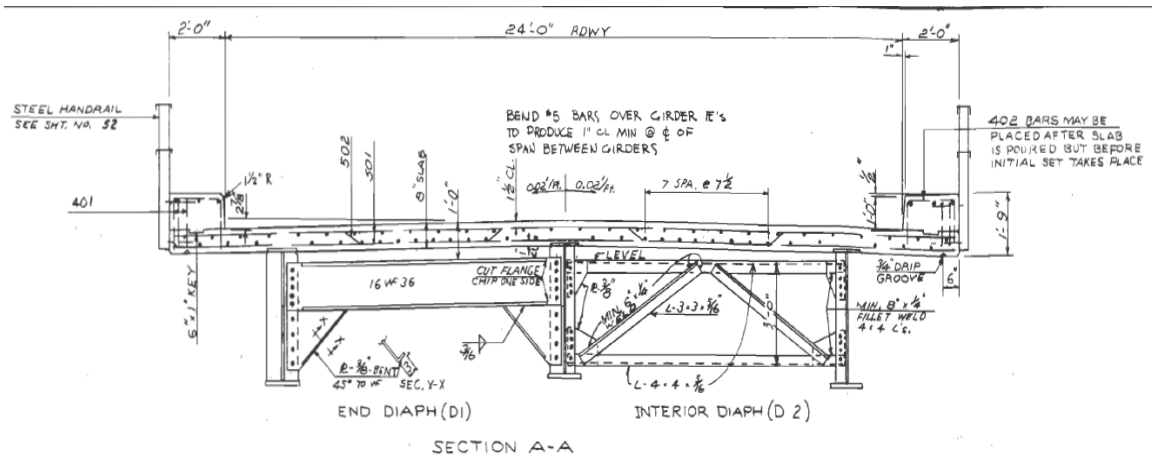

Figure 7.3 Slab geometry described in the construction documents (Courtesy CDOT)

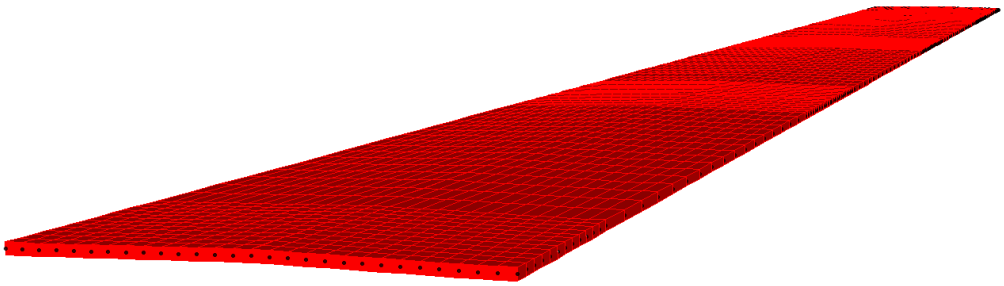

Figure 7.4 Finite element model illustration of super-elevation described in the construction documents

The bridge's bearings transfer the superstructure load to the pier caps. The bearings for the steel bridge disallow translation and allow rotation at the end of each girder. Therefore, the supports are modeled as pin connections that prevent translation in all directions and allow rotation about all axes. The boundary conditions are further discussed in Subsection 7.3.4.

A few more views of the full-scale bridge model are shown in the following figures. The different materials are represented by different colors, cyan and red, for the steel and concrete, respectively. Figure 7.5 shows an extruded view of the superstructure. Figure 7.6 shows all spans in the superstructure.

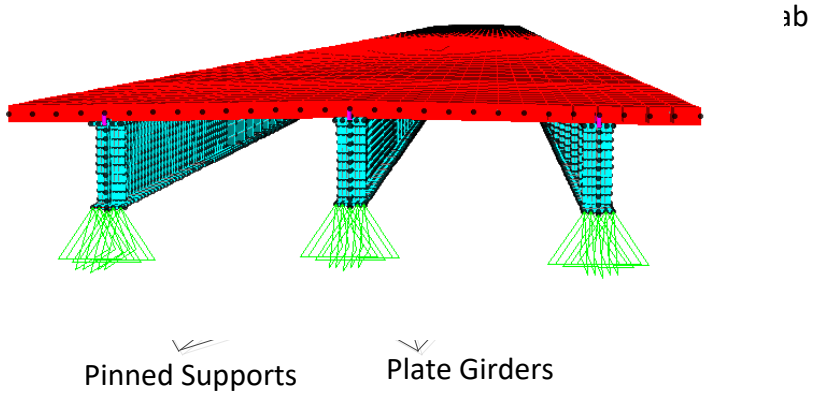

Figure 7.5 Extruded view of B-16-FM superstructure

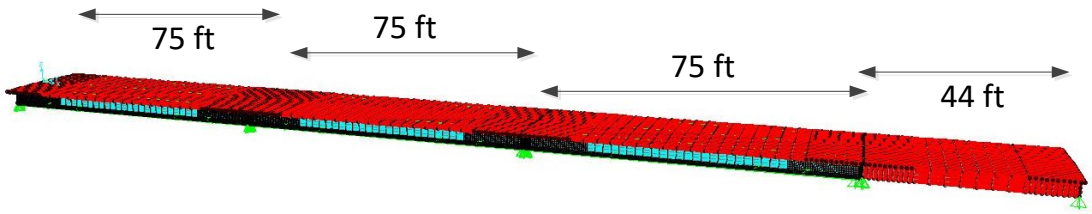

Figure 7.6 Alternative view of B-16-FM bridge model (unstressed, unloaded state)

7.3 CSi Bridge Model Methodology

A three-dimensional model was used to capture with great accuracy both the localized behavior at the joints and the global response to thermal loading. To build the three-dimensional model, shell and frame elements were used in CSi Bridge to represent various bridge elements. The model was used to examine the effects of gravity loading, dynamic loading, thermal loading (both uniform temperature changes and non-uniform gradients), and deck joint performance on the behavior of the bridge. After validating the model's responses, the model was used to perform the parametric study discussed in Section 6.

7.3.1 Shell and Frame Elements

Shell elements were used for the majority of the structural elements in the bridge. Flange, web, intermediate stiffeners, and bearing stiffeners were modeled individually with properties of grade 50 steel and with the thickness as described in the construction documents. The built up plate girder was connected to the slab with shear studs composed of appropriately sized, steel frame sections. Finer mesh sizes were utilized in areas of interest near the joints and for more detailed thermal gradients.

7.3.2 Composite Behavior

Short frame elements were used to model shear studs between the top of the girders and the slab component of the bridge. The total cross-sectional area of the shear studs was the same as that provided by the shear connectors described in the construction documents. In both the actual bridge and the CSi Bridge model, the concentration of the shear stud elements was greater near the supports to accommodate greater shear transfer in regions of high shear demand. The spacing of the studs in the model differed slightly from those on the actual bridge due to node locations in the model that accommodated the changing of the flange thicknesses along the length of the span.

The frame elements used to model shear studs were connected from a node of the girder to a node of the slab directly above. The frame elements were given a modulus of elasticity of 29,000 ksi, typical of steel, and were assigned a yield strength of grade 50 steel. However, the shear studs are not anticipated to yield in this study, and all behavior is considered linear-elastic. The top of the web section is connected to the centroid of the slab section with these frame elements. The frame elements were assessed for proper behavior and shear transfer. Figure 7.11 shows the shear load in the frame elements for one girder under self-weight. Shear lag behavior is evident directly above the supports. The maximum shear force is observed near the supports. The minimum shear force is observed at mid-span and the shear load switches direction at mid-span. This behavior is reasonable and expected.

7.3.3 Thermal Analysis

Shell and frame elements were assigned temperatures in degrees Fahrenheit to simulate thermal loading scenarios. Various temperature loads were assigned to flanges, web, and slab elements to simulate vertical temperature gradients and uniform temperature changes. The thermal gradients considered were put into the model by determining an equivalent piece-wise distribution such that individual shell elements could be assigned one temperature. Prior to using this method in the bridge model, validation analysis was conducted to ensure that this procedure yielded reasonable results. The number of shell elements in the depth of the plate girder varied between five and 10 elements, depending on proximity to the joint. Further information on this validation is discussed in Subsection 4.4.

7.3.4 Boundary Conditions

A pinned boundary condition refers to a joint restraint that allows free rotation with respect to the x-, y-, and z-axes, but does not allow translation in the x-, y-, or z-axes. A fixed boundary condition refers to a joint restraint that does not allow rotation or translation in any direction or axis. The bearings on the steel bridge display behavior that is very close to that of pinned joints. Therefore, the supports at the ends of the girders were modeled in this manner.

Due to the shell element configuration of the model, many nodes were available upon which the pinned boundary conditions can be imposed. The boundary conditions had to be applied to multiple nodes in the model to achieve pinned support behavior. Figure 7.7 shows an end view of one of the girders. Each node with a triangle beneath it has had the translation restrained, but not the rotation. Different configurations of joint restraints were considered without significant effects on the global performance of the bridge. However, the boundary configuration chosen, and indicated in the figure, was that which displayed the greatest similarity to the expected localized stress distributions at a pinned joint due to shear lag behavior. The local behavior at the joints was crucial enough to the study that this boundary condition was investigated in detail.

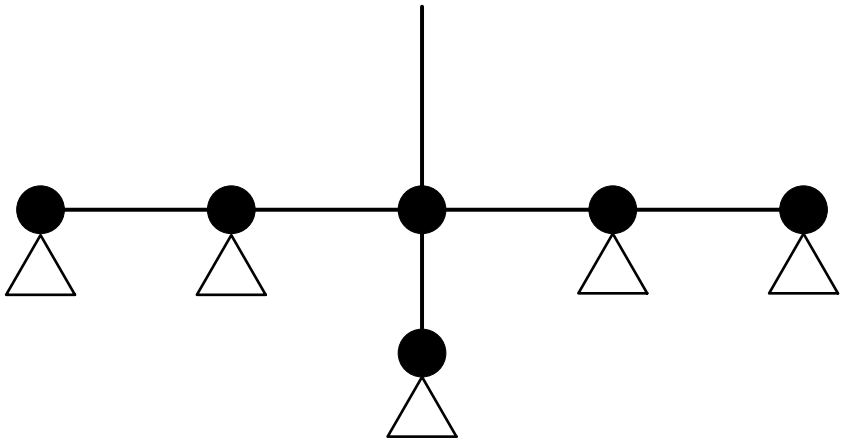

Figure 7.7 Nodes pinned to simulate pinned boundary condition at support

Figure 7.8 gives the stress distribution in the model for the boundary condition scenario shown in Figure 7.7. The shear lag behavior is clear.

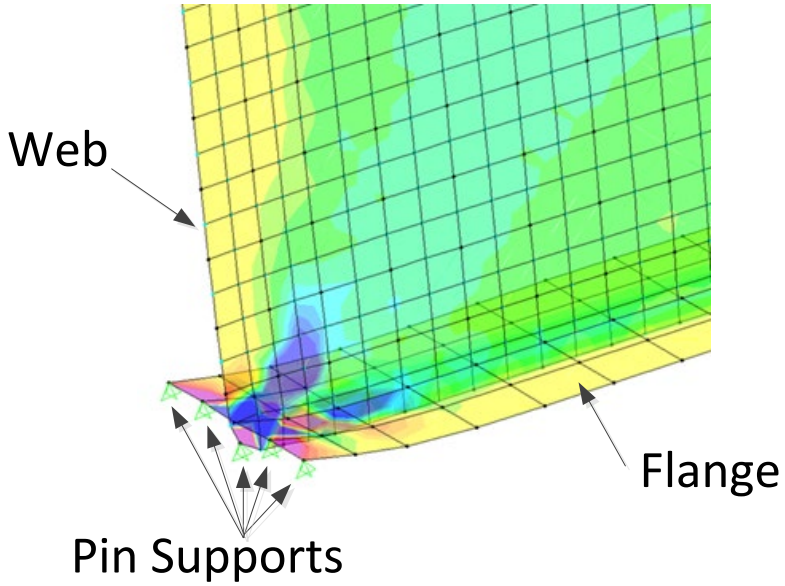

Figure 7.8 Girder stress distribution under self-weight showing shear lag behavior

7.4 Joint-Removing Connection Types Considered

While it is recognized there are numerous alternatives for connecting two spans following the removal of a joint, this parametric study focuses on previous alternatives considered common among transportation agencies. This allows the results of this study to be related to typical field practices. Specifically, connection types used in the two-dimensional study performed by Tsaistas and Boardman (described in Chapter 2) were examined with the three-dimensional model developed for this project. This provided an opportunity to compare results and draw conclusions about how necessary a three-dimensional model is to assess joint removal and thermal loading. The four connection types chosen were 1) deck only, 2) deck and top flange, 3) deck, top flange, and bottom flange, and 4) full-moment splice. Localized stresses and alterations in bending behavior were assessed for each connection type.

To model the deck only connection, the slab was connected in the finite element model using the same types of shell elements. Flanges were connected similarly, by connecting the steel sections with the same shell elements. The full moment splice was achieved by connecting the slab, web, and both flanges with their respective shell elements. The bearing was retained as a pinned boundary condition (allowing rotation, but no translation).

7.5 Thermal Gradients Considered

To assess the effect of removing joints on the superstructure's response to different thermal loading scenarios in the modeled bridge, three vertical thermal distributions were utilized. Two of the distributions had a gradient while the third had a uniform thermal distribution. The first thermal gradient considered was adopted from the AASHTO LRFD Bridge Design Specifications and the second thermal gradient considered was based on the New Zealand bridge design code. This New Zealand code was selected because a previous study conducted by French et al. (2013) (see Section 2) showed reasonable agreement between this fifth order gradient curve and the field-measured thermal loading on the bridge. Lastly, a uniformly distributed temperature change of 50°F was applied. Both the AASHTO and New

Zealand distributions are described in detail in Section 2.8.4. The uniform temperature distribution entailed an increase of 50°F, which was applied to the entire cross-section along the length of the spans in order to determine how thermal stress and behavior from a uniform thermal gradient compares with varying vertical thermal gradients. An increase of 50°F was chosen because all bridges in Colorado experience this temperature change over the course of one year.

7.6 Connection Link Stiffness Considered

Previous research described in Section 2 identified that joints are commonly clogged with debris quickly after they are put into service. To model this in CSi Bridge, links were used and axial stiffness coefficients were assigned to the links to simulate a bridge joint clogged with debris. The axial stiffness coefficients were assigned based on the moduli of elasticity of soils known to clog these joints: sand and gravel. Typically, stiffness values (commonly assigned the variable 'k') are found as EA/L, where E represents the modulus of elasticity, A represents the cross-sectional area, and L represents the length of the element.

To calculate the axial stiffness of the links to reasonably represent the clogged joint, the structural element considered is the soil volume blocking the joint. Common moduli of elasticity for gravel and sand are ~22 ksi (150 MPa) and ~7 ksi (50 MPa), respectively (Briaud, 2013). The length of the debris clog being modeled as an additional structural element is taken as the joint opening, as described in the construction documents (L=0.625 in). The area is found by multiplying the transverse dimension of the bridge by the height of the debris that is causing the clog. The height of the clogged debris was assumed to be three inches (76.2 m). This depth was chosen because three inches is a common depth of compression seals used at the expansion joints. Using these assumptions, a total stiffness of the debris clogging the joint is determined. The stiffness is then distributed evenly across the joint in the model with a link every foot in the transverse direction. This method assumed that the joint is evenly clogged, and thus there are no resulting torsional effects. Using this method, stiffness coefficients of 30 kip/in for a totally gravel-filled joint and 10 kip/in for a totally sand-filled joint were selected. Additionally, a stiffness of 20 kip/in was selected for a joint clogged with a mixture of sand and gravel. These stiffness values were implemented in the parametric study.

7.7 Parametric Study Matrix and Overview

In order to examine the effects of different combinations of connection types, clogged joints, and vertical thermal gradient on local behavior and global performance, a parametric study matrix was developed, and is shown in Figure 7.9. Two categories of joint alterations (connection types and clogged joints) were analyzed with each type of thermal gradient. All analyses took place in the finite element model described in Section 4 and Section 5. Results and conclusions drawn are discussed in Subsection 6.6.

		Stiffness of Deck Clogging Links Between Spans			Connection Types			
		10 kip/in	20 kip/in	30 kip/in	Deck Only	Deck and Top Flange	Deck, Top Flange, and Bottom Flange	Full Moment Connection
Temperature Gradient	AASHTO							
	New Zealand							
	Uniform (+50°F)							

Figure 7.9 Parametric study matrix

7.8 Results

The results of the parametric study are subdivided into two sections: results associated with clogged joints and results associated with various connection types. The numerical results from the analysis of different connection types are shown in bar charts, because the connection types are discrete, qualitative variables. However, the stiffness values assigned to the two-joint links are quantitative, continuous variables, and the results from these analyses are presented in line graphs.

To analyze the effect that different connection types and clogged joints had upon the global performance and local behavior of the bridge, three different loading scenarios were considered: 1) temperature gradient load only, 2) truck loading only, and 3) temperature gradient loading combined with truck loading. An AASHTO HS20-44 truck was used for the truck loading and is shown in Figure 7.10.

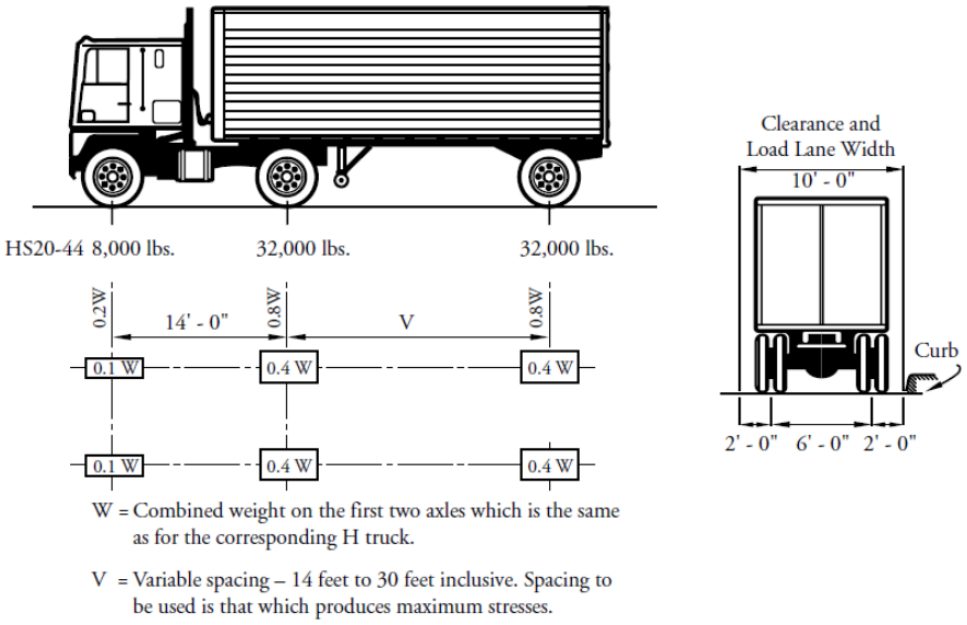

Figure 7.10 AASHTO HS20-44 truck (Precast/Prestressed Concrete Institute, 2003)

An influence line analysis was conducted to determine the location of the truck that resulted in the maximum moment demand on the bridge spans. This location was determined to be when the font axle was at the over the bearing, near the beginning of the span, and the last two axles were placed 14 feet from one another (when $V = 14$ feet in Figure 7.10). For the remainder of the chapter, *truck loading* refers to this AASHTO HS20-44 in this position on the superstructure.

7.8.1 Effect of Clogged Joints

Examination of the influence of clogged joints in the parametric study was conducted in a similar manner as the examination of the influence of connection type. The location of the truck loading was not changed. However, since the value of stiffness of the links is a continuous variable, line graphs instead of bar charts are used to present the results of the study. Three values for link stiffness ($k = 10$ kip/in., 20 kip/in., and 30 kip/in.) are examined with the thermal gradients described above. Local behavior and global performance were evaluated.

First, the compressive stress at the bottom of the girders near the bearings due to only temperature gradient was determined for each vertical gradient option for different two-joint link stiffness options. Figure 7.11 shows the results of this analysis. The model exhibited the maximum compressive stress, 60.29 ksi, when the uniform temperature increase of 50°F is applied and a link stiffness of 30 kip/in. is considered. Of the clogged joint stresses ($k > 0$), the minimum compressive stress, 26.91, was exhibited in the model when the AASTHO thermal gradient was applied with a link stiffness of 10 kip/in. Though the stresses shown in the figure exceed the yield stress, the analysis was conducted considering only the thermal loads and the dead load because the self-weight of the superstructure is neglected. The self-weight will always be present on the bridge in the field, and so the compressive stresses will be less than what is pictured in the figure that is only representing thermal loads.

The clogged joints (symbolized in the figure below by link stiffness values) do not have a significant effect on the global demand on the bridge superstructure, as seen in Figure 7.11 below. The compressive stress range on the girders for the different stiffness of links are 0.80 ksi (~5.5 MPa), 0.16 ksi (~1.1 MPa), and 0.08 ksi (~0.55 MPa) for New Zealand gradient, uniform temperature increase, and AASHTO gradient, respectively.

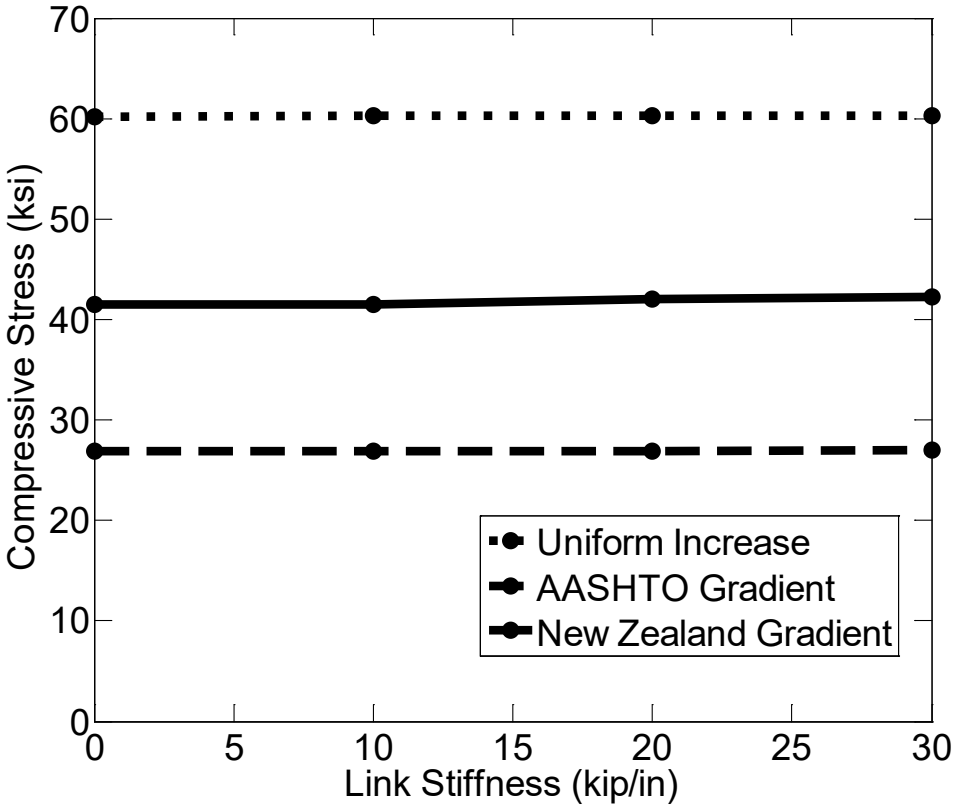

Figure 7.11 Compressive stress at bottom of girder

Figure 7.12 shows the results of the analysis from Figure 7.11 normalized to the maximum value of compressive stress in the bottom of the girders for the uniform temperature increase thermal gradient (60.29 ksi (~416 MPa)). The stress resulting from the gradient described by AASHTO is less than that of New Zealand by approximately 25%.

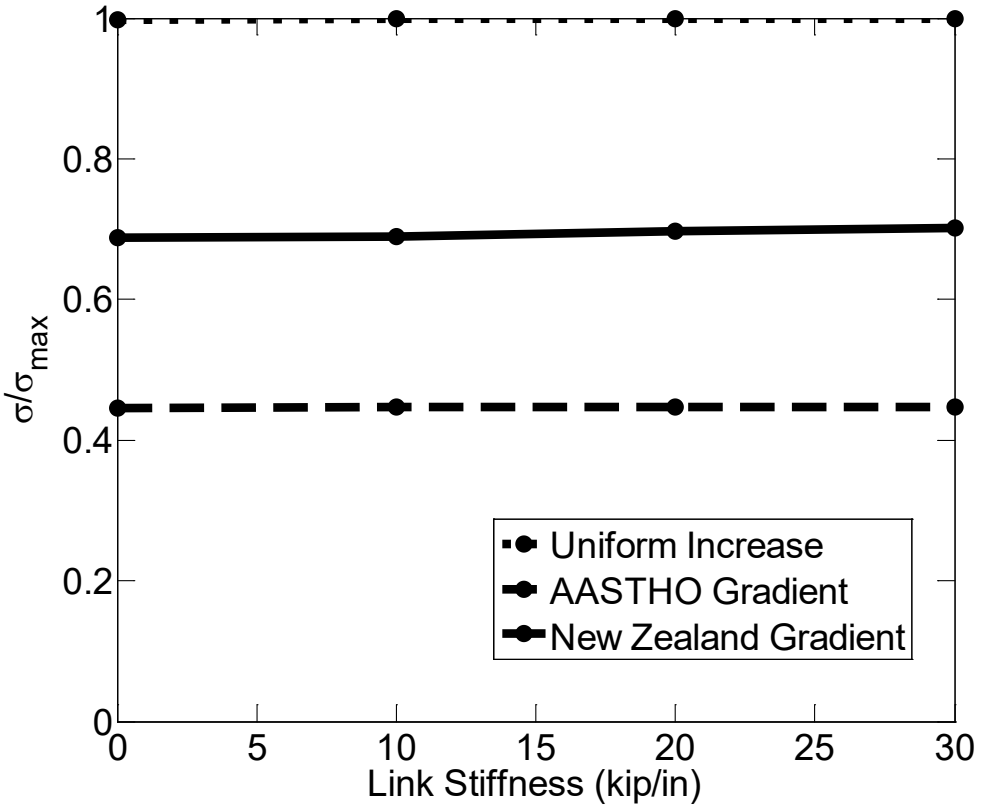

Figure 7.12 Compressive stress at bottom of girder (normalized)

Figure 7.13 shows the local compressive stress in the concrete deck for the different thermal gradients and link stiffness options. The largest, middle, and smallest localized compressive stress in the slab for each link stiffness type was exhibited by the New Zealand, uniform, and AASHTO gradients, respectively. This result is in line with what was expected, because the temperature values of the thermal gradient nearest the top of the concrete deck for New Zealand, uniform, and AASHTO distributions were 69.01°F, 50°F, and 23.33°F, respectively.

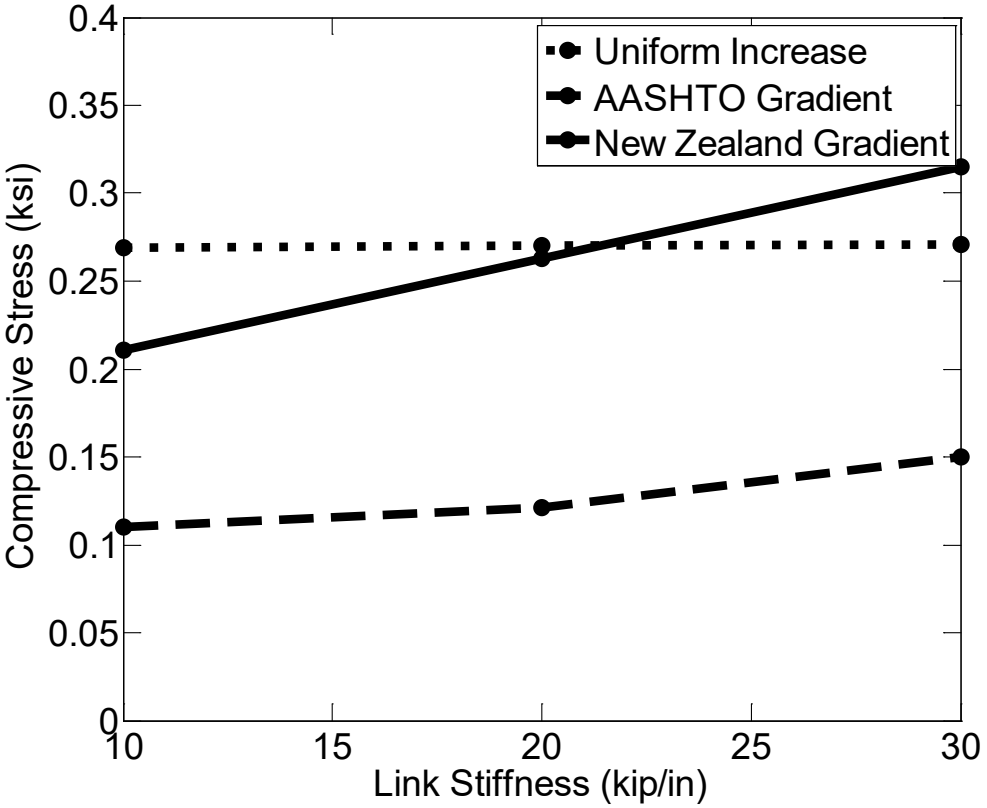

Figure 7.13 Local compressive stress in deck due to thermal loading

Figure 7.14 shows the results of the analysis from Figure 7.13 normalized to the maximum value of 0.315 ksi. This figure shows that the AASTHO gradient results in localized compressive stress less than 40% of what results with a uniform temperature increase of 50°F.

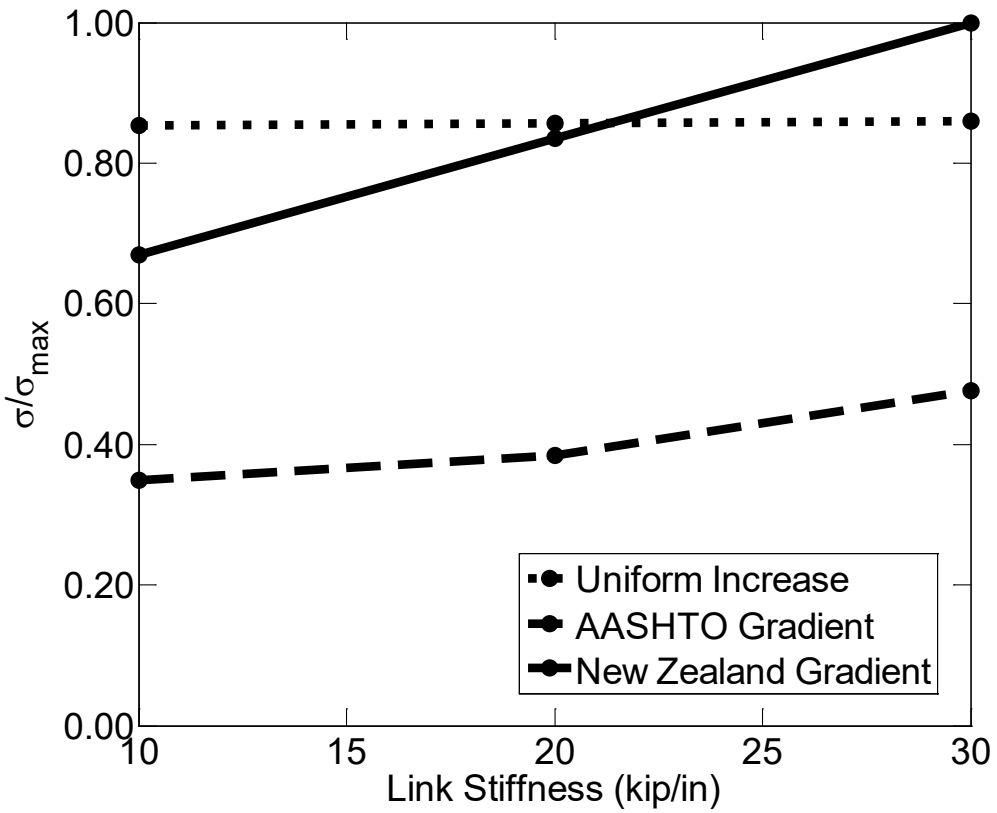

Figure 7.14 Local compressive stress in deck due to thermal loading (normalized)

Figure 7.15 shows the results of the model when only a truck load is considered. There is a slight decrease in moment demand on the bridge due to the clogged joints modeled by the links, because they simulate a clogged joint holding the concrete deck together in a negative moment region. Unlike an unclogged joint then, some moment is transferred in the negative moment region and the moment demand in the positive moment region decreases slightly. However, this decrease of tensile stress demand under the truck load is less than 0.1 ksi (~6.9 MPa), which is 0.7%.

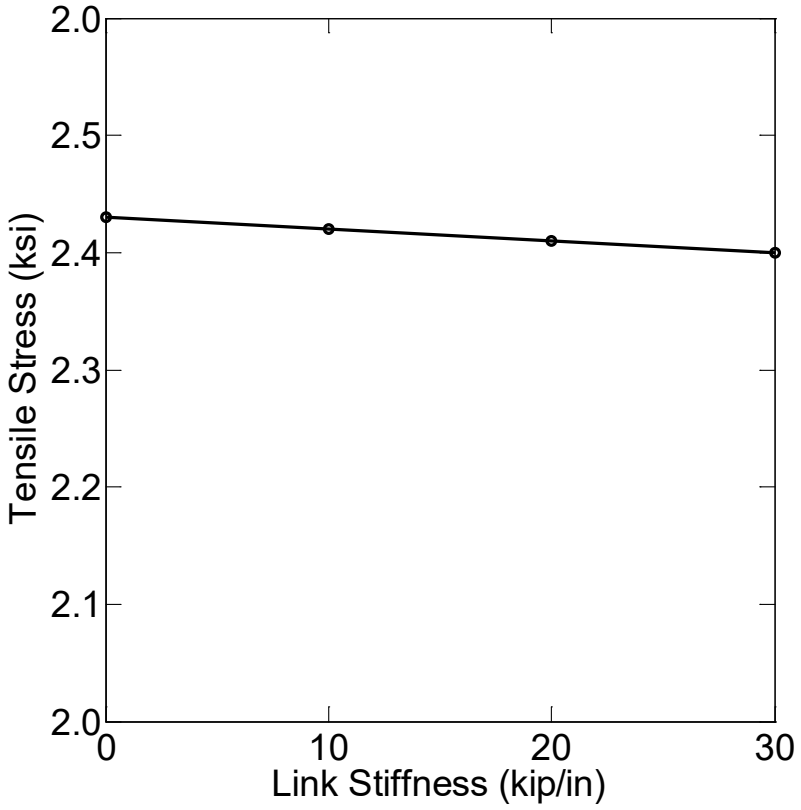

Figure 7.15 Tensile stress at bottom of girder due to only truck loading

After competition of analysis with separate thermal and truck loading, analysis was conducted with both loads applied, and the results are shown in Figure 7.16. For each thermal gradient, the stresses remained compressive. Uniform temperature increase, New Zealand gradient, and AASHTO gradient exhibited the greatest, middle, and least compressive stresses, respectively.

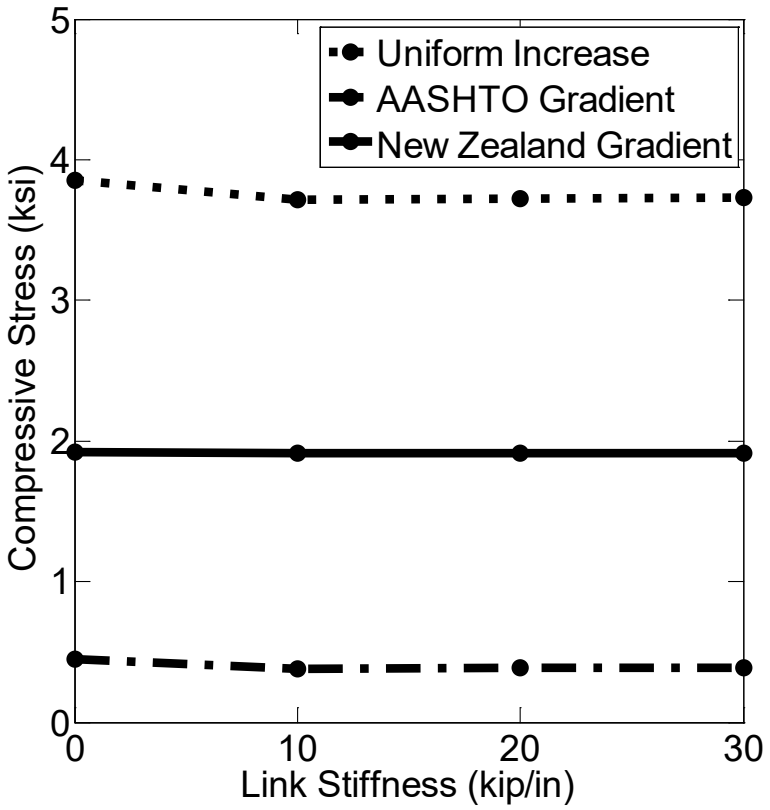

Figure 7.16 Stress at bottom of girder under the truck load due to thermal and truck loading

Figure 7.17 shows the results of the analysis from Figure 7.16 normalized to the maximum compressive stress value of 3.85 ksi (~26.6 MPa).

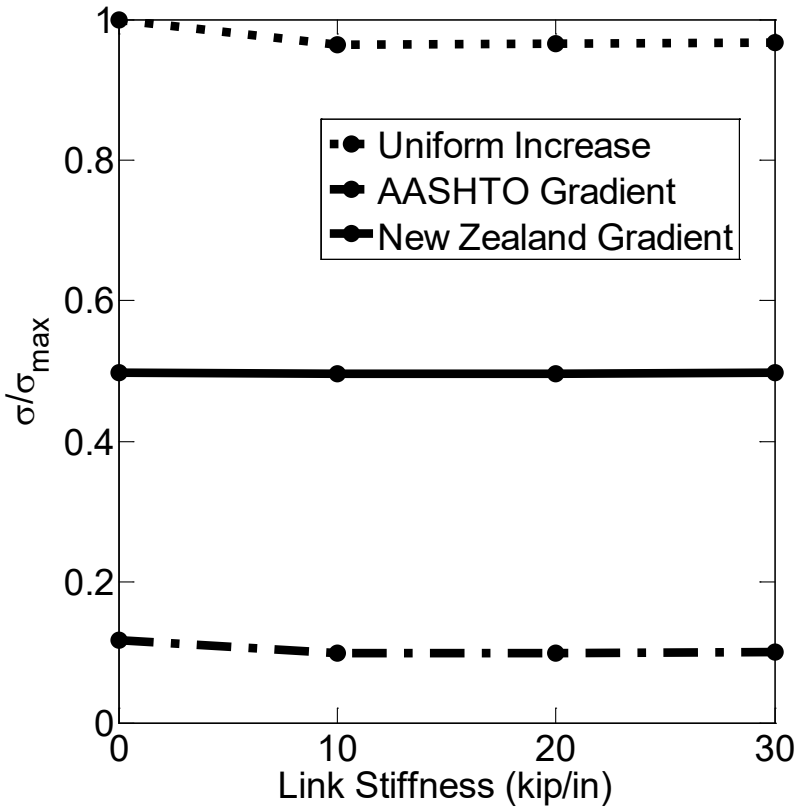

Figure 7.17 Stress at bottom of girder due to thermal and truck loading (normalized)

7.8.2 Effect of Connection Types

First, the compressive stress near the bearings in the bottom of the girders due to only temperature gradient was determined for each vertical gradient option and connection type. Figure 7.18 below shows the results of this analysis. The stresses induced by the AASHTO recommended thermal gradient are lower than those induced by the New Zealand gradient. Both of these gradients still result in lower stresses than the stresses a uniform temperatures increase of 50°F induces in the structure. The minimum compressive stress at the bottom of the girders, 7.1 ksi, is found when a Full-Moment Splice connection and the AASHTO defined vertical temperature gradient are considered. This is likely because the AASHTO thermal gradient is the least intense of the thermal loading and the Full-Moment Splice transfers moment from one span to the other. The Full-Moment Splice induces a lower neutral axis (the *y* in the equation of stress, $\sigma = (M*y)/I$, is reduced). Therefore, less stress exists at the most extreme bottom fiber of a cross-section because the moment demand is lowered at the bottom of the cross-section. Similar to the clogged joint analysis, the stresses shown in the figure below (and exceeding the yield point) are only depicting the effect of thermal loading, and will be lower in the field when the self-weight of the superstructure is present.

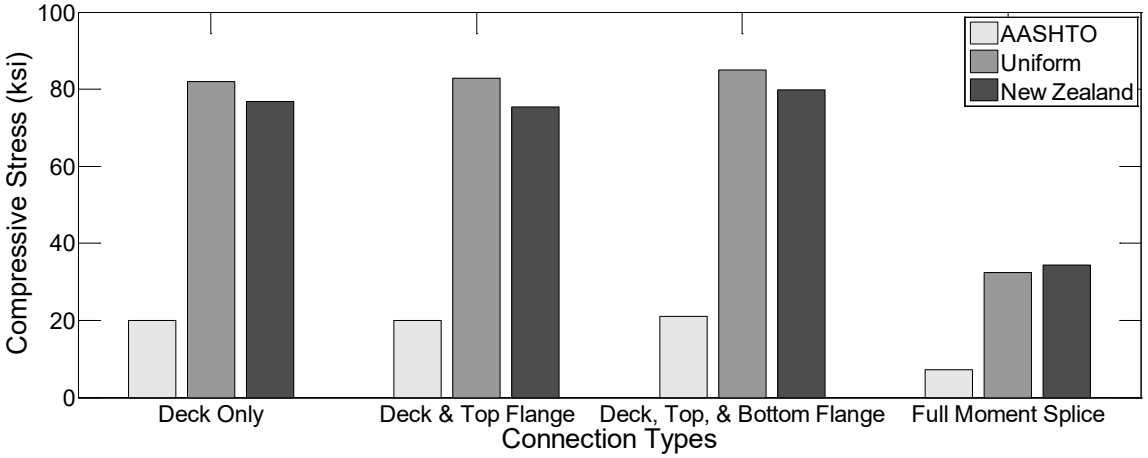

Figure 7.18 Compressive stress at bottom of girder due to only thermal loading

Figure 7.19 shows the results of the analysis conducted in Figure 7.18, but normalized to the maximum value. The maximum compressive value of stress was 85.0 ksi (~586 MPa) and was found when the compressive stress due to a uniform temperature increase of 50°F and a deck, Top, and Bottom Flange connection was considered.

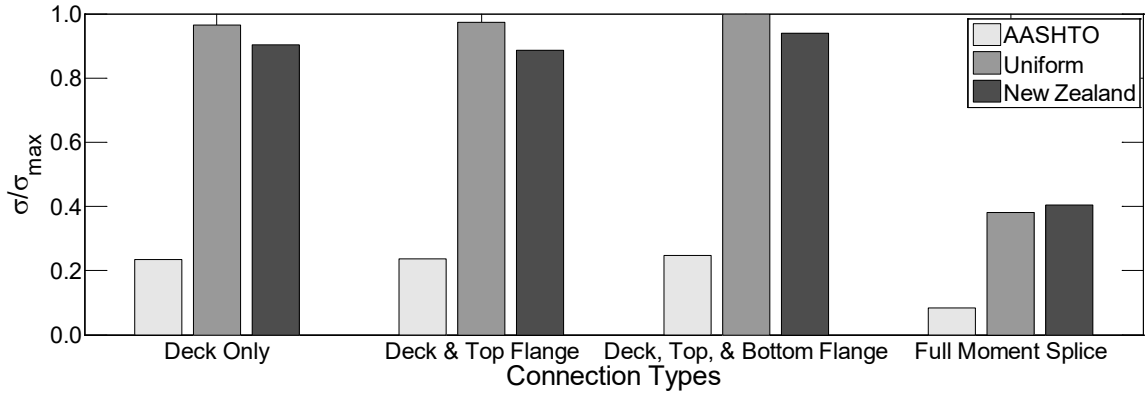

Figure 7.19 Compressive stress at bottom of girder due to only thermal loading (normalized)

To examine the localized behavior at the joints that each thermal gradient and connection type induces into the structure, the compressive stress at the joint was retrieved from the model results (considering only thermal loading). Figure 7.20 shows the results of this analysis. The localized compressive stress induced was the greatest for each thermal gradient when considered with the deck only connection. The localized compressive stress did not significantly decrease, however, when the connectivity at the joint is increased by attaching more than one plate girder flange. In other words, the deck and top flange, deck, top, and bottom flange, and full moment splice connections did not have progressively lower localized compressive stress.

The largest, middle, and smallest localized compressive stress in the slab for each connection type was exhibited by the New Zealand, uniform, and AASHTO gradients, respectively. This result is in line with what was expected, because the temperature values of the thermal gradient nearest the top of the concrete deck for the New Zealand, uniform, and AASHTO distributions were 69.01°F, 50°F, 23.33°F, respectively.

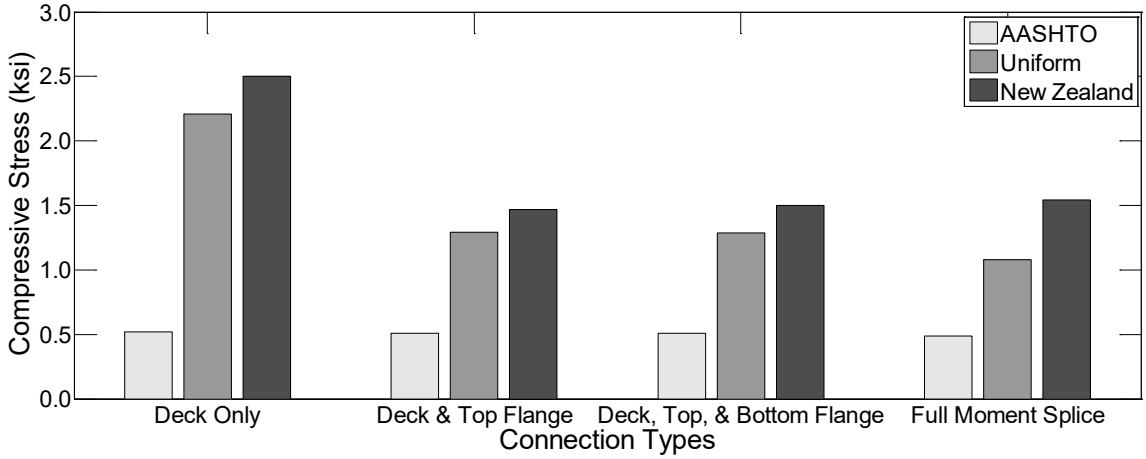

Figure 7.20 Local compressive stress in concrete deck due to only thermal loading

Figure 7.21 shows the results of the analysis conducted in Figure 7.20, but normalized to the maximum value of local compressive stress. This value was found to be 2.5 ksi (~17.2 MPa) when the New Zealand vertical temperature gradient was placed on the structure with a deck only connection.

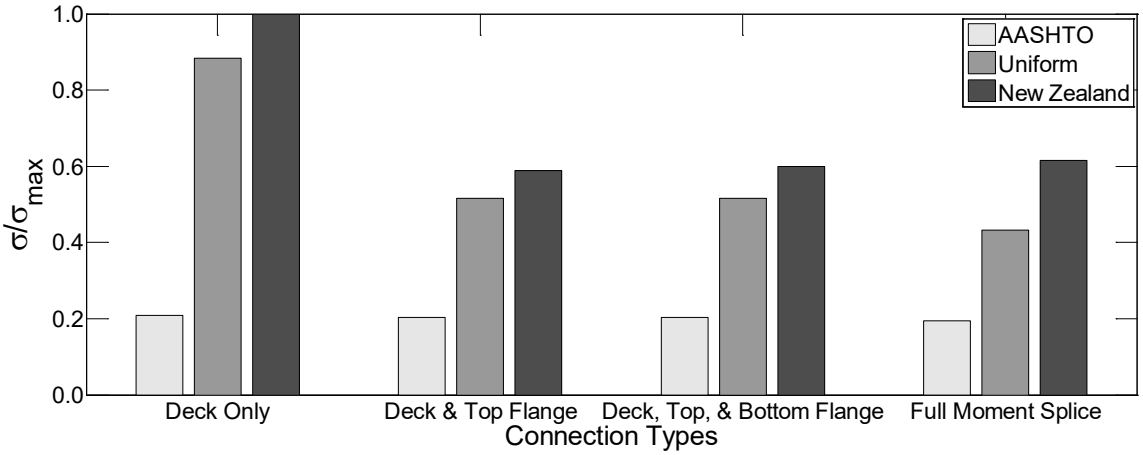

Figure 7.21 Local compressive stress in concrete deck due to only thermal loading (normalized)

To evaluate the potential increase in moment capacity of the span for the four connection types considered at the joint, analysis was conducted with only the truck loading and the connection types being investigated. The maximum tensile stress in the bottom of the girder system was taken as a measure of the moment demand on the superstructure for a given connection type and the truck loading. The results of this analysis are shown in Figure 7.22. The moment demand on the structure did not decrease considerably until the Full-Moment Splice connection was utilized. The tensile stress for the deck only, deck and top flange, and deck, top, and bottom flange was 3.22 ksi (~22.2 MPa). However, when a full moment splice was analyzed, a reduction of the tensile stress to 2.51 ksi (17.3 MPa) was observed in the span. This corresponds to a 22% decrease in the moment demand on the superstructure.

It is also important to note that connecting the flanges at the joint did not result in a significant increase in moment capacity of the bridge. Therefore, the additional cost of increasing connectivity beyond the "deck only" connection may not be beneficial. This is because connecting only the flanges does not result in sufficient increase in the rotational stiffness of the connection; hence, the moment transfer to the

connection is limited. Instead, if higher moment capacity increase is desired, a Full-Moment Splice connection should be utilized.

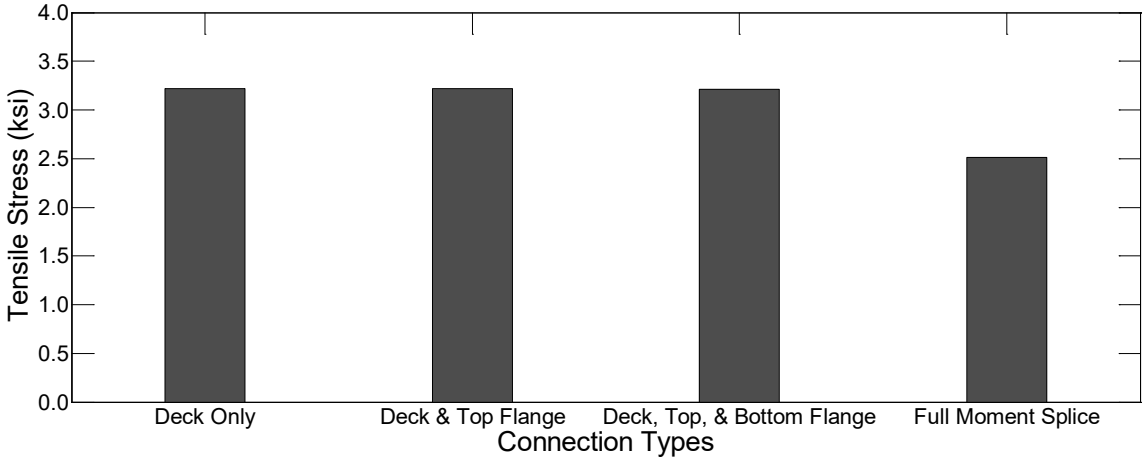

Figure 7.22 Tensile stress at bottom of girder due to only truck loading

Figure 7.23 shows the results of the analysis shown in Figure 7.22 normalized to the maximum value of tensile stress in the bottom of the girders. The maximum value is 3.22 ksi (~22.2 MPa) (found for the deck only, deck and top flange, and deck, top, and bottom flange connection). The moment demand on the superstructure for the Full-Moment Splice connection is approximately 78% of the moment demand with the other connection types.

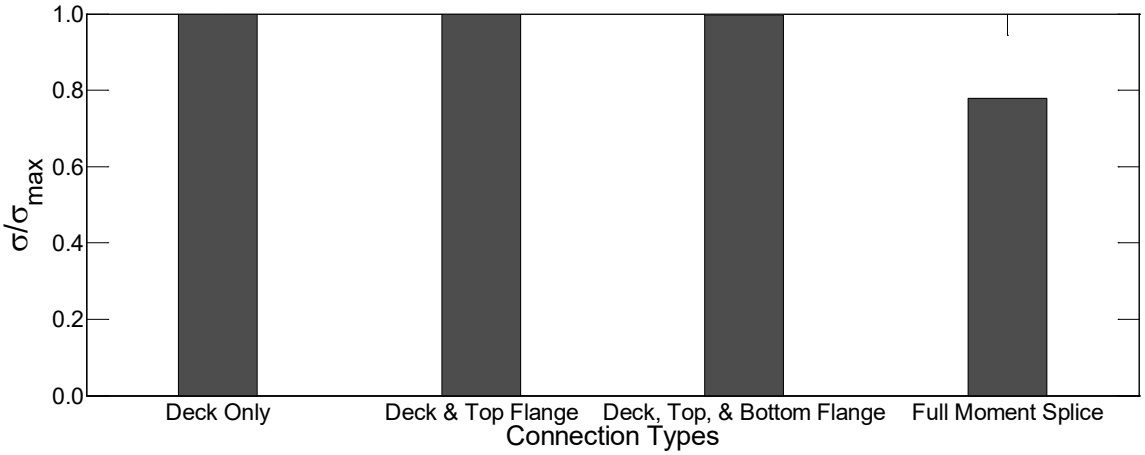

Figure 7.23 Tensile stress at bottom of girder due to only truck loading (normalized)

After completion of analysis with separate thermal and truck loading, analysis was conducted with both loads applied. The results are shown in Figure 7.24. Due to the lesser amount of compression resulting from the AASHTO thermal gradient (when only thermal loading is considered), the stress at the bottom of the girders under combined AASHTO thermal gradient and truck loading resulted in a tensile stress at the bottom of the girders. However, the uniform and New Zealand vertical thermal gradients induced enough compressive stress into the superstructure that the value of stresses in the bottom of the girders remained compressive while the truck load was applied.

The maximum compressive stress demand in the girders near the bearings due to thermal and truck loading was found when the deck only connection type was considered. The maximum compressive stress demand in the girders when considering thermal gradients increased when the connectivity of joint increased and the maximum values were found with a Full-Moment Splice connection. These results reiterate that the connection type at the joint influences the global performance and moment demand on the bridge.

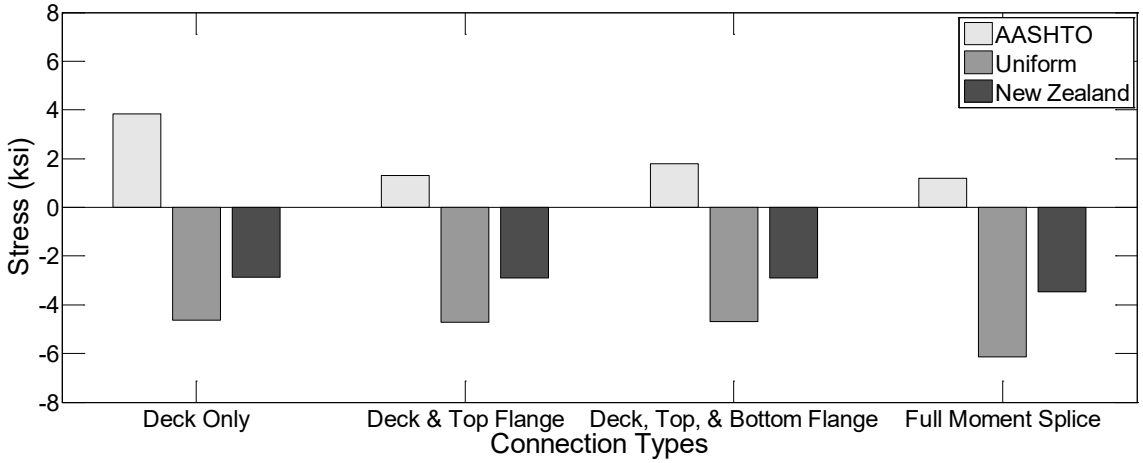

Figure 7.24 Stress at bottom of girder due to thermal and truck loading

Figure 7.25 shows the results of the analysis from Figure 7.24 normalized to the maximum value of tensile stress in the bottom of the girders for the AASHTO thermal gradient (3.84 ksi [~26.5 MPa]). The compressive values from the uniform and New Zealand thermal gradients are normalized to the maximum value of compressive stress in the bottom of the girders (-6.15 ksi [~42.4 MPa]).

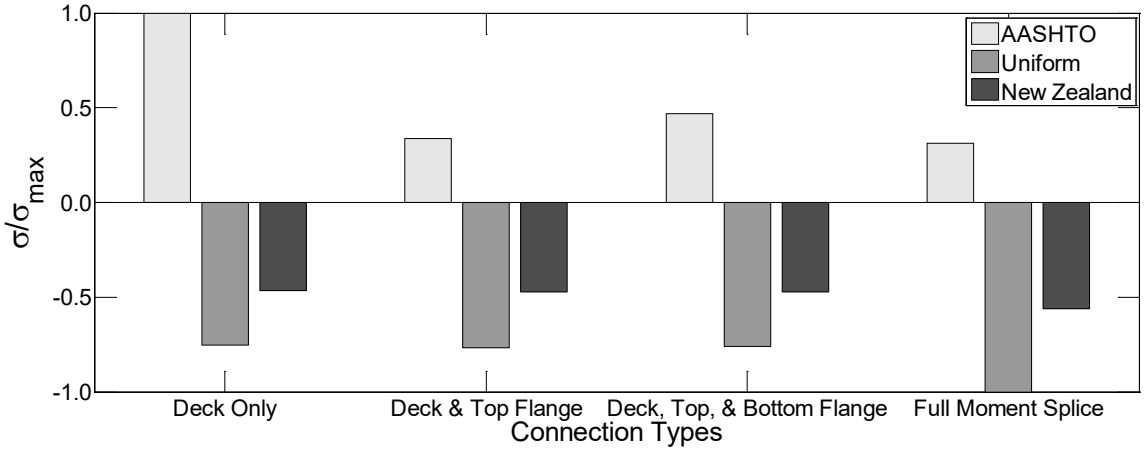

Figure 7.25 Stress at bottom of girder due to thermal and truck loading (normalized)

7.9 Conclusion

The parametric study results highlighted differences between the thermal gradients considered. The AASHTO described thermal gradient consistently resulted in lower stress demand on the structure compared with the New Zealand thermal gradient. The results from the field data will aid in further examination of the AASHTO described thermal gradient for bridges in Colorado.

The results also highlighted the extent of the effect that joint-removing connection types have compared with clogged joints. The effect of the clogged joints was primarily localized at deck surface behavior. However, the joint-eliminating connection types influenced the global performance of the bridge as well. No significant decrease in moment demand on the superstructure was observed until a full-moment splice was utilized.

8. LIFE-CYCLE COST ANALYSIS

8.1 Life-Cycle Cost Analysis Model

The goal of this chapter is to present and examine an LCCA that can be used to determine if it is more cost effective to continue replacing bridge expansion joints as they deteriorate (i.e., ***no change*** to current proactive) or to ***retrofit*** joints to be continuous. The approach is intended to be applicable to any existing steel girder/concrete deck bridge; the characteristics of one typical northern Colorado steel plate girder bridge with reinforced concrete abutments, deck, and pier caps are used as an example. The example bridge is located in Northern Colorado and has three 75 ft. (22.9 m) spans with five 44 in. (1.1 m) deep steel plate girders each, an 8 in. (203mm) thick reinforced concrete composite deck, and finger expansion joints.

An important step in conducting an LCCA is determining the appropriate costs to include in the analysis. Two different LCCA cost scenarios are examined. Cost Scenario 1 considers costs directly associated with expansion joints only, while Cost Scenario 2 considers costs associated with expansion joints and damage to pier caps caused by leaking joints. It should be recognized that poorly maintained expansion joints can lead to damage on other portions of a bridge. For example, road dirt and gravel can clog joints, preventing them from closing when bridge temperatures increase. The clogging can lead to damage at the joint as well as damage at abutments. Abutment damage can be a significant cost, and would ideally be considered in LCCA; however, the amount of damage is very dependent on the abutment design and properties of the supporting soil. The potential for abutment damage is thus much more bridge dependent and harder to generalize.

For each cost scenario, the first alternative is the current practice of replacing the joints after failure without maintenance, also known as the do-nothing or no change to current practice alternative. The second alternative is retrofitting the joints after failure and accounting for cracking of the bridge deck due to the negative moment induced at the continuous connection. Within each alternative, differences in results between two general locations, mountains and plains, will also be examined. Figure 8.1 shows the flow chart of cost scenario to alternative to topographic location.

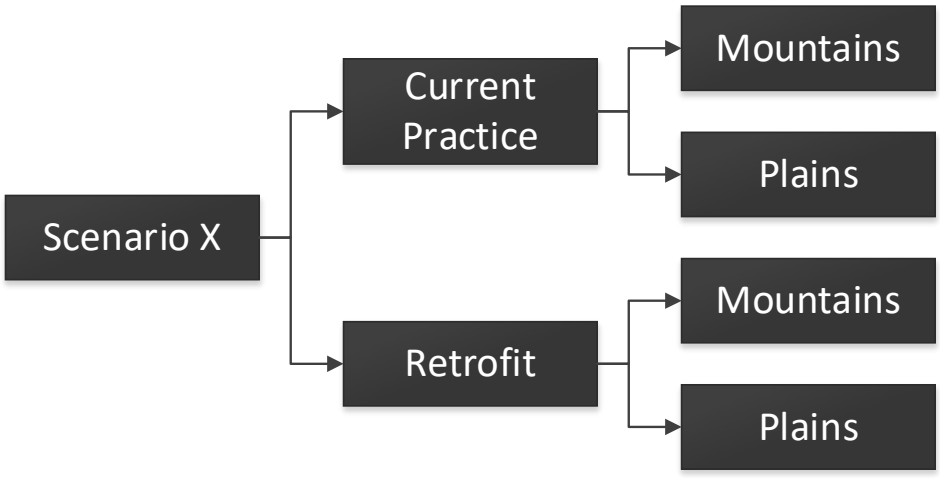

Figure 8.1 LCCA cost scenario

8.2 Life-Cycle Cost Analysis Equations and Variables

If all parts, consequences, and alternative actions on a structure, a bridge in this case, can be expressed monetarily, then the best combination of actions or alternatives can be determined as the one that minimizes the total LCC of keeping the bridge in service. If each of the parts, consequences, and alternatives are quantified, there is also a probability that the consequence or action will occur and cause that cost to become real.

There are two general LCC equations serving as the basis for this analysis, one for each alternative. These general equations, shown below, include all possible parameter costs, where Eq. (8.1) is the LCC for no change to current practice and Eq. (8.2) is the LCC for joint retrofitting.

$$LCC_{NC} = C_i + C_{cm} + C_o + C_mP_m + C_rP_r + C_{cc}P_{cc} + C_uP_u - SV \quad \text{(Eq. 8.1)}$$

$$LCC_{JR} = C_i + C_{cm} + C_R + C_s + C_o + C_mP_m + C_rP_r + C_{cc}P_{cc} + C_uP_u - SV \quad \text{(Eq. 8.2)}$$

Where C_i, C_{cm}, C_o, C_R, and C_s are the initial, construction, operation, retrofitting, and crack sealing (if retrofit) costs. C_mP_m, C_rP_r, $C_{cc}P_{cc}$, and C_uP_u are the maintenance, replacement, cost of capital and user costs and their respective probabilities of occurrence. The maintenance term is composed of two parts, $C_mP_m = C_cP_c + C_{pcr}P_{pcr}$, the joint maintenance (cleaning) and pier cap repair/maintenance and associated probabilities. Finally, SV is the salvage value of the structure at the end of its life span.

While some of these costs and probabilities are obtainable or calculable based on information from CDOT or testing, some are more ambiguous or not applicable to this particular LCCA. The initial and construction costs are not applicable, as this paper focuses on maintenance and repair decisions for existing bridges only. The operation cost does not apply since this analysis is not focusing on drawbridges or other bridges with daily operations. The user costs (cost of time and convenience to the using public) and capital costs (costs of initial investment) are more ambiguous and cannot be easily quantified. As such, they are left out in the analysis. Finally, because this study focuses on the impact of expansion joints on the LCC of a bridge, the salvage value is not directly impacted and will show little variation under different joint alternatives. For these reasons, it is also left out of the analysis. The adjusted equations are shown below as Eq. (8.3) and (8.4). Additional terms will multiply costs in order to account for the number of joints or linear feet of joints on the bridge.

$$LCC_{NC} = C_cP_c + C_{pcr}P_{pcr} + C_rP_r \quad \text{(Eq. 8.3)}$$

$$LCC_{JR} = C_cP_c + C_{pcr}P_{pcr} + C_rP_r + C_R + C_s \quad \text{(Eq. 8.4)}$$

Data collection and analysis were conducted to identify values for each of the variables indicated in Eq. (3) and (4). The costs associated with expansion joints and pier caps are shown in Table 8.1. The costs were obtained from the CDOT business website from the 2014, 2015, and 2016 cost data books (Colorado Dept. of Transportation, 2016). These costs were taken as present value costs. According to procedures described by the Federal Highway Administration, when performing an LCCA, future costs are determined by applying an inflation rate to present costs, while future costs are brought back to the present by applying a discount rate. (FHWA, 2002). Inflation rates and, especially, discount rates can be difficult to determine. This analysis used the present value costs directly, which assumes that the interest rate used to bring these costs to future values throughout the LCC and the discount rate used to bring them from future value back to present value offset each other.

Table 8.1 Assumed costs based on CDOT data (Colorado Dept. of Transportation 2016)

Variable	Value
Cost of Cleaning a Joint (C_c)	\$20/LF
Cost of Replacing a Joint (C_r)	\$350/LF
Cost of Removing/Retrofitting a Joint (C_R)	\$205/LF
Cost of Sealing Cracks (C_s)	\$0.75/LF
Cost of Repairing Damaged Pier Caps (C_{pcr})	\$2000/item[a]

[a] These are estimates from CDOT, the costs are variable and site-specific. Costs depend on amount of damaged material and ease of access, and both depend on extent of damage, traffic, and location of bridge.
[b] Average life spans of bridge joints are based on CDOT personnel experience.

Other terms in the LCCA equation depended on agency practice or were bridge dependent. Values for these variables are shown in Table 8.2. Case A represents CDOT general practices, according to CDOT personnel in the Division of Project Support, and assumptions based on those practices. Because Case A considers estimates and assumptions, Cases B and C consider two additional variations. Case B considers increasing the time until joint replacement. Case C examines the effects of increasing the remaining design life of the bridge, i.e., extending the period of analysis. Those values that are assumed are listed first, as noted in the table, with the bridge dependent variables following. The agency practice values are values that would vary depending on the exact DOT district practices. Bridge dependent variables include the remaining design life of the bridge, the number of joints and abutment joints, and the width of the bridge/length of the joint.

Table 8.2 Test matrix considering agency and bridge dependent variables

Variable	**Case A** Common CDOT Practice	**Case B** Longer Joint Replacement Time	**Case C** Longer Remaining Design Life
Prompt joint replacement [a]	0.5 yrs.	1 yrs.	0.5 yrs.
Max time to replace joint [a]	3.5 yrs.	4 yrs.	3.5 yrs.
Frequency a joint should be cleaned[a]	0.5 yrs.	0.5 yrs.	0.5 yrs.
Probability a joint will be cleaned regularly [a]	0.0000001	0.0000001	0.0000001
Remaining design life (DL)	30 yrs.	30 yrs.	50 yrs.
Number of joints total	4	4	4
Number of abutment joints	2	2	2
Width of bridge	7.3 m (24ft)	7.3 m (24ft	7.3 m (24ft

[a] Assumed values based on CDOT general practices and discussions

For the LCC discussion and analysis, the LCCs from Case A are presented in tables for comparison and discussion. The LCCs from Case A are used for analysis and discussion, with the LCCs from Cases B and C variables used for comparison when applicable.

8.3 Cost Scenario Equations, Variables, and Calculations

Each cost scenario adapts the two basic equations to its particular analysis of costs and variables. The following describes the equations particular to each cost scenario and how the different variables are calculated. Calculations for each cost scenario were conducted in MATLAB using the costs in Table 8.1 and agency practices in Table 8.2.

8.3.1 Cost Scenario 1

For Cost Scenario 1, equations (8.3) and (8.4) were modified to equations (8.5) and (8.6). The probability for cleaning is assumed to be nearly zero, as seen in Table 8.2, because CDOT and other DOTs do not have the personnel or resources to clean/maintain expansion joints. This means the cost of joint cleaning is effectively zero and was considered negligible in the calculations.

$$LCC_{NC} = C_r\,(l_j)\,(n) \qquad \text{(Eq. 8.5)}$$

$$LCC_{JR} = Cr\,(l_j)\,(n) + C_R(N) + C_s(N)\,(DL) \qquad \text{(Eq. 8.6)}$$

When calculating the costs for the **no change** alternative, the cost of a joint replacement, C_r, was treated as a constant \$350/linear ft. and l_j was taken as the total length of joints needing replacement. The number of times joints were replaced on a bridge, n, was determined by simulating the bridge's remaining life. The joint life and time to failure were randomly simulated repetitively until the cumulative time spent with intact and damaged joints reached the target for the remaining design life (DL). Uniform distributions were assumed for the time to joint failure and the time to joint replacement. Typical joint life spans were provided by CDOT personnel in the Division of Project Support as two ranges, one for the plains and one for the mountains. The joints located in the plains have a typical joint life span of seven to ten years, and joints located in the mountains have a typical joint life span of three to six years. Simulations of bridges on the plains thus assumed joint life span was uniformly distributed between seven and 10 years, for example. The time to repair was simulated based on the typical repair times shown in Table 8.2. For example, for Case A, the time to repair was assumed to be uniformly distributed between 0.5 and 3.5 years. All joints on a bridge were assumed to fail and be repaired at the same time. This assumption was based on the thought that it would be most efficient for repairs to take place on all joints at the same time, and joint repairs on a bridge would not occur until all joints were in need of repair. The life cycle costs were simulated a total of 10,000 times.

The cost calculation for the **joint retrofit** option was made for two different situations: retrofitting only the deck joints – leaving the abutment joints in place, and retrofitting all joints on the bridge. When only deck joints were retrofit, the length of joints needing repair, l_j, included only the abutment joints; when all joints were retrofit, l_j was set equal to zero as the bridge had no remaining joints. When abutment joints were left in, the cost for repair of abutment joints was calculated in the same way as the **no change** case, using random distributions to represent joint life and time to repair. C_R is the cost to retrofit a joint to make it continuous, and was taken as a fixed \$205/linear ft. N is the number of joints that were retrofit (either two or four depending on if the abutment joints were left in place or not). C_S is the cost of crack sealing. Crack sealing is only needed for those locations where a joint was removed and replaced with continuous concrete. Crack sealing was assumed to occur once per year, and DL is the remaining design life assumed for the analysis.

8.3.2 Cost Scenario 2

Cost Scenario 2 takes the equations from Cost Scenario 1 and adds the costs due to pier cap corrosion due to leaking joints, as shown in equations (8.7) and (8.8).

$$LCC_{NC} = C_r\,(l_j)\,(n) + C_{pcr}\,(m) \qquad \text{(Eq. 8.7)}$$

$$LCC_{JR} = Cr\,(l_j)\,(n) + C_R(N) + C_s(N)\,(DL) + C_{pcr}\,(m) \qquad \text{(Eq. 8.8)}$$

In addition to the variables determined for Cost Scenario 1, the number of times pier caps must be repaired for corrosion damage during the remaining design life of the bridge, m, is needed. To estimate this number, it was assumed that in the time between joint failure and joint repair, the leaking joint allowed chloride containing water to reach the pier caps below the bridge. Chlorides could then accumulate on the surface of the pier and begin to diffuse through the concrete. When a sufficient concentration of chlorides accumulated at the level of the reinforcement, corrosion could then begin, leading eventually to cracking and spalling damage to the pier. The concentration of chlorides present on the pier cap is dependent on the length of time the joint is leaking and the location of the bridge, i.e., how heavily de-icing salts are used. The threshold concentration needed to start corrosion of the rebar is determined by the concrete mix, clear cover, and type of rebar used (e.g., traditional bare bars, epoxy coated, stainless steel). In this analysis, the threshold concentration and time to reach the threshold concentration were determined using the software Life-365, developed under the American Concrete Institute (ACI) Committee 365 "Service Life Prediction" and sponsored by ACI, the National Institute of Standards and Technology (NIST), and the American Society for Testing and Materials (ASTM) in 1998.

Life-365 is an LCC and service life prediction tool for reinforced concrete structures exposed to chlorides. The version used for this research is Version 2.2.2 released July 2013. The Life-365 software does not account for carbonation, as it has a low probability of occurrence and is often associated with poor quality concrete (Life-365^{TM} Consortium III, 2014). The software analysis is composed of four main steps: predicting the corrosion initiation period, predicting the propagation period, estimating the frequency and promptness of repair, and estimating the LCC. The repair and LCC portions of the software are intended for concrete members and did not allow for including the costs related to bridge expansion joints. Therefore, for the purpose of this research, results from the first two steps were utilized to determine the time and concentration needed to corrode the rebar in bridge pier caps. The initiation period is estimated using a simplified method based on Fickian diffusion. This method requires only a few inputs from the user, as discussed below. Furthermore, the model assumes that diffusion is the dominant mechanism at play and that there are no cracks in the concrete in question. The diffusion coefficient used is a function of time, temperature, and concrete mix composition. The equations for the diffusion coefficient can be found in the Life-365 User's Manual Section 2.1.1 (Life-365^{TM} Consortium III, 2014).

Life-365 uses the type of structure, the geographical location, and the environmental exposure input by the user to calculate the maximum chloride surface concentration corresponding to the threshold chloride content at the level of the rebar and time to reach that concentration. The temperature profile uses data compiled from meteorological data based on the user's geographical location input. The user can also manually input a temperature profile. The user can also define the concrete mix composition and type of rebar present.

For the LCCA of leaking expansion joints in Colorado, Life-365 was utilized to determine the time and chloride concentration at which corrosion was expected to begin and until the rebar becomes too corroded to function. Urban bridges were selected as the structure type, the location chosen was Denver, the temperature profile for that location was used, and a basic concrete mixture without special additives was assumed. Once these inputs were in place, the model was run. The model produces a graph of chloride surface concentration vs. time in years, as seen in Figure 8.2; this graph indicates that the critical chloride concentration is reached after 9.2 years. As the remaining design life of the bridge was simulated, the time to joint failure was randomly selected from the uniform distributions described previously. Next, the time until joint repair was randomly selected. During this time when the joint was waiting for repair, it was assumed that chlorides could leak though the joint and accumulate on the pier cap. When the total time of leaking reached 9.2 years, it was assumed that corrosion would initiate within the pier cap. Life-365 then assumes it would take six years (for uncoated reinforcing steel) for corrosion damage to propagate through the pier cap to the point of requiring repair. As in Cost Scenario 1, the remaining bridge service life was simulated 10,000 times.

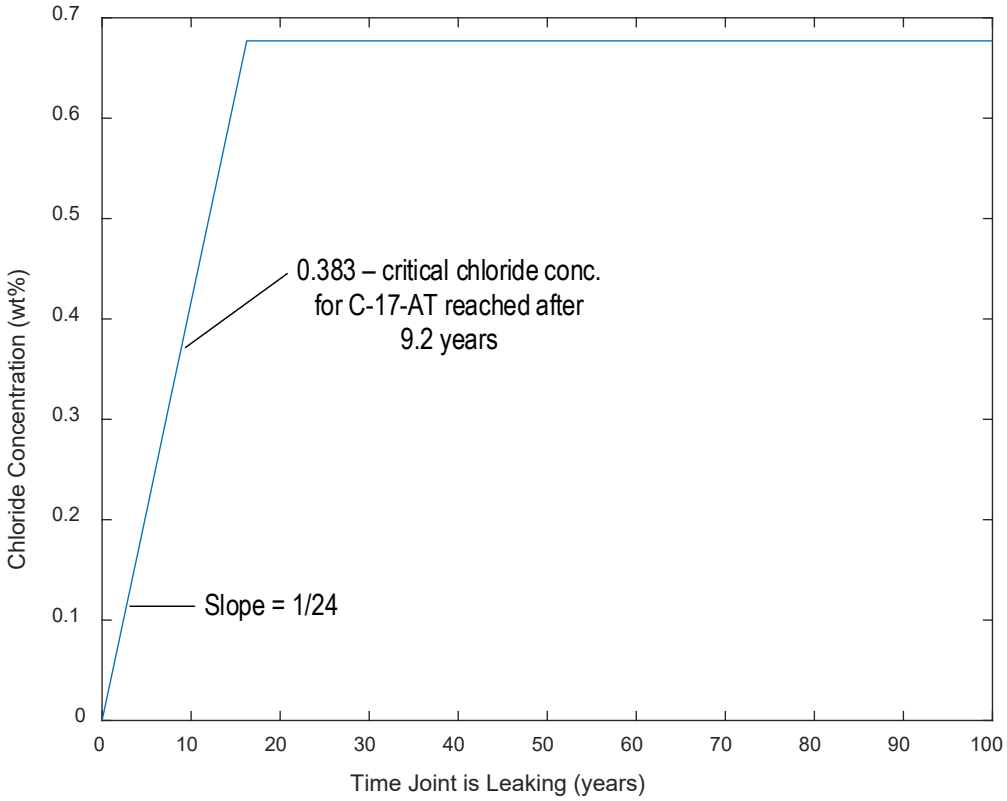

Figure 8.2 Life 365 chloride surface concentration vs. time (years) for Colorado

It should be noted that in this analysis, the chloride concentration on the pier caps is assumed to start from zero. This is equivalent to assuming that calculations are being conducted on a brand new bridge, or one that has just had its pier caps rebuilt. An existing bridge likely has an initial chloride concentration on the pier caps, and this would lead to a faster corrosion initiation and the possibility that additional pier cap repairs would be needed in the remaining service life, thus increasing the LCC for the structure.

The estimated costs for pier cap repair were assumed to affect piers or abutments under all joints for the **no change** alternative. For the **joint retrofit** alternative, when only deck joints were retrofit, corrosion damage was assumed to be a possibility under the abutment joints. When all joints were removed and replaced with continuous deck, costs for pier cap or abutment corrosion were assumed to vanish as the continuous deck with crack sealing would prevent leaking of chloride solution onto the elements below the deck.

8.4 Results

The MATLAB code was run for each combination of cost scenario and alternative agency practice, as shown in Table 8.2. The results of these analyses were compiled to determine the most cost-efficient solution for existing bridge expansion joints.

8.4.1 Cost Scenario 1 Results

Cost Scenario 1 examines the LCCs for existing bridge joints only, without considering costs associated with damage to the bridge's superstructure. The costs associated with the two maintenance alternatives and different topographical locations are shown in Table 8.3.

Table 8.3 LCC for cost scenario 1

		Agency Practice Cases								
		A			B			C		
		Mean	Std. Dev	COV	Mean	Std. Dev	COV	Mean	Std. Dev	COV
Mountains	Leave Joints In-place	$138,805	$15,729	0.11	$128,328	$15,669	0.12	$242,199	$19,916	0.08
	Retrofit deck joints only	$80,292	$7,801	0.10	$75,153	$7,754	0.10	$132,874	$9,876	0.07
	Retrofit deck and abutment joints	$21,840	--	--	$21,840	--	--	$23,280	--	--
Plains	Leave Joints In-place	$75,301	$14,373	0.19	$69,878	$9,100	0.13	$140,673	$13,102	0.09
	Retrofit deck joints only	$48,782	$7,311	0.15	$45,834	$4,511	0.10	$81,795	$6,423	0.08
	Retrofit deck and abutment joints	$21,840	--	--	$21,840	--	--	$23,280	--	--

For both the mountains and plains, and for all agency practice cases, there are significant cost savings associated with retrofitting the bridges to remove expansion joints. Removing just the deck joints can result in a 30% to 40% cost savings over the design life. Removing all bridge joints results in even greater savings. The cost savings are highest in the mountains, because the typical life of a joint in the mountains is much shorter, and thus when joints are allowed to remain in the bridges they will need to be replaced much more often. The costs for agency practice case B are lower than those for case A, because the time until joints are replaced is longer, which means there will be fewer joint replacements over the remaining life. The costs associated with leaving joints in place and continuing to repair/replace them when necessary are much higher in agency practice case C, and the potential savings associated with removal of joints are even larger.

This analysis shows that even on a single bridge there is the potential for significant savings by removing either deck joints, or deck and abutment joints. When prioritizing bridges for the joint retrofit, the greatest future savings can be achieved by retrofitting bridges in the mountains and those with longer remaining design lives first. There is uncertainty associated with all of these cost estimates. Each individual bridge and joint will behave in its own way, and the probabilistic distributions assumed in this analysis are approximations based on prior CDOT experience. Given the assumed distributions, for most of the alternatives and agency practice cases the coefficient of variation (COV) of LCC is in the range of 10%. There is higher variation for the plains and agency practice Case A, because the combination of average joint life and average time to replacement is such that there is more variation in the number of times the joints will be replaced within the remaining design life.

8.4.2 Cost Scenario 2 Results

Cost Scenario 2 examines the LCCs for existing bridge joints and their impact on pier caps, taking the costs considered in Cost Scenario 1 and adding the costs of repairing pier cap damage due to corrosion. The LCCs for both maintenance alternatives are shown in Table 8.4.

Table 8.4 LCC for Cost Scenario 2

		Agency Practice Cases								
		A			B			C		
		Mean	Std. Dev	COV	Mean	Std. Dev	COV	Mean	Std. Dev	COV
Mountains	Leave Joints In-place	$138,536	$15,499	0.11	$128,436	$15,361	0.12	$250,108	$20,234	0.08
	Retrofit deck joints only	$83,975	$7,937	0.09	$75,202	$7,657	0.10	$132,676	$9,826	0.07
	Retrofit deck and abutment joints	$21,840	--	--	$21,840	--	--	$23,280	--	--
Plains	Leave Joints In-place	$75,324	$14,387	0.19	$69,871	$9,090	0.13	$140,361	$12,845	0.09
	Retrofit deck joints only	$48,631	$7,223	0.15	$45,830	$4,506	0.10	$81,938	$6,537	0.08
	Retrofit deck and abutment joints	$21,840	--	--	$21,840	--	--	$23,280	--	--

Comparing the LCCs shown in Table 8.4 with those in Table 8.3 indicate there is a slight increase in savings associated with deck retrofits to remove joints when the additional costs of pier cap corrosion are included. The overall trends in LCC when pier cap corrosion is included are the same, and the largest cost savings can still be obtained by retrofitting mountain bridges and those with longer anticipated remaining service lives.

8.5 Conclusion

In conclusion, expansion joints have a significant impact on the LCC of any existing bridge. The number of joints, topographical location, and remaining design life of the bridge affect the overall LCC. Corrosion of pier caps does increase the LCC if a bridge has leaking expansion joints. However, the cost of joint replacement is still the dominant component in the total LCC, and for the purpose of making decisions about which bridges should be retrofit, a simplified LCCA considering only the joints themselves should give appropriate information for decision making.

Retrofitting bridge deck joints while leaving the abutment joints in place creates a semi-integral bridge design. This design still produces significant cost savings but allows the abutment joints to remain and serve as thermal stress mediators. Additional study of the costs and consequences of abutment damage due to clogged joints and/or retrofit of abutment joints to be continuous is recommended before bridges are retrofit to remove all joints.

9. SUMMARY AND CONCLUSIONS

9.1 Summary

To gain further knowledge of thermal loading and its influence on expansion joint removal practices, several tasks were performed in the completion of this thesis. First, an extensive literature review was conducted to gain an understanding of the current research completed in this field of study. Moreover, a steel plate girder bridge and a reinforced concrete bridge in Colorado with simply supported spans separated by expansion joints were selected for field instrumentation, load testing, and long-term monitoring. In addition, a three-dimensional finite element model of this bridge was developed using shell elements in CSi Bridge.

The selected bridges were instrumented with thermocouples, linear potentiometers, strain gauges, and a scratch gauge. The sensors installed on the bridge provide thermal loading data throughout the depth of the girders. The strain gauges provided information on bridge performance and local behavior at the joint. The linear potentiometers provided information about how much the joint is moving throughout the seasons and the day. The strain gauges installed at the center girder at midspan of the bridge were used to validate the finite element model, and an excellent match was achieved.

Following field instrumentation, load testing, and validation of the numerical models, a parametric study was performed to examine the effects of different connection types at the joint, different thermal gradients, and the effect of clogged joints. For the steel bridge, the moment demand on the structure was not significantly reduced until a full moment splice connection was implemented. The clogged joints did not affect the global behavior of the bridge significantly. The AASHTO described thermal gradient resulted in smallest thermal stresses on the superstructure compared with the New Zealand thermal gradient. A future analysis with measured thermal gradient information collected from the bridge can further calibrate the numerical model using a realistic thermal distribution.

In order to conduct an LCCA to compare joint maintenance options and expand knowledge of thermal gradient effects on expansion joints in existing bridges, several tasks were conducted for the completion of this thesis. First, an extensive literature review was conducted to further understanding of current research into LCCA for expansion joints on existing bridges. From this literature review, general LCC equations were generated for existing bridges with expansion joints and for retrofitting bridges to remove joints. The LCCA was conducted using MATLAB as the main coding tool and data from CDOT, LIFE 365, and the CSiBridge models. This analysis examined costs associated with bridge expansion joints alone as well as those costs to the bridge superstructure, such as the bridge abutments and pier caps, due to failing expansion joints. The analysis accounted for the bridge's remaining design life, material, and location, where appropriate. The analysis was conducted for three different test scenarios, each with varying parameters in order to provide a more comprehensive analysis. The analysis found that retrofitting all joints, except abutment joints, to be continuous was the most cost effective in most cases, assuming expansion joints will not be cleaned and maintained regularly.

9.2 Significance and Further Research

The significance of this work includes the results of the data collection and analysis, the parametric study, and the LCCA findings. The daily temperature changes, thermal gradients, and overall shifts in temperature due to changing seasons have a significant effect on bridge expansion joints in Colorado. The potential for 0.01 in. of movement and 0.5 ksi of stress increase on concrete bridges consistently and 0.5 in. movement and 5 ksi stress on steel bridges regularly is not negligible. The preliminary data on the concrete bridge C-17-AT presented in this report only account for mid-winter and do not account for the hottest or coldest days of the year with the most movement. However, these limited observations do imply that if CDOT is interested in removing an expansion joint, the bridge superstructure and retrofit option would need to support the movement of the bridge. Additionally, there are clear differences between the AASHTO gradient and what was observed in this study; and there is greater interest around the country in bridges with fewer joints (either integral, semi-integral, or retrofitted). Undoubtedly, instrumenting bridges for temperature effects is an important topic that might warrant a pooled fund study to further evaluate the conclusions made in this study.

The parametric study and data analysis of thermal gradients indicate a great need for further research into thermal gradients experienced by bridges. The current standards of AASHTO and New Zealand thermal gradients appear overly conservative and in need of refinement regarding shape compared with the measured data. The extent of conservatism in the AASHTO gradient results, varying from approximately 1.5 to 15 times that of the uniform gradient in this study, will depend largely on the bridge configuration and type as well as the components for which the stresses are calculated.

Finally, the LCCA concluded that a semi-integral bridge design, which retrofits the interior expansion joints of an existing bridge, would provide the most cost effective design by decreasing joint replacement costs and pier cap corrosion. Further research could expand on this LCCA by examining environmental impacts and costs to users due to deteriorated expansion joints.

REFERENCES

AASHTO LRFD Bridge Design Specifications. (2012).

Agency, Highways, and River Severn. 2000. “Assessment of Composite Bridges,” 219–30.

Albhaisi, S., and Nassif, H. (2014). *Simple Approach to Calculate Displacement and Rotations in Integral Abutment Bridges*.

Al-Wazeer, Adel, Bobby Harris, and Christopher Nutakor. 2005. “Applying LCCA to Bridges.” *Public Roads* 69 (3): 9–9.

Basim, Mohammad Ch., and Homayoon E. Estekanchi. 2015. “Application of Endurance Time Method in Performance-Based Optimum Design of Structures.” *Structural Safety* 56. Elsevier Ltd: 52–67. doi:10.1016/j.strusafe.2015.05.005.

Board, Capital Development. 1998. “Life Cycle Cost Analysis Service.” *World Pumps* 1998 (376): 4. doi:10.1016/S0262-1762(98)90545-4.

Briaud, L. (2013). *Geotechnical Engineering: Unsaturated and Saturated Soils.* Wiley, New YorkCDOT. (2012). *Bridge Design Manual*.

Burke Jr., M. P. (1990). “The Integrated Constuction and Conversion of Single and Multiple Span Bridges.” *Bridge Management*, 677–693.

“Congress Approves the Federal-Aid Highway Act.” (n.d.). United States Senate: Art & History, <https://www.senate.gov/artandhistory/history/minute/Federal_Highway_Act.htm> (Mar. 7, 2014).

CDOT. 2015. “Bridge Expansion Device (0-4).” Colorado Dept. of Transportation. (2016). “Engineering Estimates and Market Analysis.” <https://www.codot.gov/business/business/eema> (Jan. 19, 2017).

Chen, Q. (2008). “Effects of Thermal Loads on Texas Steel Bridges.”

Federal Highway Administration. (n.d.). “History of the Interstate Highway System.” <http://www.fhwa.dot.gov/interstate/history.htm> (July. 8, 2016).

French et al. (2013). “Investigation of Thermal Gradient Effects in the I-35W St. Anthony Falls Bridge.” *J. Bridge Engineering* 18(1), 890-900

Frangopol, D M, and M Liu. 2007. “Structure and Infrastructure Engineering: Maintenance, Management, Life-Cycle Design and Performance.” *Structure and Infrastructure Engineering: Maintenance, Management, Life-Cycle Design and Performance*. doi:10.1080/15732479.2013.769013.

Girmscheid, G. n.d. “Probabilistic Risk-Based LC NPV Model.” Zurich, Switzerland.

Goh, K. C., and Yang, J. 2014. “Managing Cost Implications for Highway Infrastructure Sustainability.” *International Journal of Environmental Science and Technology*, 2271–80. doi:10.1007/s13762-014-0572-5.

Hatami, A. and Morcous, G.. 2014. “Life-Cycle Cost Analysis for Bridge Managment An Application to Nebraska Bridges.pdf.” ASCE.

Hawk, H.. 2003. *Bridge Life-Cycle Cost Analysis*. Edited by Transporation Research Board. Washington, DC: National Cooperative Highway Research Program.

Husain, I., and Bagnariol, D. (2000). “Design and Performance of Jointless Bridges in Ontario.” *Transportation Research Record*, (1696), 109–121.

Kang, J, S Lee, T Hong, K.-J. Koo, C.-T. Hyun, and D Lee. 2007. “Life-Cycle Cost Analysis in Bridge Structures: Focused on Superstructure.” *5th IABMAS Workshop on Life-Cycle Cost Analysis and Design*

of Civil Infrastructure Systems, LCC05. London: Taylor & Francis Group. http://www.scopus.com/inward/record.url?eid=2-s2.0-84863266867&partnerID=40&md5=a7c7295395f718eee0e37cfdfb29a443.

Kassimali, A. (2012). Matrix Analysis of Structures, 2nd Ed., Cengauge Learning, Independence, KY

Kim, S-H, Kim, J-H., Jung, C-Y., and Ahn, J-H. 2010. "Life-Cycle Cost Analysis of a TPSM Applied Continuous Composite Girder Bridge." *International Journal of Steel Structures*. doi:10.1007/BF03215824.

"Life Cycle Cost Optimisation in Highway Concrete Bridges Management.pdf." n.d. Life-365™ Consortium III. (2014). "Life-365™ User Manual." < http://www.life-365.org/download/Life365_v2.2.1_Users_Manual.pdf> (Feb. 20, 2017).

Lam, C., Lai, D., Au, J., Lim, L., Young, W., and Tharmabala, B. (2008). "DEVELOPMENT OF CONCRETE LINK SLABS TO ELIMINATE BRIDGE EXPANSION JOINTS OVER PIERS." *Annual Conference of the Transportation Association of Canada*, Toronto, Ontario, 1–20.

Li, D., Maes, M. A., and Dilger, W. H. (2008). "Evaluation of Temperature Data of Confederation Bridge : Thermal Loading and Movement at Expansion Joint."

Loveall, C. L. (1985). "Jointless Bridge Decks." *ASCE Journal of Civil Engineering*, 55(11), 64–67.

Mao, S., and Huang, R-Y. 2015. "Lifecycle Assessment of Maintenance Repair and Rehabilitation Costs: A Deterioration Modeling Approach for Bridge Components." *Journal of the Chinese Institute of Civil and Hydraulic Engineering*.

Lima, J. and de Brito, J.. 2010. "Managment Systems for Expansion Joints of Road Bridges.pdf."

Milton, J. (2013). "Joint Maintenance and Best Practices in Deck Joint Replacement." *2013 Virginia Concrete Conference*, Virginia Department of Transportation.

Moorty, S., and Roeder, C. W. (1992). "Temperature-Dependent Bridge Movements." *Journal of Structural Engineering*, 118(4), 1090–1105.

Ontario Ministry of Transportation. (2014). "Pulling the Teeth on Old Bridge Structures." *Road Talk*, <http://www.mto.gov.on.ca/english/transtek/roadtalk/rt17-1/#a8> (Apr. 9, 2014).

Osman, H. 2005. "Risk-Based Life-Cycle Cost Analysis of Privatized Infrastructure." *Transportation Research Record*. doi:10.3141/1924-24.

Ozbay, K., Jawad, D., Parker, N., Hussain, S.. 2004. "Life Cycle Cost Analysis: State-of-the-Practice vs State-of-the-Art." Washington D.C.: National Academy of Science.

Precast/Prestressed Concrete Institute. (2003). Chapter 7: Loads & Load Distribution. In PCI Bridge Design Manual. Chicago.

Pugasap, K., Kim, W., and Laman, J. A. (2009). "Long-Term Response Prediction of Integral Abutment Bridges." *Journal of Bridge Engineering*, 14(April), 129–139.

Roeder, C. W. (2003). "Proposed Design Method for Thermal Bridge Movements." *Journal of Bridge Engineering*, 8(1), 12–19.

Rogers, C. E., and Schiefer, P. (2012). "Region Bridge Support Unit Bridge Field Services." (January).

Rogers, C. E., Schiefer, P., and Bouvy, A. (2012). *Alleviating the Effects of Pavement Growth on Strucutres*.

Rager, K. 2016. "Joint Elimination retrofits and Thermal Loading Analysis In Plate Girder Bridge Using Health Monitoring and Finite Element Simulations." Colorado State University.

Reigle, Jennifer A., and John P. Zaniewski. 2002. “Risk-Based Life-Cycle Cost Analysis for Project-Level Pavement Management.”

Riedel, T, Tiemann, N. Wahl, M., Ambler, T. 1998. “LCCA-Life Cycle Cost Analysis.”

RStudio. "RStudio." < https://www.rstudio.com/> (Feb. 10, 2016)

Safi, M., Sundquist, H. and Karoumi, R. 2015. “Cost-Efficient Procurement of Bridge Infrastructures by Incorporating Life-Cycle Cost Analysis with Bridge Management Systems,” 1–12. doi:10.1061/(ASCE)BE.1943-5592.0000673.

Savioz, P. Spuler, T. 2014. “Minimally Invasive Maintenance Refurbishment Options for Bridge Expansion Joints.” Leiden: The Netherlands: CRC PRess/Balkema.

Tsiatas, G., and Boardman, W. G. (2002). *Expansion Joint Elimination For Steel Highway Bridges*. Kingston, RI, 1–129.

University, Standford. 2005. “Guidelines For uidelines for Life Cycle Cost Analysis (LCCA); October 2005,” no. October.

Vasseghi, A. (2013). “Effect of Pier Section Reinforcement on Inelastic Behavior of Steel I-Girder Bridges.” *Journal of Bridge Engineering*, 18(January), 31–41.

Wasserman, E. P. (1987). “Jointless Bridge Decks.” *American Institute of Steel Construction, Inc.*, 24(3), 93–100.

Wasserman, E. P. (1999). “Tennessee State Route 50 Bridge Over Happy Hollow Creek.” *American Pci Journal* 44(5):26-36.

Wasserman, E. P. (2014). “Tennessee State Route 385 over the Wolf River Wetlands - A Precast Solution” *PCI National Bridge Conference*.

Zhu, Z., Davidson, M. T., Asce, A. M., Harik, I. E., Asce, M., Sun, L., and Sandefur, K. (2010). “Effect of Superstructure Temperature Changes on Intermediate Pier Foundation Stresses in Integral Abutment Bridges.” 1–11.

APPENDIX A.
INSTRUMENTATION PLAN FOR C-17-AT

Overview

Bridge C-17-AT will be partially closed to allow CSU research group to instrument the bridge. The bridge to be closed is on I-25. The instrumentation will take approximately 12-16 hours. 2 flaggers will be needed from CDOT. Proper PPE will be worn by all present. 4 to 6 members of the CSU research team will be on site. Jessica Martinez and possibly David Weld of CDOT will be on site as well.

Steps to Instrumentation

1. **If necessary, close East lane of bridge – Instrumentation will be on the east side of the bridge – Might not be necessary**

2. **Locate inspection truck near joint between span 2 and span 3 under the north lane of bridge.**
   a. Install 3 linear potentiometers on joint. This is the east side and north end of the bridge.
      i. C17AT_LP_1 is installed at mid-thickness on the concrete deck about 3.75" from the top of the deck. The exact distance from the center of the linear potentiometer and the top of the deck is recorded. This sensor will be installed on the east side of the deck joint.
      ii. C17AT _LP_2 is installed on the concrete girder about 3" from the bottom of the deck/top of the girder. The exact distance from the center of the linear potentiometer to the top of the deck is recorded. This sensor will be installed on the east side of the deck joint.
      iii. C17AT_LP_3 is installed on the concrete girder about 3" above the bottom of the girder. The exact distance from the center of the linear potentiometer to the top of the deck is recorded. Approximately 21" from the top of the girder. This sensor will be installed on the east side of the deck joint.

   b. Install 4 thermocouples on girder near the joint
      i. C17AT_TH_1 is installed on the concrete deck at about 2" from the top of the deck. The exact distance from the center of the thermocouple and the top of the deck is recorded. This distance should be about 2 inch. This sensor will be installed on the north side of the deck joint (the northward girder).
      ii. C17AT _TH_2 is installed on the concrete girder about 2" from the top of the girder. The exact distance from the center of the thermocouple and the top of the girder is recorded. This distance should be about 2 inch. This sensor will be installed on the north side of the joint (the northward girder).
      iii. C17AT _TH_3 is installed on the north side of the joint. It will be located in the center of the vertical face of the girder. The exact distance from the center of the thermocouple and the top of the deck is recorded. This distance should be approximately 19-20.5 inches.
      iv. C17AT _TH_4 is installed on the north side of the joint. It will be located at about 2" from the bottom of the girder. The exact distance from the center of the thermocouple and the top of the deck is recorded. This distance should approximately 22 inches from the top of the girder/2 inches from the bottom of the girder.

   c. Install 8 strain gauges on girder near the joint
      i. C17AT _SG_1 is installed on the concrete deck as close to the top of the deck as possible. The distance from the center of the strain gauge and the top of the deck is recorded. This distance should be about 1 inch. This sensor will be installed on the south side of the deck joint (the southward girder).
      ii. C17AT _SG_2 is installed on the concrete deck as close to the top of the deck as possible. The distance from the center of the strain gauge and the top of the deck is recorded. This distance should be about 1 inch. This sensor will be installed on the north side of the deck joint (the northward girder).

iii. C17AT _SG_3 is installed on the north side of the joint on the concrete deck as close to the bottom of the deck as possible. The distance from the center of the strain gauge and the top of the deck is recorded. This distance should be about 6.5 inches from the top of the deck (about 1in from the bottom of the deck). This sensor will be installed on the north side of the deck joint (the northward girder).

iv. C17AT _SG_4 is installed on the north side of the joint. It will be located as close to the top of the girder as possible. The distance from the center of the strain gauge and the top of the deck is recorded. This distance should be about 8.5 inches (about 1 in below the top of the girder/bottom of the deck). This sensor will be installed on the north side of the deck joint (the northward girder).

v. C17AT _SG_5 is installed on the north side of the joint. It will be located at mid depth of the girder (about 12" from the bottom of the girder). The exact location from the bottom of the girder will be measured and recorded. This sensor will be installed on the north side of the deck joint (the northward girder).

vi. C17AT _SG_6 is installed on the south side of the joint. It will be located at the base of the girder. The exact distance from the center of the strain gauge and the top of the girder is recorded. This distance should be about 23 inches/1 inch above the bottom of the girder. This sensor will be installed on the south side of the deck joint (the southward girder).

vii. C17AT _SG_7 is installed on the north side of the joint. It will be located at the base of the girder. The exact distance from the center of the strain gauge and the top of the girder is recorded. This distance should be about 23 inches/1 inch above the bottom of the girder. This sensor will be installed on the north side of the deck joint (the northward girder).

3. **Locate instrumentation Truck near mid-span of northernmost span under the East lane of the bridge.**
   a. Install 1 strain gauge on web of girder near bottom of web at mid-span. C17AT _SG_8 will be installed as close to the bottom of the girder at mid-span as possible.

4. **Zero strain gauges and record linear potentiometer measurements for Control Load Testing??**

5. **Control Load Testing – To be done in the evening – Date & Time: TBA**
   a. Close easternmost (right) lane of bridge entirely – Drive truck over during gaps between northbound traffic
   b. During gaps in traffic drive CDOT specified truck to drive over bridge on closed lane 3x at 5 mph
   c. During gaps in traffic drive CDOT specified truck to drive over bridge on closed lane 3x at 30 mph
   d. During gaps in traffic drive have CDOT specified truck sit with front axil over midspan for 5 minutes
   e. During gaps in traffic drive have CDOT specified truck sit with back axil over midspan for 5 minutes
   f. Clean Up
   g. Open bridge entirely

Detour Information

During the controlled load testing of the bridge, the east lane will need to be closed


12'-10"

APPENDIX B.
DECK JOINT REMOVAL SURVEY

The Colorado Department of Transportation and the research team were interested to understand the level of interest in deck joint removal on a nation scale. Therefore, a survey was developed and administered to all states' departments of transportation and all members on the AASHTO SCOBS list using a Google Form. Interest and the current state of deck joint removal were the main focus of the survey. The results of the survey indicated a strong interest in removing deck joints in existing bridges. Key results are highlighted in this Appendix and the survey is also presented. 62% of the Department of Transportation responded to the survey.

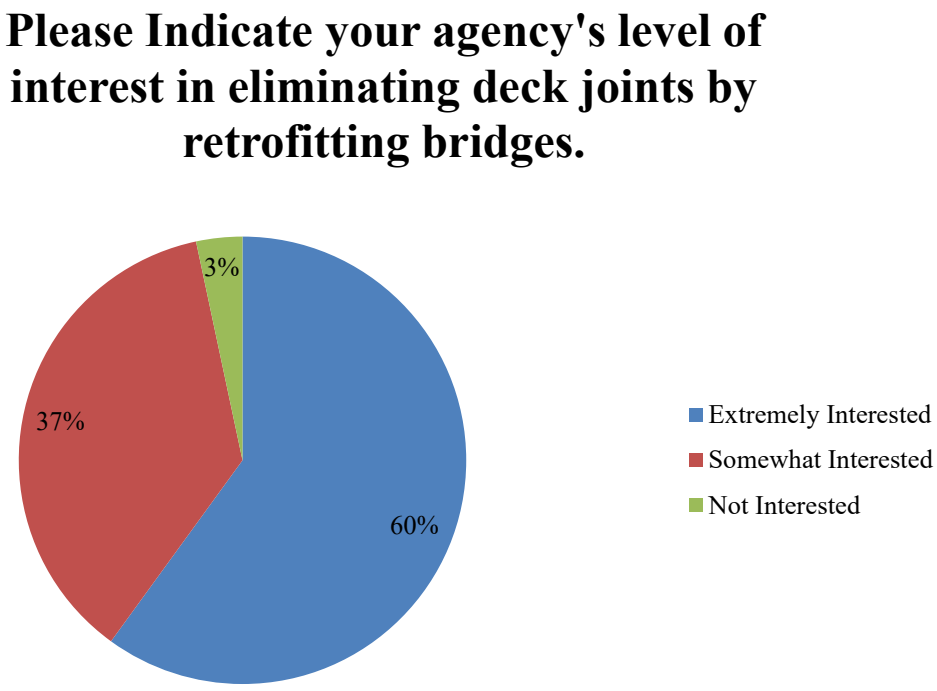

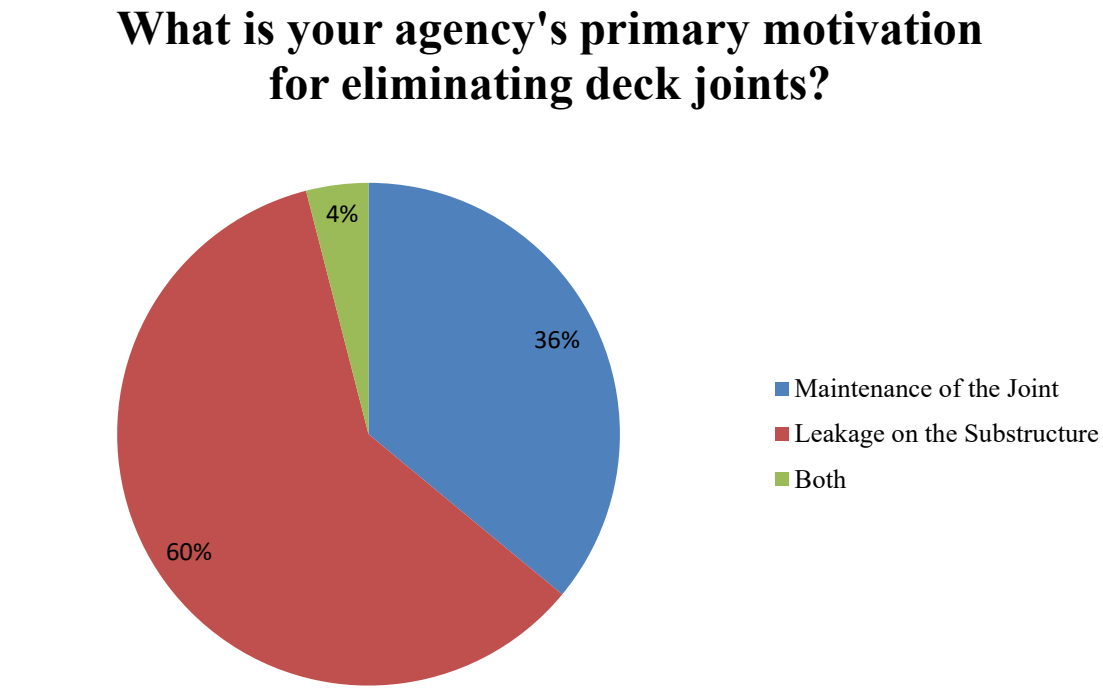
What is your agency's primary motivation for eliminating deck joints?
4%
36%
60%
Maintenance of the Joint
Leakage on the Substructure
Both

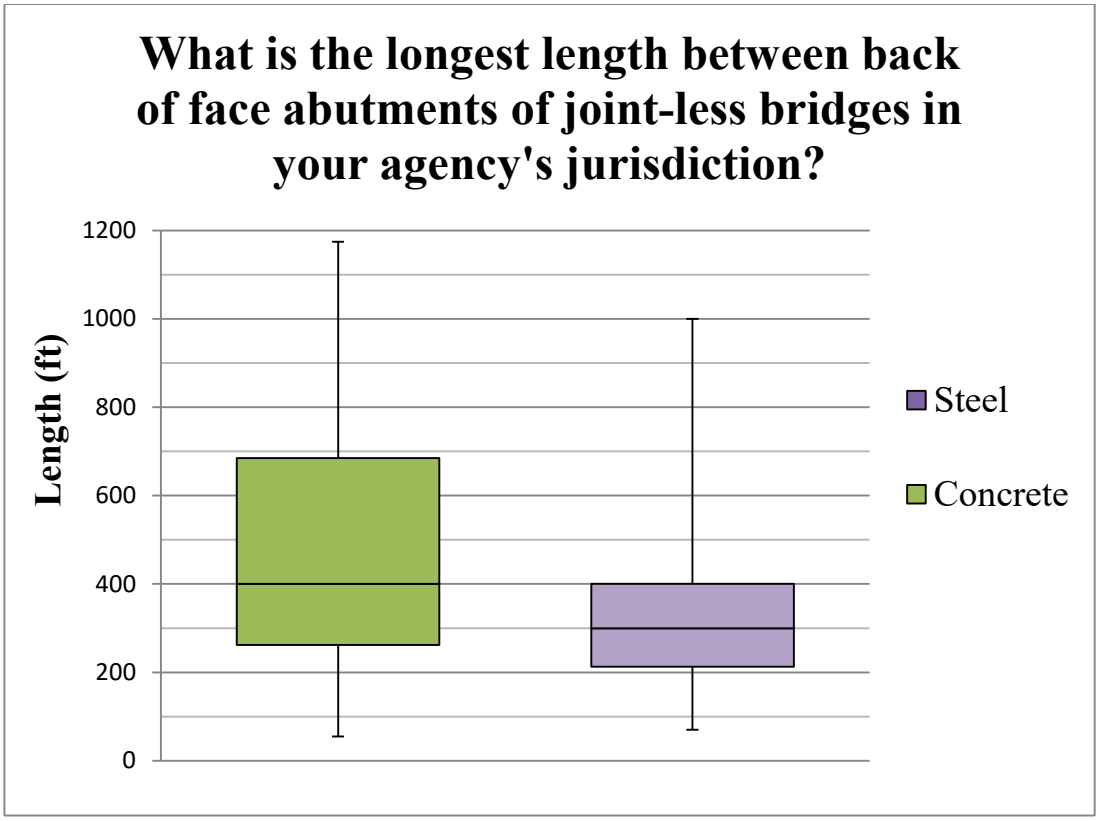
What is the longest length between back of face abutments of joint-less bridges in your agency's jurisdiction?
Length (ft)
1200
1000
800
600
400
200
0
Steel
Concrete

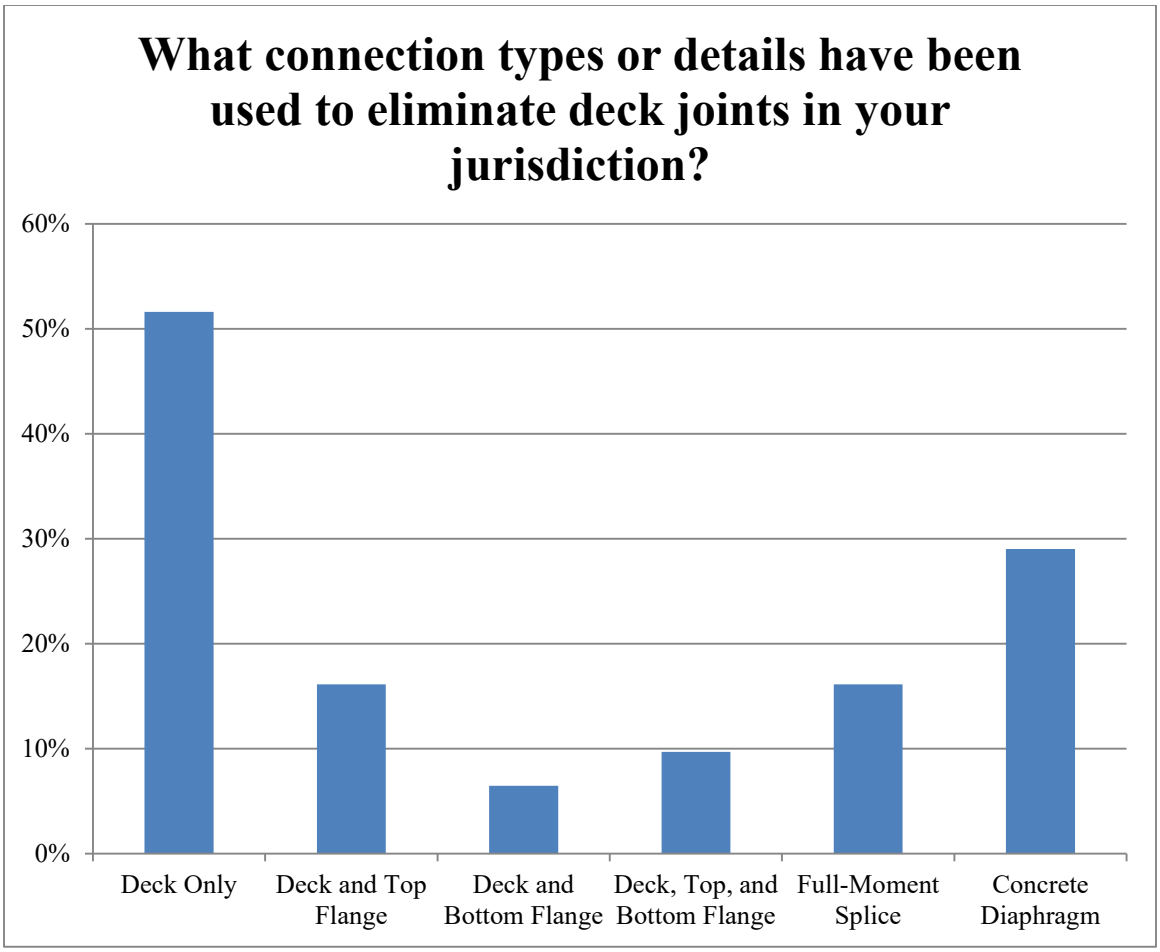
What connection types or details have been used to eliminate deck joints in your jurisdiction?
60%
50%
40%
30%
20%
10%
0%
Deck Only
Deck and Top Flange
Deck and Bottom Flange
Deck, Top, and Bottom Flange
Full-Moment Splice
Concrete Diaphragm

Have improvements in maintenance costs or other life cycle costs for retrofitted bridges been observed as a result of deck joint elimination?

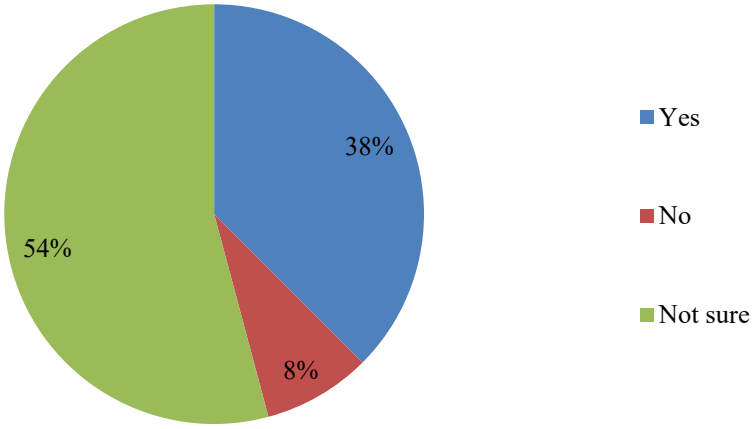

Does your agency promote newly constructed bridges to be designed and built without deck joints?

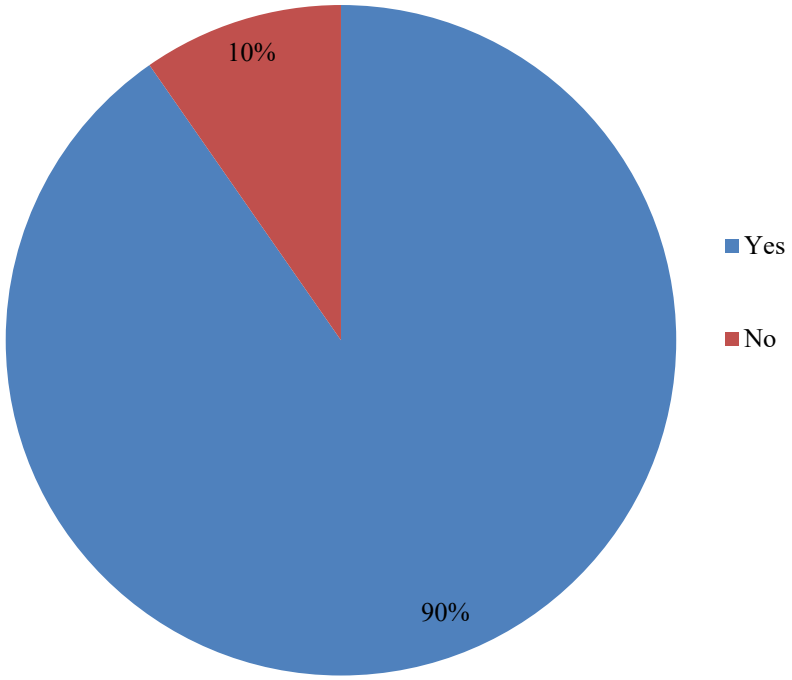

Deck Joint Removal Implications

Research funded by the Colorado Department of Transportation

* Required

Please indicate the agency you are representing.

Please indicate your agency's level of interest in eliminating deck joints by retrofitting bridges.

- Extremely Interested
- Somewhat Interested
- Not Interested

What is your agency's primary motivation for eliminating deck joints?

- Maintenance of the Joint
- Leakage on the Substructure
- Other:

In joint-less steel bridges in your jurisdication, what is the longest total length between back faces of abutments?

In joint-less concrete bridges in your jurisdication, what is the longest total length between back faces of abutments?

Has your agency already eliminated deck joints by retrofitting bridges? *

- Yes
- No

Does your agency provide a specific procedure (design guidelines and/or construction detail) for removing deck joints in bridges?

- Yes
- No

Continue »

Experience with Deck Joint Retrofits

What resources are available to guide the design of retrofits for deck joint elimination? Please check all that apply.

- [ ] Design Manuals
- [ ] Design Guidelines
- [ ] Design Examples
- [ ] Worksheets
- [ ] Other:

How many bridges have been retrofitted to eliminate deck joints in your jurisdiction? May provide answer numerically as an exact number, an approximation, or an approximate percentage. Please feel free to expand or explain your answer further as needed.

Have deck joints been eliminated in steel bridges, concrete bridges, or both?

- ( ) Steel
- ( ) Concrete
- ( ) Both

What connection type or detail was used to eliminate deck joints? Circle all that apply. *

- [ ] Deck Only
- [ ] Deck and Top Flange
- [ ] Deck and Bottom Flange
- [ ] Deck, Top, and Bottom Flange
- [ ] Full-Moment Splice
- [ ] Concrete Diaphragm
- [ ] Other:

Have improvements in maintenance costs or other life cycle costs for retrofitted bridges been observed as a result of deck joint elimination?

- ( ) Yes
- ( ) No
- ( ) Not Sure

Please use the space below to expand on any lessons learned from eliminating deck joints in your jurisdiction.

Deck Joints in New Bridge Construction

Does your agency promote newly constructed bridges to be designed and built without deck joints? *

- Yes
- No

« Back Continue »

Additional Comments

Would your agency be interested in the results of this survey and reading the final research report? If so, please provide an e-mail address of who to e-mail the report to.

If there are other comments, questions, concerns, or heightened interested in the implications of eliminating deck joints, please feel free to express them below.

Minimizing Deck Joints in New Bridge Construction

Do you promote elimination of deck joints in the following types of bridges? Please select one.

- ◯ Concrete
- ◯ Steel
- ◯ Both

What provisions or guidelines are used to implement this preference of minimizing deck joints in new bridge construction? Please check all that apply.

- ☐ Design Manuals
- ☐ Design Guidelines
- ☐ Design Examples
- ☐ Worksheets
- ☐ Other:

Consideration of Thermal Loading

Are the following thermal gradients considered in the design of the retrofit used to eliminate a deck joint? Please check all that apply.

- [ ] Vertical Gradient
- [ ] Transverse Gradient
- [ ] Longitudinal Gradient
- [ ] None of the above are considered
- [ ] Bridge Dependent
- [ ] Unsure

Is the consideration of a vertical thermal gradient considered when designing a new bridge or when eliminating a deck joint? *

- ( ) Yes
- ( ) No

« Back Continue »

Vertical Thermal Gradient

What design provisions are used for the consideration of a vertical thermal gradient?

- ( ) AASHTO LRFD Specifications (Section 3.12.3)
- ( ) Jurisdiction-Specific Procedure
- ( ) Both of the above
- ( ) Other:

How confident are you in designing for the thermal vertical thermal gradient demands given the procedure selected above?

- ( ) Extremely Confident
- ( ) Somewhat Confident
- ( ) Not Confident

Would a more clearly defined procedure in the AASHTO LRFD Bridge Design Specifications improve your agency's ability to consider vertical thermal gradients in new bridge design?

- ( ) Yes
- ( ) No
- ( ) Maybe

Information and Resources Needed

Would a more clearly defined procedure in the AASHTO LRFD Bridge Design Specifications improve your ability and confidence when choosing to retrofit bridges to eliminate deck joints?

- ◯ Yes
- ◯ No
- ◯ Maybe

What tools and information are still needed in order to help with the decision making process regarding deck joint elimination? Please check all that apply.

- ☐ Analytical Tools
- ☐ Design Procedures
- ☐ Field Data
- ☐ Life-Cycle Assessment
- ☐ Other:

« Back Continue »

Additional Comments

Would your agency be interested in the results of this survey and reading the final research report? If so, please provide an e-mail address of who to e-mail the report to.

If there are other comments, questions, concerns, or heightened interested in the implications of eliminating deck joints, please feel free to express them below.

APPENDIX C.
INSTRUMENATION PLAN FOR B-16-FM

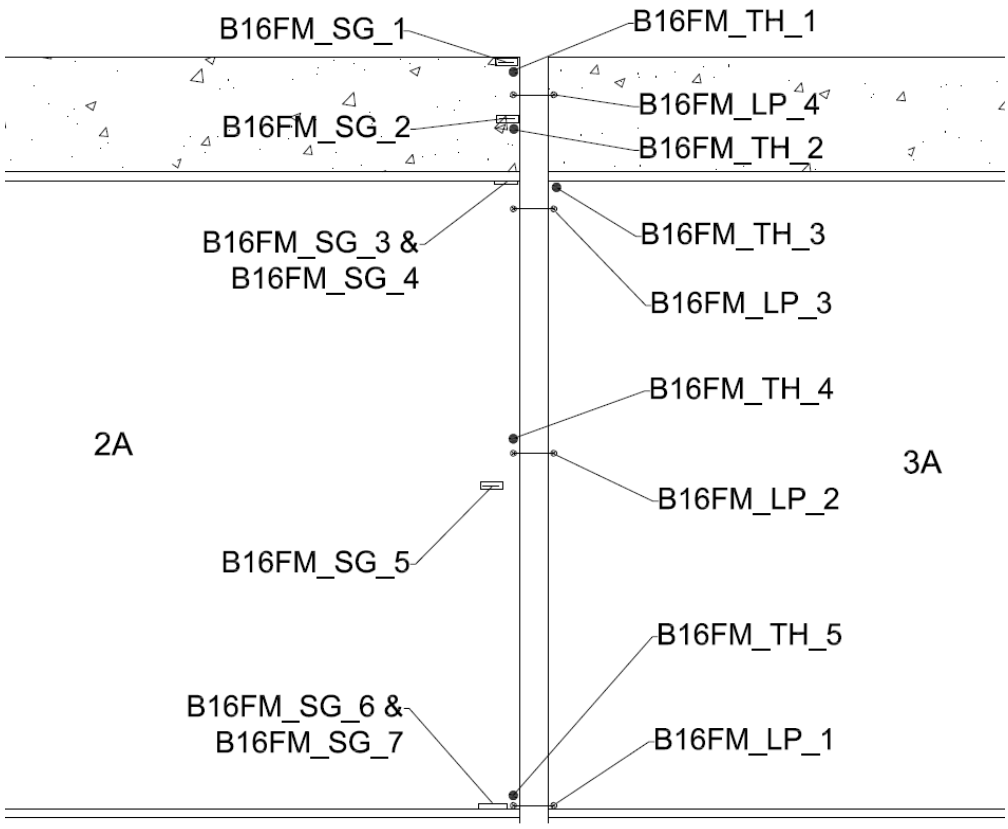

Legend

Thermocouple

Strain Gage

Linear Potentiometer

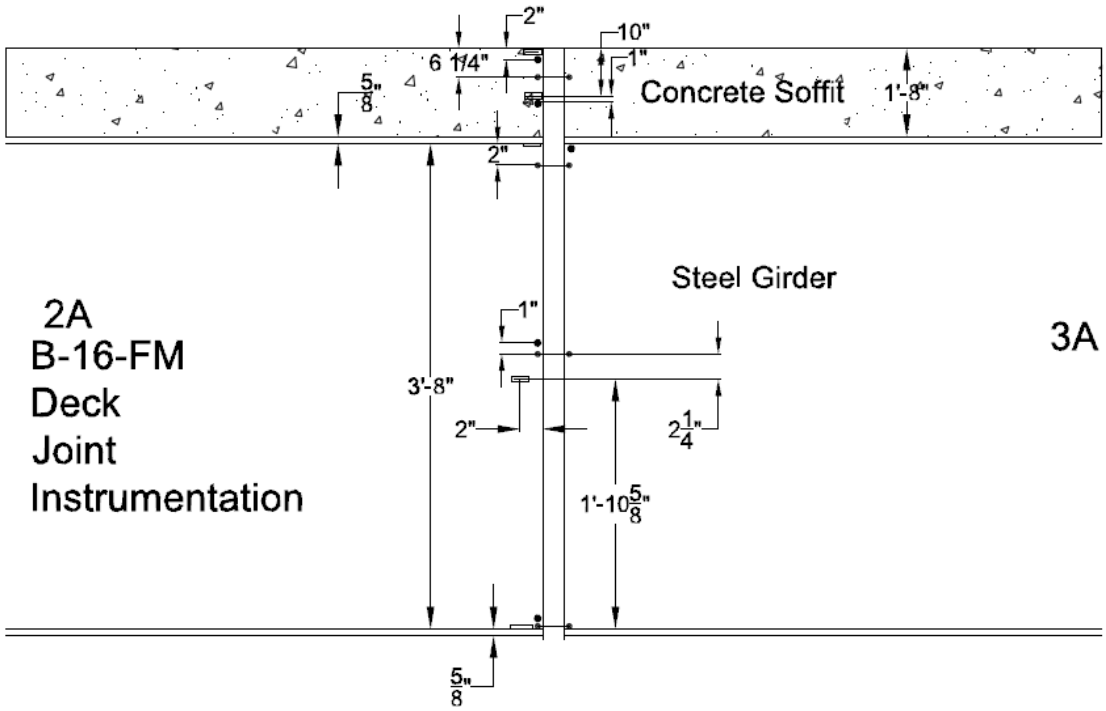
2"
10"
6 1/4"
1"
5/8"
Concrete Soffit
1'-8"
2"
Steel Girder
2A
B-16-FM
Deck
Joint
Instrumentation
1"
3A
3'-8"
2"
2 1/4"
1'-10 5/8"
5/8"